Observation of solar neutrons in association with solar flare using an international network of new type of solar neutron detector

(新型太陽中性子検出器を用いた国際ネットワークによる
太陽中性子の観測)

Doctoral Thesis

Harufumi Tsuchiya

Abstract

High energy neutrons are produced at the solar surface in association with a solar flare. Such neutrons are called solar neutrons. Solar neutrons are produced by nuclear interactions between accelerated ions and the solar atmosphere. Therefore, the observation of solar neutrons provides us valuable information on the high energy ion acceleration mechanism at the solar surface. For the purpose of detecting the solar neutrons accompanied by solar flares on the ground and to understand the ion acceleration mechanism, solar neutron detectors of a new type were installed at various sites between 1990 and 1998.

On November 6th 1997 and November 28th 1998, X9.4/2B and X3.3/3N solar flares occurred at the solar surface. In both events, the solar neutron detector installed on Mt. Chacaltaya in Bolivia (S16°E295°, 5250 m above sea level) and Yangbajing in Tibet (N30°E90°, 4300 m a.s.l.) detected remarkable signals due to solar neutrons. The statistical significance for 3 minute counting rate was 3.9σ and 4.2σ respectively. Although significant signals were obtained in both events, it was thought to be impossible to detect solar neutrons from these flares because of the thick air mass for both events. However, the Monte Carlo simulation in this thesis indicates that it is possible to detect solar neutrons taking account of the refraction effect of solar neutrons in the atmosphere, even if the atmospheric depth is large due to the large zenith angle of the sun. From the data obtained by the Tibet solar neutron detector, the neutron flux at the top of the atmosphere was derived. Making a comparison of the derived neutron spectrum with the neutron flux obtained from the past solar neutron events, it was found that the flux on 1998 November 28th event was relatively weaker than those for the past results. According to the detection of solar neutrons using the Tibet solar neutron detector, it was demonstrated that measurement of arrival direction of solar neutrons was very effective especially for weak flux of solar neutrons.

The data obtained at Mt. Chacaltaya showed a very strange behavior, in that a clear signal was detected about 10 minutes before the time when the X9.4 solar flare occurred. At the corresponding time, a C4.7 solar flare

occurred. However, up to now, there have been no observation of solar neutrons in association with C class solar flares. For solving this mystery, escape probability of neutrons and 2.223 MeV gamma ray lines from the solar atmosphere was calculated. According to the result of the calculation, it was found that the 2.223 MeV line was strongly attenuated by thick solar atmosphere if production region of the line was deeper than 300 km from the boundary between the photosphere and the chromosphere. Therefore, it was found that there was a possibility that solar flares in no association with gamma rays could cause the ion acceleration and produce neutrons. In this thesis, the question of whether or not the signal obtained by the Bolivian solar neutron detector is due to solar neutrons will be discussed under the calculation of the escape probability.

Contents

List of Figures

List of Tables

1 Introduction

Particle acceleration is a phenomenon which can be found at various places in the universe. However, our knowledge on the acceleration mechanism of particles is still not adequate. Since cosmic rays were discovered, it has been a fundamental subject in astrophysics to understand where and how particles are accelerated. Cosmic rays consist of mainly protons and helium; in other words, they are charged particles. Information on the acceleration site is not available from those charged particles, because their paths are bent by the magnetic field in the Galaxy while traveling from the source to the earth (except for very high energy cosmic rays). On the other hand, neutral particles, for example, photons, neutrons and neutrinos do not have their paths diffused by the magnetic field between the source and the earth, therefore these particles can provide information on the acceleration site.

For determination of particle acceleration model, it is necessary to measure as wide energy spectrum of particles as possible. Figure 1 shows that the energy spectrum of cosmic rays extends over a very wide energy range from 10^9 to 10^{20}eV. The spectrum can be roughly represented by a power law function. Below 10^{15} eV, the power law function has a power index -2.7. As a general understanding, a shock acceleration process in the supernova remnants is thought to be possible acceleration model for cosmic rays below 10^{15} eV. However, around and above 10^{15} eV, the spectrum becomes steeper a little. It is still uncertain that such spectrum change is due to the change of the acceleration mechanism around 10^{15} eV (Asakimori et al., 1998 [1]). Observation of a cosmic ray with energy 3×10^{20}eV has been reported in the past. (Bird et al., 1993 [2]; Nagano and Watson, 2000 for review [3]). However, the process of making such high energy particles is not also still clear since arrival rate of such ultra high energy particles is less than 1 particle /100km^2/year.

Recently, from observation of X rays and gamma rays, the acceleration site and acceleration mechanism of electrons have been gradually revealed. X rays and gamma rays directly arrive at the earth without being disturbed by the magnetic field. Observations of SN1006 in the X ray region indicated that electrons were accelerated to high energies up to 100 TeV in the supernova remnants by the shock acceleration process(Koyama et al., 1995 [4]). Perhaps, this may suggest that protons and heavier ions are also acceler-

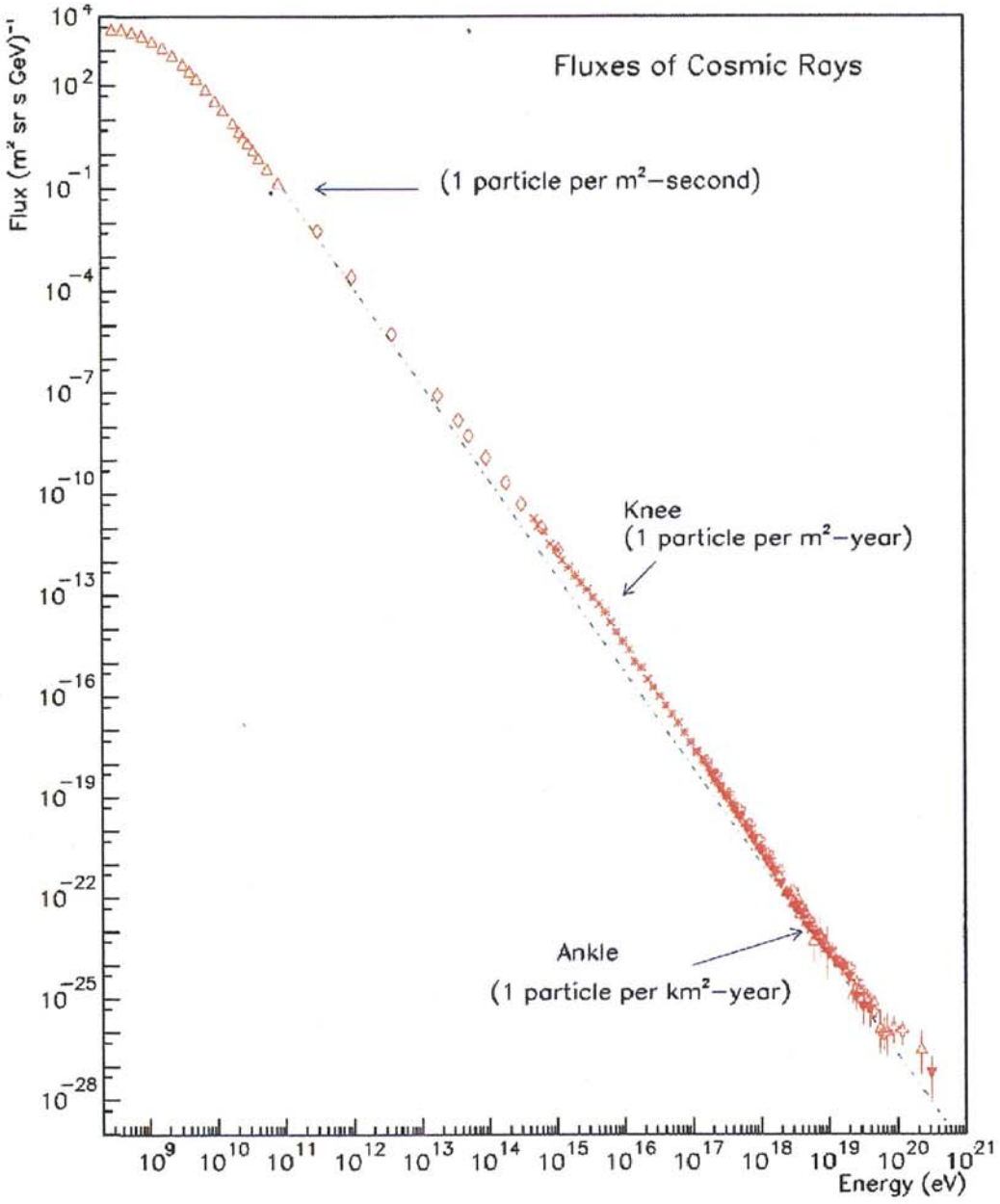

Figure 1: Observed energy spectrum of primary cosmic rays over the energy range of $10^9 - 10^{20}$ eV. The bump at around the energy of 10^{15}eV is called the knee. At 10^{19}eV spectrum becomes harder, which is called the ankle. The arrival rate above the knee and ankle is approximately $1/\mathrm{m}^2/\mathrm{year}$ and $1/\mathrm{km}^2/\mathrm{year}$, respectively.

ated in the same place by the shock. However, observations of X rays relate specifically to acceleration of the electrons and not the acceleration of the ions. This situation is also the same for gamma ray observations of SN1006 in multi-TeV energy regions(Tanimori et al.1998 [5]; Naito et al., 1999 [6]). From the observations of the Crab nebula, gamma rays with energies of TeV have been detected using the atmospheric Cherenkov technique(Vacanti et al., 1991 [7]; Tanimori et al., 1998 [8]) and by data from the air shower array installed on a high mountain in Tibet(Amenomori et al., 1999 [9]). Gamma ray emissions with the energies of TeV from the Crab can be explained by inverse Compton scattering process between accelerated electrons and soft energy photons. As plausible source for such soft energy photons, photons produced by synchrotron emission of the accelerated electrons themselves can be picked in the case of the Crab, which is called Synchrotron Self Compton (SSC) model(de Jager et al., 1996 [10]). Candidate for soft energy photons is 2.7 K cosmic microwave background in the case of SN1006.

As mentioned above, it is very useful for elucidating the acceleration mechanism, to detect neutral particles because they can travel directly from the source to the earth. Although neutrons are produced by nuclear interactions between accelerated ions and interstellar matter, neutrons have a lifetime of about 15 minutes in the rest frame. Therefore, neutrons from astrophysical objects except for the sun which do not have ultra high energy cannot reach the earth before their decay.

The sun occasionally produces detectable flux of neutrons near the earth in association with solar flares. Production of neutrons is evidence that ion acceleration occurs at the flare site during a solar flare. Therefore, we can see the rare scene in which the ion acceleration takes place through a observation of such neutrons. Hereafter, we call neutrons produced in association with solar flares solar neutrons. A solar flare is an enormous explosion and an amount of energy of $10^{29} - 10^{33}$ ergs is emitted over an interval of few minutes to a few tens of minutes at the solar surface. Released energy by a solar flare is sometimes very large, in the largest solar flares it reaches $\sim 10^{34}$ ergs (Kane et al., 1995 [11]). It has been also a long standing problem of how solar flares produce such large amounts of energy(Golgate, 1978 [12]; Choe, G. S.& Cheng, C. Z., 2000 [13]). From recent observations, the release of stored energy in the magnetic field via magnetic reconnection

is believed to be the source of energy of solar flares (Tsuneta et al., 1997 [14]; Shibata, 1998 [15]; Kocharov et al., 2000 [16]; Nishio et al., 2000 [17]). The released energy is thought to be used not only in particle acceleration but also in plasma heating (Simnett, 1991 [18]) and in creating CMEs (Coronal Mass Ejection)(Antiochos et al, 1999 [19]; Innes et al., 1999 [20]). Therefore investigations of particle acceleration mechanisms at the solar surface are very meaningful in terms of understanding solar flare mechanism itself as well as particle acceleration.

Flare-accelerated particles produce many secondaries via interactions with the solar atmosphere. They include a wide energy range of electromagnetic waves (from radio wave to gamma ray), charged particles and neutrons(Cliver et al., 1991 [21]; Trottet et al., 1994 [22]; Chupp, 1995 [23]; Trottet et al., 1998 [24]; Laitinen et al., 2000 [25]). As a result of electron acceleration, soft and hard X rays as well as radio waves are produced through bremsstrahlung and synchrotron radiation processes. From observations using the soft and hard X ray telescopes on board Yohkoh, electron acceleration at the solar surface has been gradually better understood. When a solar flare occurred on 1992 January 13, a flaring loop structure and hard X ray sources were detected by Yohkoh. In this flare, the flare loop contained hot plasma and hard X ray sources were located at the apex and each footpoint of the loop (Masuda et al., 1994 [26]). The scenario for this loop structure was described as follows. As a result of the magnetic reconnection, Alfvenic upward and downward outflows were generated at the reconnection point. The downward outflow exceeded local Alfven velocity and the fast shock was formed by interactions between the Alfvenic outflow and the magnetic field near the top of the loop. Due to this fast shock, electrons were accelerated near the top of the loop and streamed down to the sun's chromosphere along the magnetic field lines in the flaring loop. Hard X rays were produced by bremsstrahlung from accelerated electrons at the top of the loop because the plasma density increased due to the downward outflows. Furthermore, hard X rays were produced at each footpoint which was located in the chromosphere. Soft X rays resulted from evaporation of the chromosphere heated by downward streaming electrons.

Concerning ion acceleration in association with solar flares, neutrons and gamma rays provide us valuable information, since they are produced by

interactions between accelerated ions and the solar atmosphere. Of course, direct observations of the accelerated ions would provide information on the ion acceleration mechanism. However, the paths of ions are bent by the interplanetary magnetic field and/or ions are trapped in a closed magnetic field at the flare site. Therefore, information on the production time of ions is lost. On the other hand, neutral particles can directly travel from the production site to the earth without losing the information on the production time which is connected with acceleration time of ions.

As characteristic features of gamma rays produced by solar flares, the gamma ray spectrum for energies greater than a few hundred keV shows line and continuum structures (Ramaty et al., 1979 [27]; Cliver et al., 1983 [28]). Figure 2 shows the gamma ray spectrum in association with solar flare on 1991 June 4th, which was obtained by the Oriented Scintillation Spectrometer Experiment(OSSE) on board the *Compton Gamma Ray Observatory*(CGRO). The line structure originates from de-excited nuclei (1-8 MeV), electron-positron annihilation (0.511 MeV) and neutron capture (2.223 MeV) processes. Many observations of gamma rays in association with solar flares were provided by the Gamma Ray Spectrometer(GRS) on board the *Solar Maximum Mission* (SMM) in the 1980's and CGRO in the 1990's (with launches in February 1980 and April 1991, respectively). Yohkoh, which was launched in August 1991, also detected solar gamma ray emissions (Yoshimori et al., 1994 [29]). Although we can study the ion acceleration mechanism using line gamma rays, if electron acceleration is more dominant than ion acceleration, line structure is masked with continuous gamma rays produced by the electron bremsstrahlung process (Such flares are called electron rich flares). Moreover, in the case of a large solar flare, protons and heavier ions are accelerated up to GeV energies well beyond the MeV energy region. Therefore, it is difficult to understand the ion acceleration mechanism observing only the line gamma rays from solar flare, because line gamma rays are produced mainly by ions with energies of 1 - 100 MeV/n.

Low energy solar neutrons can be detected in space while high energy solar neutrons can be detected on the ground. Simultaneous detection of solar neutrons in space and on the ground provides us a wide range of energy spectrum of solar neutrons; in other words, that of accelerated ions at the solar surface. Another important piece of information on the ion accelera-

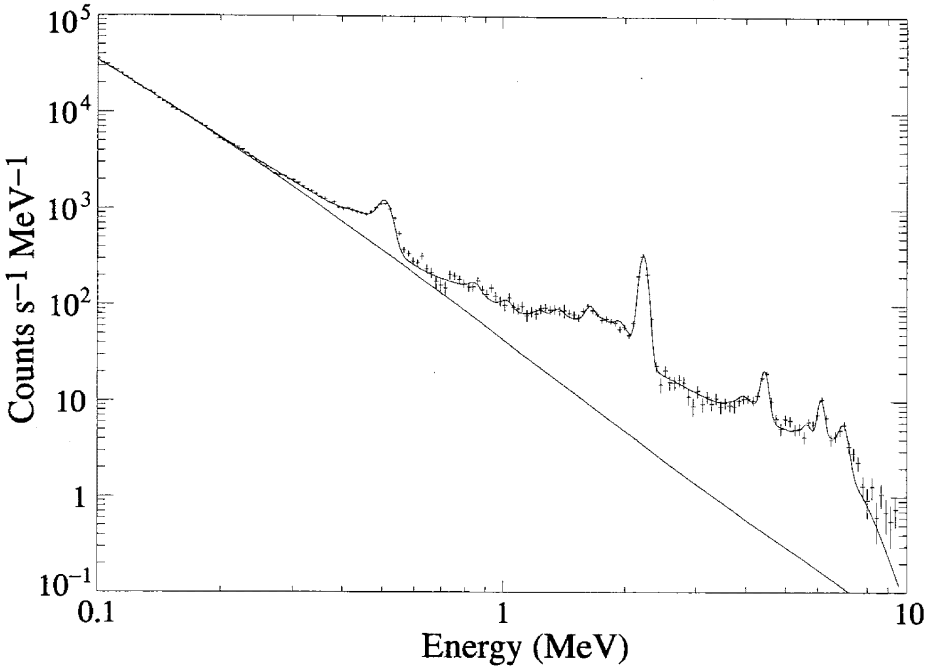

Figure 2: An example of the energy spectrum of gamma ray emissions in a solar flare on 1991 June 4. The spectrum was observed by OSSE on board CGRO.

tion is the acceleration time. By obtaining information on acceleration time, we can know whether ions are accelerated impulsively or gradually at the solar surface in association with solar flares. Furthermore, comparing with data obtained from satellites, it is possible to find out if ions and electrons are accelerated simultaneously or at different times. Therefore, the energy spectrum and the acceleration time are very important quantities for understanding the mechanism for particle acceleration. This is the reason that the observation of solar neutrons becomes very important if we wish to obtain essential information about the acceleration mechanism which gives ~GeV energies to protons and heavier ions.

The importance of observations of solar neutrons produced by accelerated protons was pointed out by Biermann et al.(1951 [30]). Lingenfelter et al.(1965 [31, 32]) also noted this importance and calculated the expected flux of solar neutrons at the earth which were produced by accelerated protons and α particles at the solar surface. They concluded that solar neutrons should be observed in the vicinity of the earth after a large solar flare. They also showed that the time dependence of the solar neutron flux was strongly dependent on the accelerated ion spectrum if neutrons were produced in a

time shorter than their travel time between the sun to the earth.

Early solar neutron observations were difficult due to the inadequate sensitivity of the detectors, although Biermann et al. predicted the arrival of solar neutrons near the earth. In 1980's, SMM was launched and made the first observation of solar neutrons during a solar flare. SMM detected 258 gamma ray emissions in association with solar flares up till 1989 (Vestrand, 1999 [33]). However, SMM detected solar neutrons, for only two events. In 1990's, CGRO was launched. CGRO also could detect not only gamma rays but also solar neutrons. On the ground, solar neutrons were first detected by the neutron monitor on 1982 June 3rd (Chupp et al., [34]). On 1991 June 4th, both the neutron monitor and our solar neutron detector at Mt. Norikura detected solar neutrons (Takahashi et al., 1991 [35]; Muraki et al., 1992 [36]; Struminsky et al., 1994 [37]; Muraki et al., 1995 [38]). However, the number of observations of solar neutrons is still inadequate both in space and on the ground to permit a full understanding of the ion acceleration mechanism.

Solar flares which produce solar neutrons occur when solar activity is near the maximum in a solar cycle. There is a close relationship between the occurrence rate of solar flares and solar activity. It is well known that the sun has variation in its activity peaking every 11 years. By measuring the number of sunspots which appear at solar surface, one can establish the level of the activity on the sun. In Figure 3, the 11 year periodicity in the sunspot numbers can be seen clearly. The occurrence rate of X class solar flares is also given in Figure 3. By comparing the sunspot number with the number of X class solar flares in Figure 3, it can be generally seen that the occurrence rate of solar flares increases as the sunspot number increases and X class solar flares occur at around the solar maximum. From 1975 to 1985 (in solar cycle 21), 157 X class solar flares were observed and 143 events were observed from 1986 to 1996 (in solar cycle 22).

With regard to the ground-level observations, the detection of solar neutrons has been reported in association with solar flares with $>$ X8 class so far besides the observations mentioned above (Shea et al., 1991 [41]; Pyle & Simpson, 1991 [42]; Shibata et al., 1993 [43]; Debrunner et al., 1997 [44]). This fact deeply relates to the small flux of neutrons and the sensitivity of detectors for neutrons. Although neutrons have been detected mainly by neutron monitors located at high mountains in the world until now (Usoskin

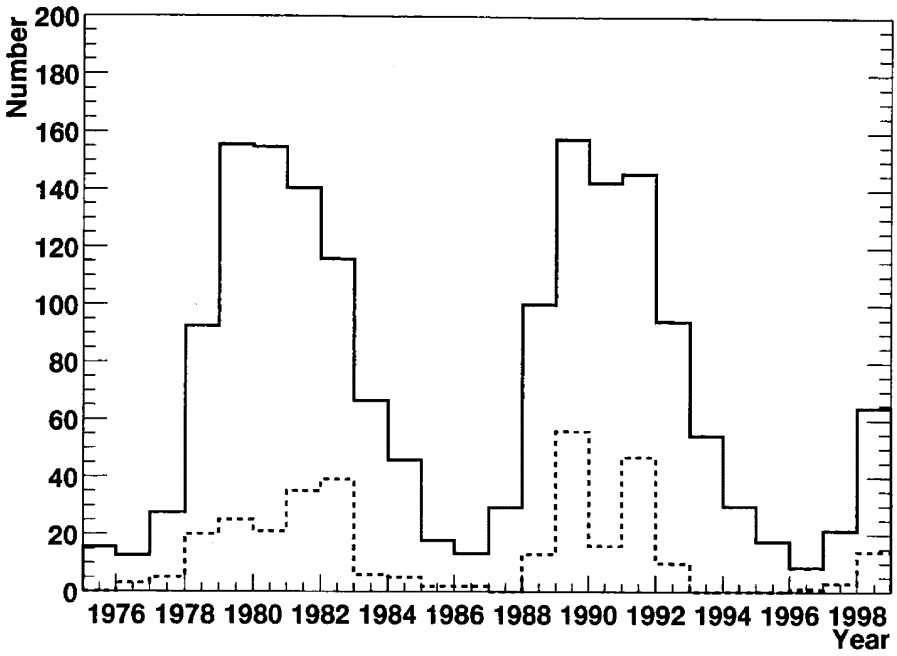

Figure 3: The variation of the number of sunspots (solid line) and X class flares (dashed line).

et al. 1997 [39]; Lockwood & Debrunner, 1999 [40]), the main aim of the neutron monitor is not for solar neutron observations but for measuring the intensity of cosmic rays continuously. For this reason, the neutron monitor does not have several important abilities to detect solar neutrons on the ground such as: (1) measuring the energy of incident neutrons, (2) measuring the arrival direction of incident neutrons, (3) distinguishing neutrons from charged particles. Therefore, it has been necessary to make a new detector which is optimum for detecting solar neutrons on the ground. Now new detectors with such properties have been installed on several high mountains in the world. Furthermore, the new detectors have been installed at various longitude points due to continuous observation of solar neutrons, and they are comprised an international network for solar neutron observation. The reason that solar neutron observation must be continuous is that we can observe solar neutrons only in the daytime. Using the international network, solar neutron observation continues for several years.

In this thesis, at first I introduce a theoretical study of particle acceleration mechanisms and neutron production in solar flares, and the past observations of solar neutrons are shown in section 2. Detectors which are

used for solar neutron observations will be discussed in section 3. In section 4 the observations of solar neutrons using our solar neutron network during solar cycle 23 are described and a discussion of the observations appears in section 5. In section 6, the conclusions and a summary are presented.

2 Theoretical studies and past observations of solar neutrons

2.1 Acceleration models for solar flares

There are various models for particle acceleration at the solar surface. As general acceleration models for solar flares, stochastic acceleration(Ramaty, 1979 [45]; Miller et al., 1990 [46]), shock acceleration(Bell, 1978 [47, 48]; Ellison & Ramaty, 1985 [49]) and direct current (DC) acceleration (Tsuneta, 1985 [50], Anastasiadis, 1997 [51]) are studied well. These models are required to explain the observational results described below:

(1) Ions are accelerated up to GeV energies during solar flares.

(2) In the case of impulsive flares, particle acceleration occurs in a very short time.

(3) Total amount of energy involved in the accelerated particles is typically $10^{29} - 10^{32}$ ergs.

Concerning (1), neutron and gamma ray observations provide the key evidence. Line gamma rays are produced mainly by ions with energies of 1 - 100 MeV/n. Gamma rays with energies > 10 MeV are produced as a result of the decay of neutral pions ($\pi^0 \rightarrow 2\gamma$) and bremsstrahlung associated with the positrons and electrons from the decay of charged pions ($\pi \rightarrow \mu + \nu$; $\mu \rightarrow e + \nu + \bar{\nu}$). These pions are produced via inelastic processes between accelerated ions and ambient matter ($pp \rightarrow d\pi^+$, $pp \rightarrow np\pi^+$, $pp \rightarrow pp\pi^0$). Since the threshold energy for producing pions through the pp reactions is about 300 MeV, in the case of pα collisions that value turns out about 200 MeV. Therefore protons are accelerated to at least a few hundreds of MeV during a solar flare. Moreover, in the flare of 1982 June 3rd, ground-based neutron monitor detected solar neutrons with energy ~ 2 GeV(Chupp et al., 1987 [34]). Also, according to the observations from GAMMA-1 (Akimov et al., 1995 [52]), gamma rays greater than 2 GeV were detected in association with a solar flare on 1991 June 15. These results suggest that ions can be accelerated up to a few GeV in solar flares.

As far as acceleration time is concerned, the time profile of hard X rays and gamma rays rises quickly from a few seconds to few tens of seconds in

the case of an impulsive solar flare. Therefore, in the case of most rapid acceleration, particles are accelerated in less than a few seconds at the solar surface. Taking account of this fact, the acceleration mechanism must involve a process in which particles gain energy very efficiently.

The last item (3) closely correlates with the cut-off energy of particle acceleration at low energies. Generally, energy spectrum forms of accelerated particles are described by a modified second-order Bessel function for the stochastic acceleration [45, 46] and by a power law function in the shock acceleration process [47, 48, 49]. In the stochastic acceleration process, the Bessel function can be applied over the range of non-relativistic energies. As regards the Bessel function form, the total energy content in accelerated ions does not diverge due to characteristic of Bessel function. But, it diverges in the case of the power law form if we do not consider the cut-off energy of lower energy part. In both Bessel function and power law cases, the high energy part does not greatly contribute to the total amount of energy in accelerated ions. Also, taking account the item (1), the cut-off energy of high energy part can be set in the range of a few GeV to a few tens of GeV.

Ramaty et al (1995 [53]) analyzed 19 X-Class events obtained by SMM. As a result of their analysis, the energy content of accelerated ions with energy greater than $> 1\mathrm{MeV/n}$ turned out to be around $10^{30} - 10^{33}$ ergs. This result is comparable to the energy content of accelerated electrons with the energy greater than > 20 keV which was derived from X ray observations generally. According to the comparable energy contents of accelerated electrons and ions, the mechanism is required to give almost the same energy to them if they are accelerated simultaneously. Given these points, it seems reasonable to consider DC acceleration as a plausible mechanism.

Considering the postulations mentioned above, it is pictured as general consideration that the acceleration model satisfied with the postulations and the magnetic reconnection model for particle injection are merged.

2.2 Past observations

After about 30 years from suggestion of Biermann et al [30], neutrons in association with solar flares were actually detected in space. The first detection of neutrons was done by GRS on board SMM on 1980 June 21st(Chupp et al., 1982 [54]). Figure 4 shows the time profile of GRS. This event was

explained clearly by Chupp et al [54]. The first peak of Figure 4 was due to high energy gamma rays and the second gradual increase was due to solar neutrons. Forrest & Chupp(1983 [55]) showed that electrons and protons were accelerated simultaneously by a single process since the time profile of hard X ray and gamma ray showed an increase at almost the same time. This observation also indicated that neutrons with energies of > 50 MeV up to at least 600 MeV were produced at the solar surface within a very short time (within 60 seconds) and so protons were accelerated up to GeV energies rapidly. Ramaty et al.(1983 [56]) and Lingenfelter et al. (1983 [57]) derived the number and the energy spectrum of accelerated protons and heavier ions at the sun from the result of solar neutron observations by SMM/GRS on 1980 June 21st. Figure 5 shows the observations by SMM/GRS and the results calculated by Ramaty et al. [56]. They calculated the time-dependent flux of high energy neutrons at the earth by using a modified second order Bessel function, which was well suited for stochastic Fermi acceleration. As a result, it was found that αT parameter and the number of protons with energy > 30MeV at the flare site were 0.02 and 1.2×10^{33} respectively. αT is the parameter characterizing the energy spectrum in the stochastic acceleration model and determines the hardness of the spectrum. The spectrum becomes harder as αT increases. α represents acceleration efficiency and T indicates the time for particles to escape from the acceleration site.

On June 3rd 1982, not only GRS on board SMM but also ground-based neutron monitors at Jungfraujoch, Lomnicky Stit and Rome succeeded in detecting solar neutrons in association with a large solar flare (Chupp et al., 1983 [58]; Efimov et al., 1983 [59]; Chupp et al., 1987 [34]; Guglenko et al., 1990 [60]). High energy gamma rays resulting from π^0 decay (Ramaty et al., 1987 [61]), radio emissions (Trottet et al., 1994 [22]) and solar neutrons decay protons (Evenson et al., 1983 [62]; Ruffolo, 1991 [63]) were also detected by SMM/HME, SMM/GRS, Nancay Radio heliograph and ISSE-3.

Figure 6 shows the time profile of SMM/GRS and the neutron monitor. Between 11:45 and 11:50 UT, neutron monitor at Jungfraujoch showed an 8.5σ increase due to solar neutrons. In this event, 2 GeV solar neutrons were detected by the neutron monitors. Therefore, accelerated protons that produced the neutrons must have had energies of several GeV at least. With regard to the acceleration time of ions, however, a problem still remains

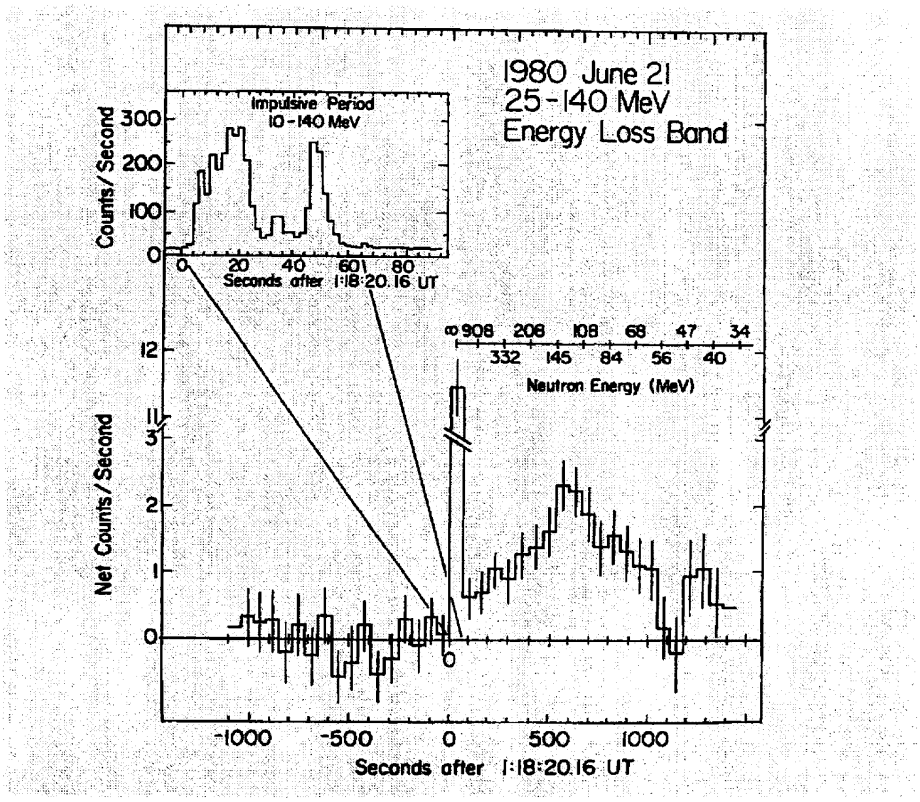

Figure 4: Time profile of photons and neutrons observed by the SMM/GRS detector on 1980 June 21st flare. This graph was shown in [54] as Figure 3.

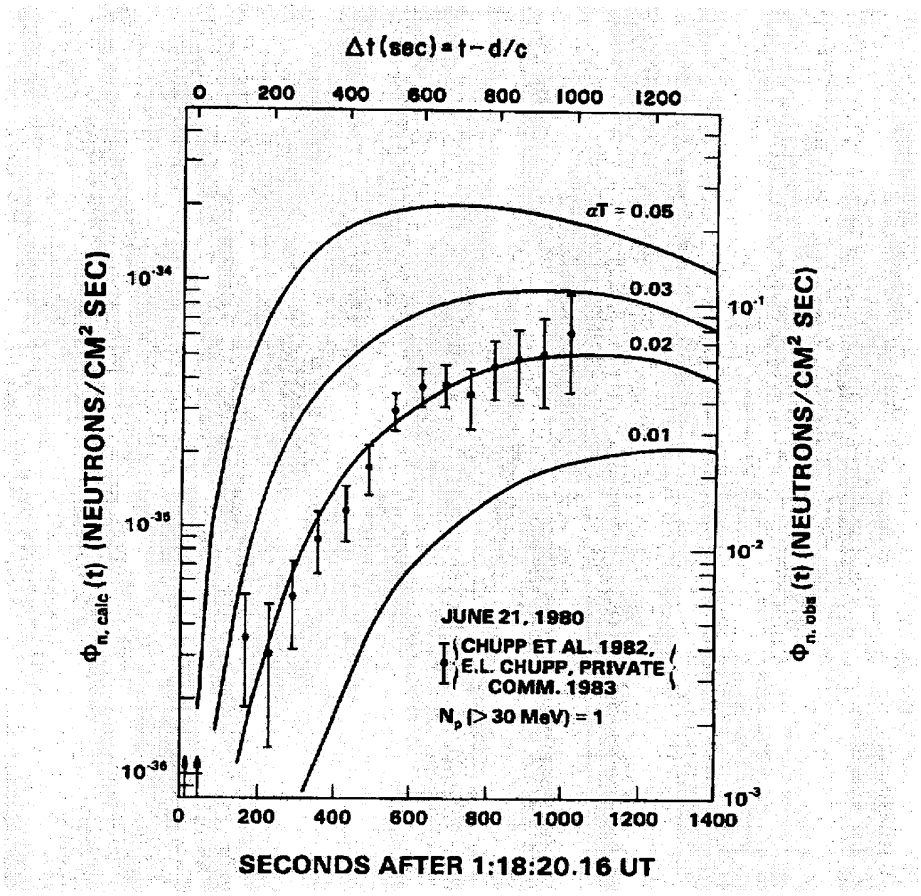

Figure 5: The calculated results given by Ramaty et al.(1983). Black points represent the observed flux of neutrons by the SMM/GRS satellite. Solid lines show the calculated neutron flux at the earth. This graph was shown in [56] as Figure 1.

as to whether ions were accelerated impulsively or continuously. Chupp et al. (1987 [34]) concluded from the SMM/GRS observation and the neutron monitor observation that solar neutrons were produced continuously and so protons were accelerated continuously at the solar surface. If neutron production occurred at only the first impulsive phase of the HE-matrix (> 25 MeV), the increase recorded by the neutron monitors after 11:50 UT could not be explained. But, according to Shibata et al.(1994 [64]) and Muraki et al.(1998 [65]), one can understand that the increase detected by the neutron monitors was produced by only the impulsive production of neutrons. As mentioned later, this discrepancy between them mainly comes from different propagation models of solar neutrons through the earth's atmosphere.

According to these observations of solar neutrons, it was found that protons and heavier ions were accelerated to $\sim$ 300 MeV/n. In some large solar flares, protons were accelerated to at least 1 $\sim$ 10 GeV. The acceleration time varies from flare to flare. Sometimes, ions are accelerated impulsively (from a few seconds to a few tens of seconds), and sometimes, gradually (from a few minutes to a few tens of minutes). But in the case of gradual event, it is difficult to distinguish real continuous acceleration from leakage of trapped particles from the magnetic field (Maddzhavidze & Ramaty, 1987 [66]). As for gradual flare, it is generally accepted that particles are accelerated by a shock accompanied by a CME(but, not all gradual flares accompany CMEs). A CME traveling in the solar corona can accelerate ambient particles, so, the composition of particles accelerated by a CME is almost the same as that in the background solar corona.

As mentioned in section 1, ground level observations of solar neutrons associated with > X8 solar flares have been reported. One of them was mentioned above, that being the 1982 June 3rd event. Table 1 lists solar flares in which the solar neutrons were detected using ground based detectors. Besides the 1991 June 4th event, solar neutrons were detected by neutron monitors.

2.3 Production of solar neutrons

Lingenfelter et al.(1965 [31]) calculated the flux of solar neutrons produced by flare-accelerated protons and they showed more than 90 % of solar neutrons were generated from the interactions between accelerated protons and

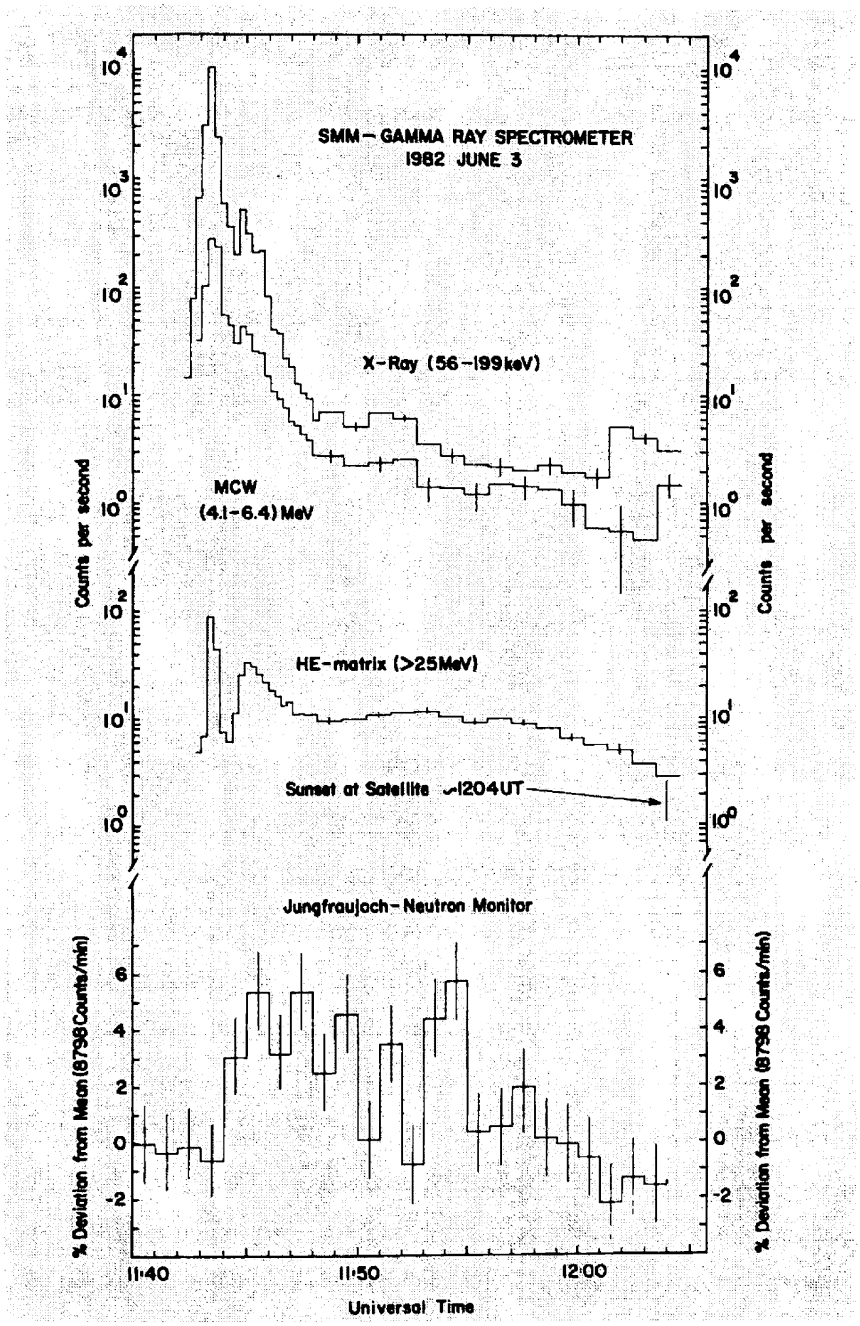

Figure 6: The time profiles of SMM/GRS data and the neutron monitor at Jungfraujoch. The time profile at the top of the Figure shows X ray data. The middle and bottom profiles show high energy gamma rays (> 25 MeV) and data from the neutron monitor obtained with a sample rate one minute. This figure is from Figure 1 in [34].

Table 1: Ground level observations of solar neutrons in association with solar flares. The observation locations of column 2 show one of the representative sites at which solar neutrons were detected.

date	Observation Location	GOES class/H_α imp.	sun
1982 6/3	Jungfraujoch(Switzerland)	X8/2B	S09E72
1990 5/24	Climax(North America)	X9/1B	N36W76
1991 3/22	Haleakala (Hawaii)	X9/3B	S26E28
1991 6/4	Mt.Norikura(Japan)	X12/3B	N30E70
1991 6/6	Mt.Norikura, Haleakala	X12/4B	N33E44

protons/helium in the solar atmosphere. Murphy et al.(1987 [67]) calculated the productivity of neutrons and gamma rays by interactions between the accelerated particles and the solar atmosphere. They evaluated the production of neutrons at the solar surface considering some compositions of the ambient medium and accelerated particles and also considered two acceleration models which were the stochastic acceleration type and the shock acceleration type. According to their calculations, for the stochastic acceleration mechanism, high energy neutrons are produced efficiently via α-p, α-α collisions and low energy neutrons are produced via p-p collisions. For the shock acceleration mechanism, low and high energy neutrons are produced mostly through p-α and p-p interactions, respectively.

Production of solar neutrons and also gamma rays is considered to take place at hydrogen densities greater than 10^{12} /cm^3 (Chupp 1984 [68]). According to the general solar atmospheric model, the atmospheric density has exponential form with scale height of about 85 km and the density at the top of the photosphere is $10^{16} - 10^{17}$ /cm^3. The density $\rho(d)$ at the depth d km from the top of the chromosphere is described by the formula,

$$\rho(d) = \rho_0 \times \exp\left(-\frac{2000 - d}{85}\right) \quad /\mathrm{cm}^3. \tag{1}$$

where the thickness of the chromosphere is 2000 km and ρ_0 represents the density at the top of the photosphere mentioned above. Using this equation, the depth at density 10^{12}/cm^3 is around 1000 km $\sim$ 1200 km. Therefore, the neutron production takes place in the region deeper than the middle of the chromosphere. Generally, the acceleration site must be a low density

region and the production site of neutrons and/or gamma rays must be a high density region. These concepts are called thin target and thick target models.

Hua and Lingenfelter (1987 [69]) calculated the depth dependence of the production point of neutrons and gamma rays caused by accelerated ions using a Monte Carlo simulation. They assumed that ion acceleration took place in the corona or the upper chromosphere at a hydrogen density less than $10^{13}/\mathrm{cm}^3$ and the composition of accelerated ions was the same as for the solar atmosphere. Under these assumptions, their calculations showed that neutron production could actually take place in the photosphere if the accelerated ions have an isotropically downward angular distribution and a harder energy spectrum than that of a Bessel function with $\alpha T \sim 0.03$ for the stochastic acceleration or power law with ~ 4 for shock acceleration The neutron production would take place in the chromosphere if ions have a softer spectrum.

But recently, it was reported that solar neutrons were produced in thin region rather than in a thick region. Ramaty et al.(1997 [70]) showed, from *Granat*/PHEBUS observations that the gamma ray line emissions in the energy range of $1.1 - 1.8$ MeV and $4.1 - 7.6$ MeV were produced in a low ambient density in the corona during a behind-limb solar flare on 1991 June 1st. At that time, a X12/1F solar flare occurred which was the largest flare of solar Cycle 22 involving a total energy $\sim 10^{34}$ ergs. They suggested that the nuclear gamma rays for a disk solar flare were almost produced in the thick region whereas, for a behind-limb solar flare, the thin target model was reasonable one. Murphy et al.(1999 [71]) also analyzed data from OSSE on board CGRO acquired on 1991 June 1st. They claimed that neutrons were detected by OSSE and those neutrons were produced in a thin region due to a limb flare. They also mentioned that the thin target interaction of particles was able to produce intense neutrons in such a case only if the accelerated particles have very hard spectrum with power index less than < 2. If solar neutrons were really produced at thin region in the corona or upper chromosphere, it could have been a very rare case as the neutron production since the general production site of neutrons is a thick region.

2.4 Directivity of solar neutrons

Using a Monte Carlo simulation, Hua and Lingenfelter(1987 [72]) investigated angular and energy distributions of escaping neutrons from the sun. They assumed that the accelerated protons and α particles had an energy spectrum form of a Bessel function and power law and three type angular distributions, which were isotropic, beaming(0°) and horizontal (89°) falling to the chromosphere. According to their calculations, in the case that accelerated ions horizontally (89°) interact with the chromosphere, the probability that neutrons escape at 1 AU is the highest in three angular distributions. The horizontal falling to the chromosphere means mirroring of accelerated particles in the magnetic loop. Since moving direction of neutrons produced by incident accelerated ions becomes predominantly the direction of incident ions. Due to this result, it is thought to be more detectable in the case of limb flares than the disk flares as long as neutrons are concerned. But, there are not yet sufficient observations of solar neutrons so as to judge that limb-brighting of solar neutrons is correct.

2.5 Solar neutron propagation in the atmosphere of the earth

Neutrons which come from the sun are attenuated by the earth's atmosphere through interactions with air nuclei. In order to estimate the flux of neutrons which come to the earth, it is necessary to know the propagation of neutrons in the earth's atmosphere. The propagation of solar neutrons has been calculated independently by Debrunner et al.(1968 [73]) and Shibata(1994 [64]) using a Monte Carlo simulation. Hereafter, the two models are called the Debrunner model and the Shibata model. The results of the calculation using two models are different in the point of threshold energy of incident neutron for reaching at certain altitude after traveling in the earth's atmosphere. This comes from the difference of nuclear interactions used in two models. In the Debrunner model, a nuclear interaction model is used called an intranuclear cascade model. The target nuclei are neutrons and protons. An incident neutron collides with each neutron and proton and induced nucleons then collide with other nucleons. These reactions occur continuously in the nucleus. Simply speaking, the Debrunner model only uses inelastic

scattering between incident neutrons and air nuclei. On the other hand, the Shibata model treats to be the inelastic scattering process and elastic scattering processes. The elastic and inelastic processes used in the Shibata model are utilized from the data obtained from accelerator experiments, which include the cross section, the differential energy distribution and the angular distribution.

As the result of two calculations using different interaction models, the interpretation of the increase of neutrons monitored at Jungfraujoch on June 3rd 1982 became different. According to the Debrunner model, only neutrons with energy > 200 MeV can reach the detector. But, neutrons with energy ~ 90 MeV can also be detected according to the Shibata model. As a consequence, the Debrunner model led us to the conclusion that solar neutrons were produced not only at first impulsive phase but also next extended phase of the flare, whereas the Shibata model led us to the conclusion that solar neutrons were produced at only first impulsive phase of the 1982 June 3rd event([34], [64, 65]).

In this section, we must mention another important concept, namely the refraction effect of solar neutrons in the atmosphere. Recently, Dorman et al. (1999 [74, 75]) calculated the propagation of solar neutrons analytically and Galicia et al.(2000 [76]) applied their result to the observations of solar neutrons in association with a solar flare on 1990 May 24th. As a result of their calculations, it was found that the attenuation rate of solar neutrons with an oblique angle was overestimated and those neutrons have an asymmetrical angular distribution instead of symmetrical distribution. The reason for overestimation of the attenuation was due to lack of consideration of the refraction effect of solar neutrons in the atmosphere. In section 4, it will be shown that there were possible solar neutron observations considering this refraction effect.

3 International network for solar neutron observation

3.1 Solar neutron detector

As mentioned in section 1, to observe solar neutrons associated with solar flares at ground level, one requires not only an optimal location for the detector but also specific instrumental capabilities.

Solar neutrons can travel from the sun to the top of the earth's atmosphere without remarkable attenuation other than decay. However, they then suffer attenuation due to the earth's atmosphere as they pass through the atmosphere to the detector. Figure 7 indicates the calculated attenuation of neutrons at various atmospheric depths in the case of vertical entrance at the top of the atmosphere. For example, in the case that 10,000 neutrons with kinetic energy $T_n = 200$ and 1000 MeV arrive at the top of the atmosphere, the number of neutrons expected at the level of 1000 g/cm^2 (this value corresponding to almost the vertical atmospheric depth at sea level (1030 g/cm^2)), become 1 and 20, respectively. Therefore, neutrons with energies less than 100 MeV rarely arrive at sea level. Attenuation of solar neutrons can not be avoided as long as we observe on the ground. Therefore, solar neutron detectors must be installed at high altitude and at as low latitude as possible to reduce the thickness of the atmosphere traveled by the neutrons. Figure 8 shows the locations of solar neutron detectors and Table 2 shows the geographical coordinates of each solar neutron detector. As seen in Figure 8 and Table 2, in order to achieve continuous observations of solar neutrons, the detectors were installed at different longitudes since it is not possible to predict the time of occurrence of solar flares.

3.1.1 Detection principle of neutrons using the solar neutron detector involving various inelastic interaction processes

Our international network for solar neutron observation has various types of detectors. All the detectors have target layers for converting incoming neutrons to protons, because charged particles can be detected much easier than neutral particles. A plastic scintillator or wood is used as producer of recoil protons. Recoil protons are produced by charge exchange reactions

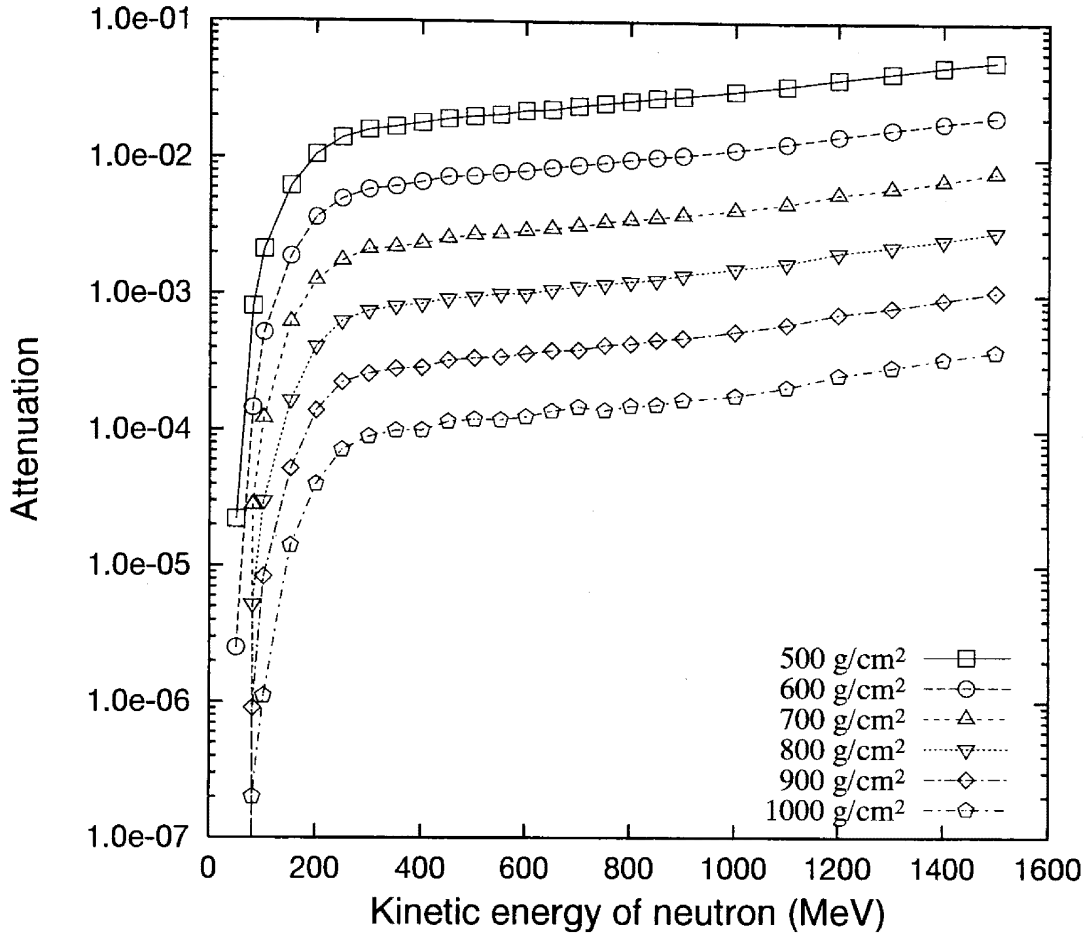

Figure 7: The attenuation of neutrons at various atmospheric depths predicted by a Monte Carlo simulation. The curve for 1000 g/cm^2 corresponds to sea level.

$n + p \rightarrow p + n$ and are also produced through the reaction $n + C \rightarrow p + X$.

In high energy interactions, pion production takes place. Inelastic collisions between neutrons and carbon targets become important at higher energies of incident neutrons. Other charged hadronic particles and electrons have masses less than a proton mass. Therefore, they can easily penetrate thick material because of their smaller ionization loss in the matter at the same energy. If an inelastic collision creates π^0, π^0 is able to produce the charged particles via $\pi^0 \rightarrow 2\gamma \rightarrow e^+e^-$ process. Therefore, if the energy of incident neutrons is higher, we must consider the process of pion production.

Figures 9a and b show the results of simulations for the Tibet solar neutron detector including all processes described above; this simulation was done using GEANT 3. The result represents the number of neutron induced charged particles which can travel to the bottom of the detector with a total

Table 2: The geographical locations of each solar neutron detector.

location (place)	height	longitude	latitude
Switzerland (Gornergrat)	700 g/cm^2 (3135 m a.s.l.)	7°.8E	46°.0N
Armenia (Aragats)	700 g/cm^2 (3200 m a.s.l.)	40°.5E	44°.2N
Tibet (Yangbajing)	600 g/cm^2 (4300 m a.s.l.)	90°.5E	30°.0N
Japan (Mt. Norikura)	730 g/cm^2 (2770 m a.s.l.)	137°.5E	36°.1N
USA (Mauna Kea)	610 g/cm^2 (4200 m a.s.l.)	203°.7E	19°.8N
Bolivia (Mt. Chacaltaya)	540 g/cm^2 (5250 m a.s.l.)	292°.0E	16°.2S

energy loss greater than 40 MeV in the scintillator. In the simulation, 10^5 incident neutrons entered the detector and two incident angles were selected, which were vertical incidence (0°) and oblique (50°) incidence. Figure 9a shows the vertical arrival and Figure 9b indicates the oblique arrival. In both cases, the contribution from the protons is dominant. However, in the case of oblique arrival, the difference between protons and other charged particles turns out to be significantly smaller than for vertical arrival. In the oblique case, the average path length of the particles is longer. Therefore, protons lose kinetic energy more in the scintillator via the ionization process and it becomes difficult for them to reach the bottom of the detector.

3.1.2 The capability of the solar neutron detector

The solar neutron detector is capable of measuring the energy of recoil protons which are produced by incident neutrons via nuclear interactions. It is a very important that the detector has an ability to measure the energy of incident neutrons, since, from this information, we can learn the acceleration time of ions at the solar surface. Neutrons have a mass and they can not

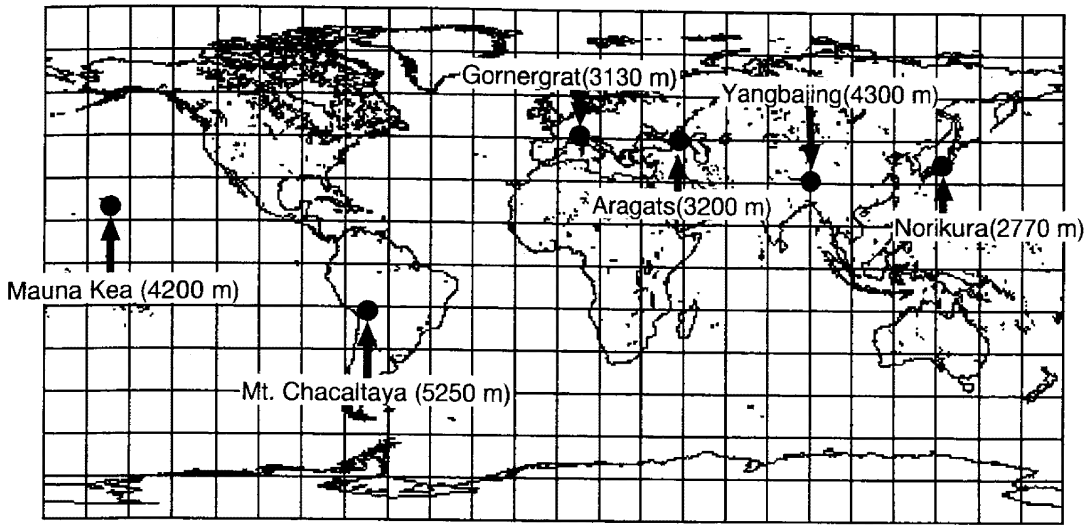

Figure 8: The locations of solar neutron detectors. Closed circles represent the places where the neutron detectors were installed. The names of the sites and their altitudes (in parenthesis) are also indicated.

travel between the sun and the earth at the light speed. The delay time (Δt) of neutrons in comparison with the arrival time of light can be represented by the following equations,

$$\Delta t = \frac{1AU}{c}(\frac{1}{\beta} - 1)$$

$$\beta = \sqrt{1 - \frac{1}{\gamma^2}}, \gamma = 1 + \frac{T_n}{M_n}$$

where γ represents the Lorentz factor for neutrons; T_n and M_n are the kinetic energy and the rest mass of a neutron; c and β are the light velocity and the ratio of velocity of neutrons to the light velocity respectively. As shown in the equation, if the kinetic energy of neutrons (T_n) can be measured, we can obtain the delay time (Δt) of neutrons for the light and convert it to knowledge of the production time of neutrons at the solar surface. However, if the detector does not have an ability to measure the energy of incident neutrons, the production time could be obtained by using the time of flight technique for neutrons and introducing an assumption. In this case, we must assume that neutrons are produced in a short time in comparison with the travel time of neutrons between the sun and the earth. As another assumption, we can also argue that the neutron production time profile is the same as the time profile of X ray and/or gamma rays. By using these assumptions, we

(a) Incident angle is 0°.

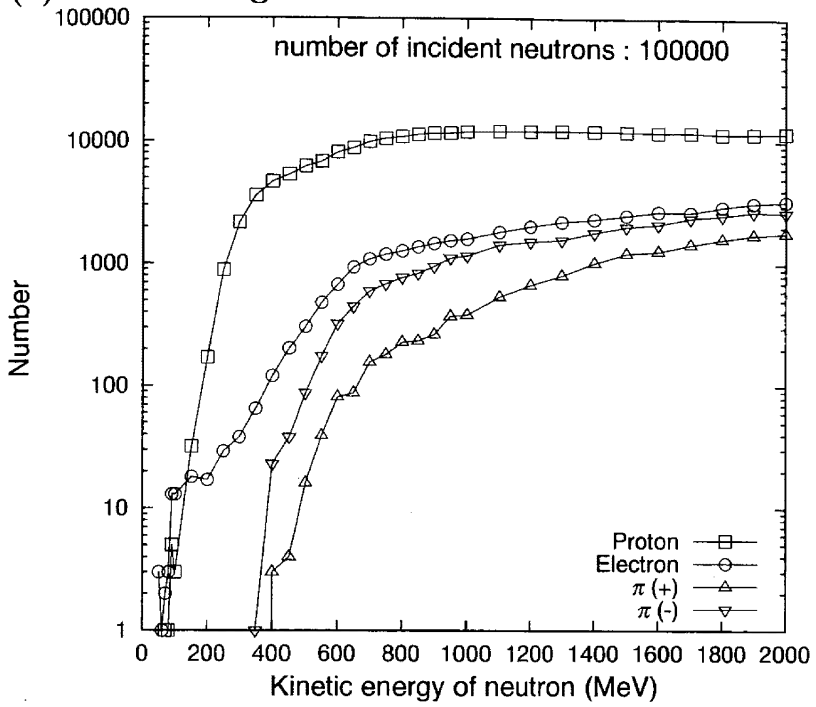

(b) Incident angle is 50°.

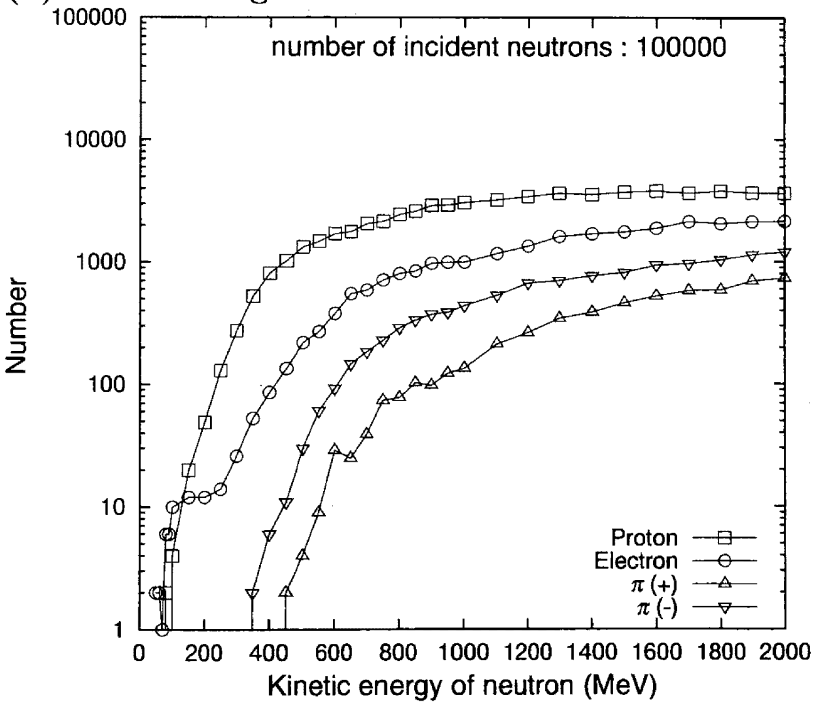

Figure 9: The number of charged particles reaching the bottom of the Tibet solar neutron detector predicted by a Monte Carlo simulation.

could also identify the ion acceleration time profile, however, the solar neutron detectors can bring us more information on the ion acceleration time since they can measure the energy of neutrons.

As next important ability for observing solar neutrons on the ground, our solar neutron detectors can measure the arrival direction of incoming neutrons. Solar neutrons arrive from the direction of the sun. Therefore, the measurement of the arrival directions of neutrons makes it possible to reduce the background from secondary neutrons produced by primary cosmic rays. Furthermore, it allows us to determine the origin of signals by comparing the flux from the solar direction with that from the anti-solar direction. The detectors which have been located at Gornergrat, Yangbajing, Mt.Norikura and Mauna Kea have the ability to measure the direction of incident solar neutrons.

All solar neutron detectors have anti-counters for rejecting charged particles produced by cosmic rays, which are mainly muons and electrons. Not only charged particles but also low energy gamma rays act as noise in terms of observation of solar neutrons. Furthermore, low energy gamma rays come from the floor, the wall and the ceiling. These gamma rays can be rejected by converting them to charged particles using lead plates in front of the detector. Two detectors located at Mt. Norikura have lead plates but others do not have them yet. In Table 3, the features of each solar neutron detector are summarized.

In this thesis, not all detectors will be described, but the detectors installed at Yangbajing in Tibet are shown. Descriptions of the solar neutron detectors are given in many publications(Miyazaki, 1992 [77]; Matsubara et al., 1993 [78]; Muraki et al., 1997 [79]; Matsubara et al., 1997 [80]; Flückiger et al., 1998 [81]; Tsuchiya, 1998 [82]; Hoshida et al., 1999 [83]; Katayose et al., 1999 [84]; Matsubara et al., 1999 [85]; Tsuchiya et al., 1999 [86]; Ter-Antonyan, 2000 [87]; Tsuchiya et al., 2000 [88]). Besides those publications, considerable information can be obtained on the Internet whose URL are shown below.

- `http://kspc4.unibe.ch/sontel.html`
- `http://crdlx5.yerphi.am/solar.html`
- `http://binary.stelab.nagoya-u.ac.jp/Neutron/index.html`

Table 3: The features of each solar neutron detector. Directional mode NS(EW) indicates a detector which can measure in the NS(EW) direction.

Place	Area	anti counter	directional mode
Gornergrat	4 m^2	Top + Side	5 NS
Aragats	4 m^2	Top	No
Yangbajing*	9 m^2	Top + Side	9 EW × 9 NS
Mt.Norikura**	64 m^2	Top + Side	5 EW × 5 NS
Mauna Kea	8 m^2	Top	3NS
Mt. Chacaltaya	4 m^2	Top + Side	No

(*) Until Sep. 1999, 5EW × 5 NS directions had been observed.

(**) At Mt. Norikura, one more solar neutron detector has been installed and operated.

3.1.3 The Tibet solar neutron detector

A schematic view of solar neutron detector installed at Yangbajing (4300 m a.s.l.) is shown in Figure 10. This detector was constructed in September 1998, and has been successfully operated until now. The detector was designed for measuring the energies and directions of recoil protons scattered by incoming neutrons. As shown in Figure 10, the detector consists of scintillation counters and proportional counters. The area of a scintillation counter is 1m × 1m, and the total area is $9m^2$. The thicknesses of scintillators placed in each scintillation counter is 40cm. The energies deposited by recoil protons are measured by a photomultiplier installed above each scintillation counter and the pulse height obtained by each photomultiplier is discriminated at four levels, which correspond to the deposit energy of recoil protons of $>$ 40 MeV, $>$ 80 MeV, $>$ 120 MeV and $>$ 160 MeV. Recoil protons with high energies can pass through the scintillator without stopping and enter the part for measuring energies and directions of recoil protons. This part consists of four layers of the proportional counters and wood. The thickness and density of the wood is 10 cm and $\sim$ 0.8 g/cm^2 respectively. It consists of carbon, hydrogen and oxygen ($C_6H_{10}O_5$). The wood is used as an absorber for low energy particles. The arrival directions are measured by using 4 layers of proportional counters under the scintillation counters, each layer of which is aligned orthogonally. Figure 11 shows the method of measuring the

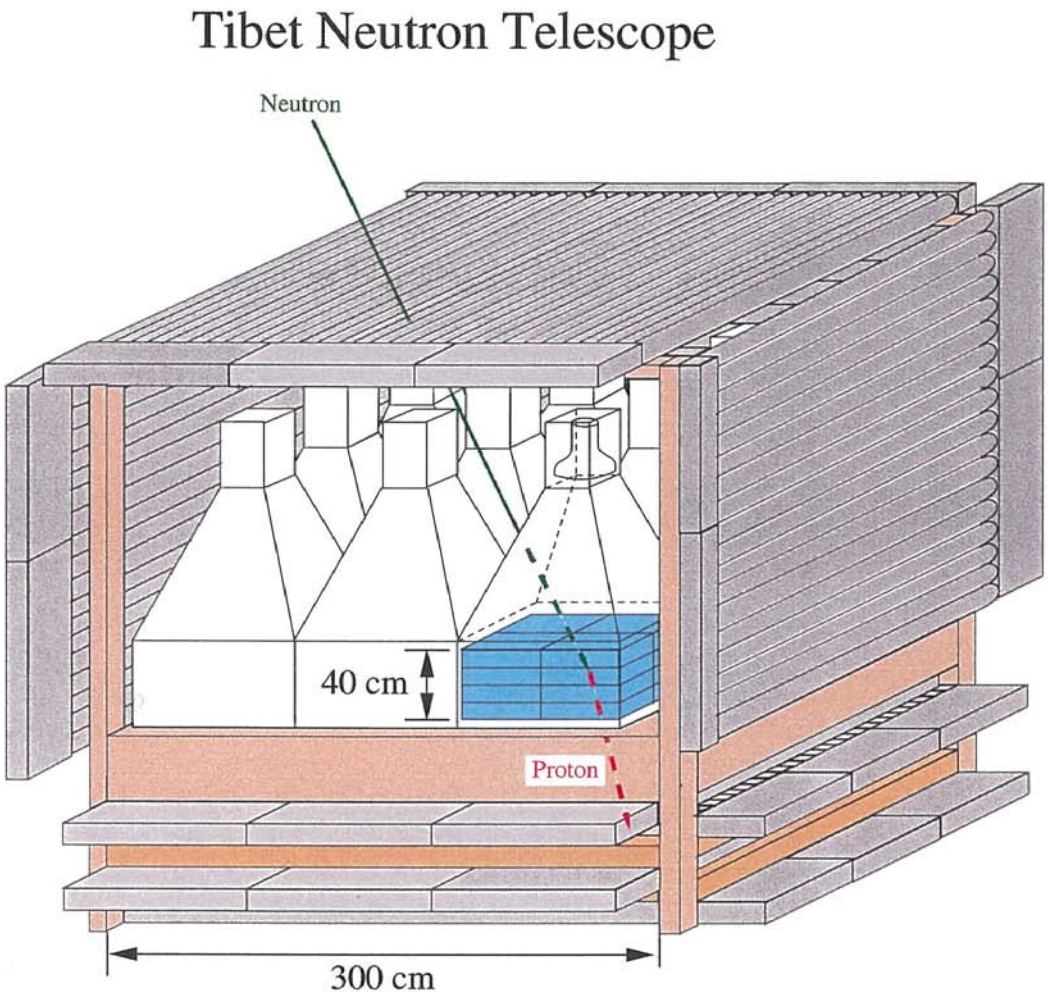

Figure 10: Schematic view of the solar neutron detector located at Yangbajing. Incoming neutrons are converted into protons by nuclear interactions in the scintillator. The directions of the neutrons are measured by using double X and Y layers of proportional counters.

arrival direction. East-West and North-South directions are divided into 9 sections and totally this detector can measure 81 directions. Until Sep.1999, the detector had been operating with 25 angular sections, but after that the detector was improved and can identify 81 directions.

Anti-counters surrounding the scintillation counters are used for rejection of charged particles. When a coincidence is required with the anti-counters, the OR counting rate ($/m^2/min$) of nine scintillation counters is reduced from $\sim 34,000$ to $\sim 8,900$ for the lowest threshold channel (> 40 MeV). Thus, the background level has been reduced to about 1/4 and the signal-to-noise ratio has been improved by about a factor of 2 in comparison to the system without anti counters.

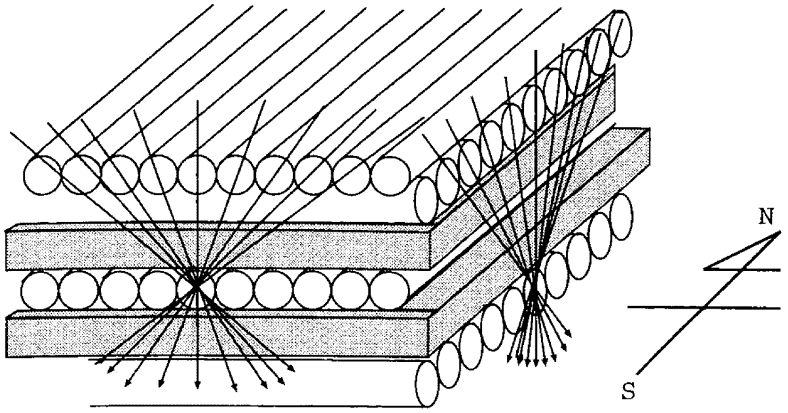

Figure 11: Schematic view of the measurement of the arrival directions for neutrons using the Tibet solar neutron detector. The arrows represent moving directions of recoil protons produced by incident neutrons.

The sensitivity of the detector for neutrons is shown in Figure 12. The sensitivity corresponds to the thinnest air mass at Yangbajing, which is 600 g/cm^2.

3.2 Neutron monitor

A neutron monitor is a traditional device for monitoring the intensity of galactic and solar cosmic rays. Table 5 shows the location of neutron monitors around the world. There are two types of neutron monitors, one being the IGY monitor and the other the NM64 monitor. The IGY neutron monitor was improved by J.A. Simpson between 1948 and 1950. During the International Geophysical Year(1957 – 1958), many IGY neutron monitors were located around the world. After that, H. Carmichael developed the NM64 neutron monitor. The neutron monitor that were developed and improved during 1950's and 1960's are still operating at many cosmic ray stations (Usoskin et al. 1997 [91]).

The schematic views and typical dimensions of two neutron monitors are given in Figure 13 and Table 4. The basic concept for detecting neutrons with a neutron monitor is the same for NM64 and IGY types. The neutron monitor mainly consists of three parts; the reflector, the producer and the counter. The main differences between the two types of neutron monitors are found in the reflector medium and its thickness. The IGY monitor uses paraffin as the reflector, while the NM64 monitor uses polyethylene. Paraffin and the

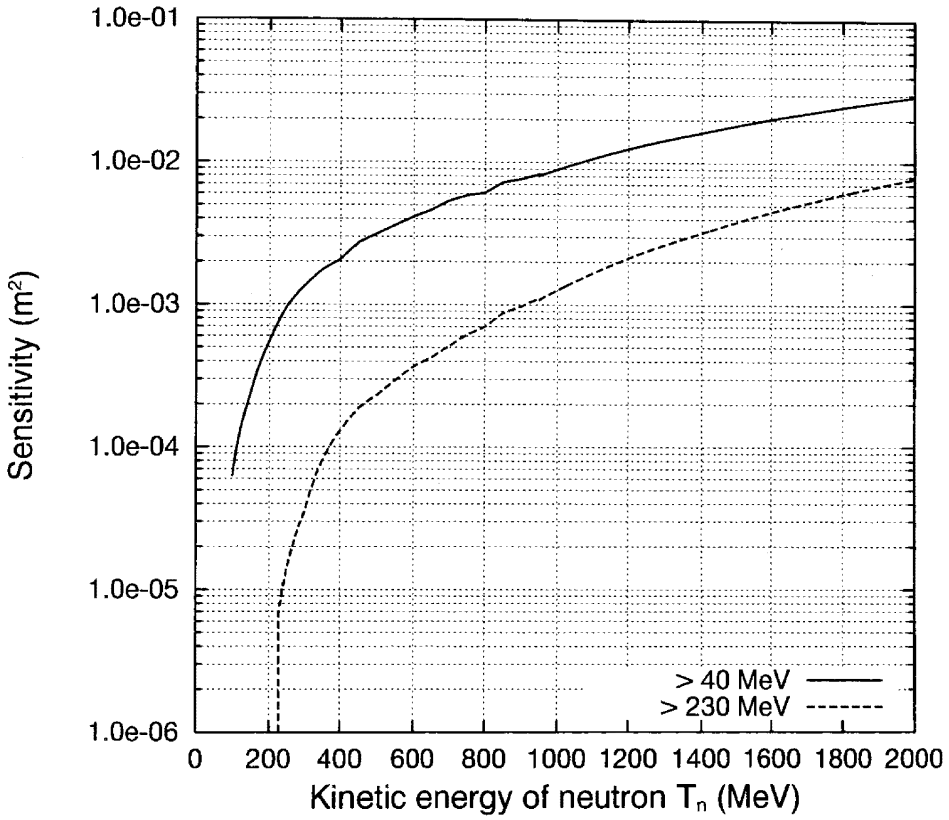

Figure 12: The sensitivity of Tibet solar neutron detector to neutrons. Upper and lower lines correspond to the sensitivity for the lowest (> 40 MeV) channel and the highest (> 230 MeV) energy channel respectively.

polyethylene both consist of carbon and hydrogen atoms and have almost the same mixing ratio between carbon and hydrogen,*i.e.*, $\sim 1/2$. Both reflectors are suitable for moderating neutrons since they have many hydrogen atoms. The role of the reflector is to reject the low energy neutrons produced in the atmosphere and in the substances close to the neutron monitor. The lead which surrounds the reflector is used as a producer. Moderated neutrons in the reflector enter the producer and are multiplied via nuclear interactions. A BF_3 counter is located inside the producer. The inner moderator for slowing down neutrons to thermal energy is prepared between the counter and producer. The thermal neutrons are easily caught using the counter by the reaction

$$^{10}_{5}\mathrm{B} + \mathrm{n} \rightarrow ^{7}_{3}\mathrm{Li} + ^{4}_{2}\mathrm{He}.$$

As a result of this reaction, the energy of a neutron is given to the Li and He. Two major channels exist in the B(n, He)Li reaction, in which the produced Li stays in the ground state (g.s.) or in the excited state (e.s.). The branching ratio of those reactions is 6 % for g.s. and 94 % for e.s. and the Q-value of the reactions is 2.79 MeV for g.s. and 2.31 MeV for e.s..

The detection efficiency of neutron monitor was calculated by Hatton (1971 [92]) and recently by Clem & Dorman (2000 [93]). Our group checked calculated detection efficiency by using an accelerator beam(Shibata et al., 2000 [94]). Figure 14 represents the calculated detection efficiency. The experimental results are also shown in Figure 14. In the energy range of our experiment, which is mainly in between 100 MeV and 400 MeV, the calculated results agreed fairly well with the experimental results. But the outside that energy range, there is rather big difference between the result of the two calculations.

Recently, a ^{3}He counter has been used instead of the BF_3 counter for the neutron monitor. It has the advantage of operating at higher pressure than the BF_3 counter, so that a stable drift velocity and high gas multiplication are achieved by a ^{3}He counter. Because of such characteristics of the ^{3}He counter, the detection efficiency for neutrons is higher than for the BF_3 counter.

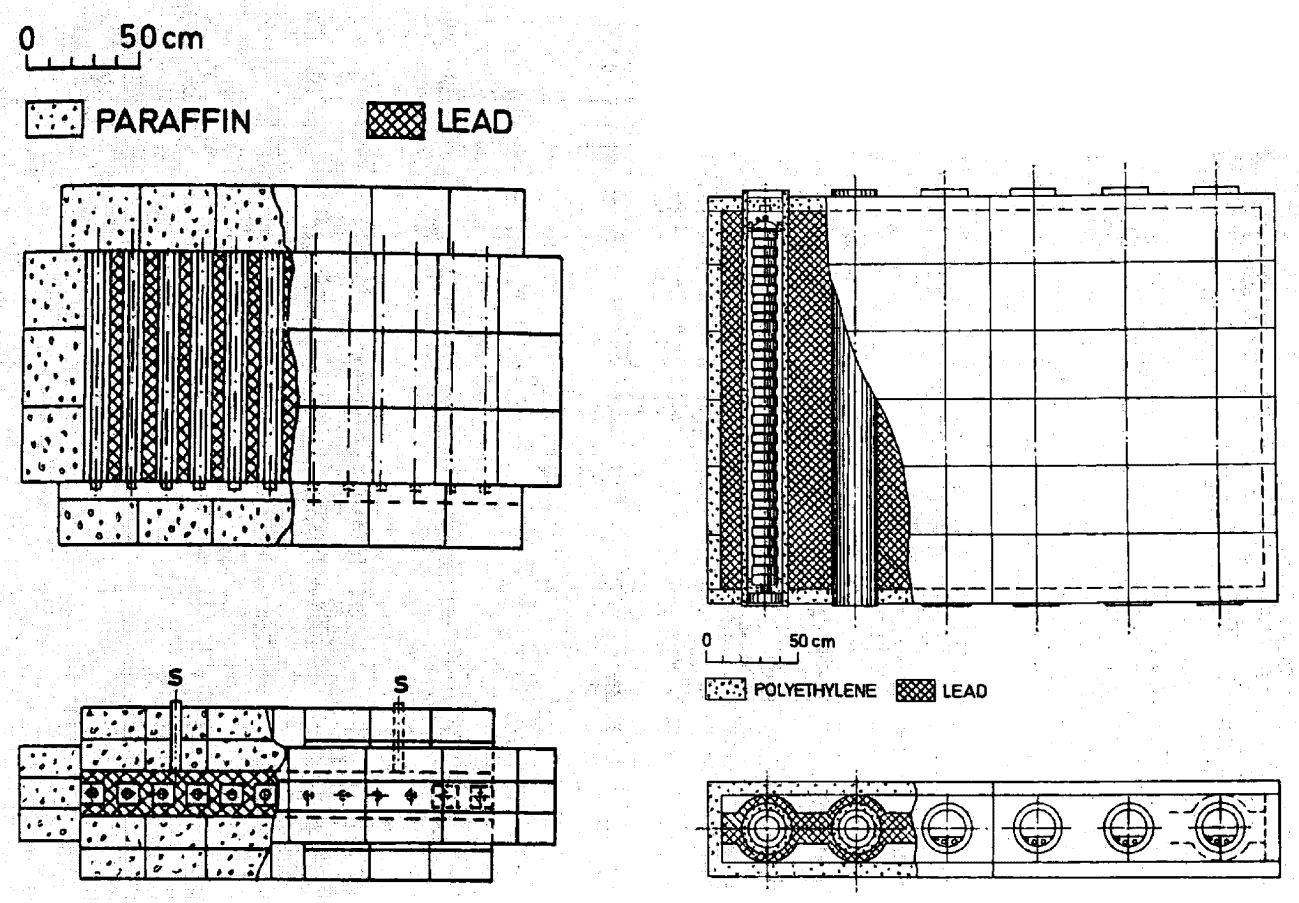

Figure 13: Schematic view of the two types of neutron monitors. Left and right side represent the IGY type and the NM64 type neutron monitor respectively.

Table 4: Typical dimensions and properties of two types of neutron monitors.

	IGY	NM 64
Active length of counter (cm)	86.4	191
Diameter of counter(cm)	3.8	14.8
Pressure (mm Hg)	450	200
Average depth of producer (g/cm^2)	153	156
Average thickness of reflector (cm)	28	7.5

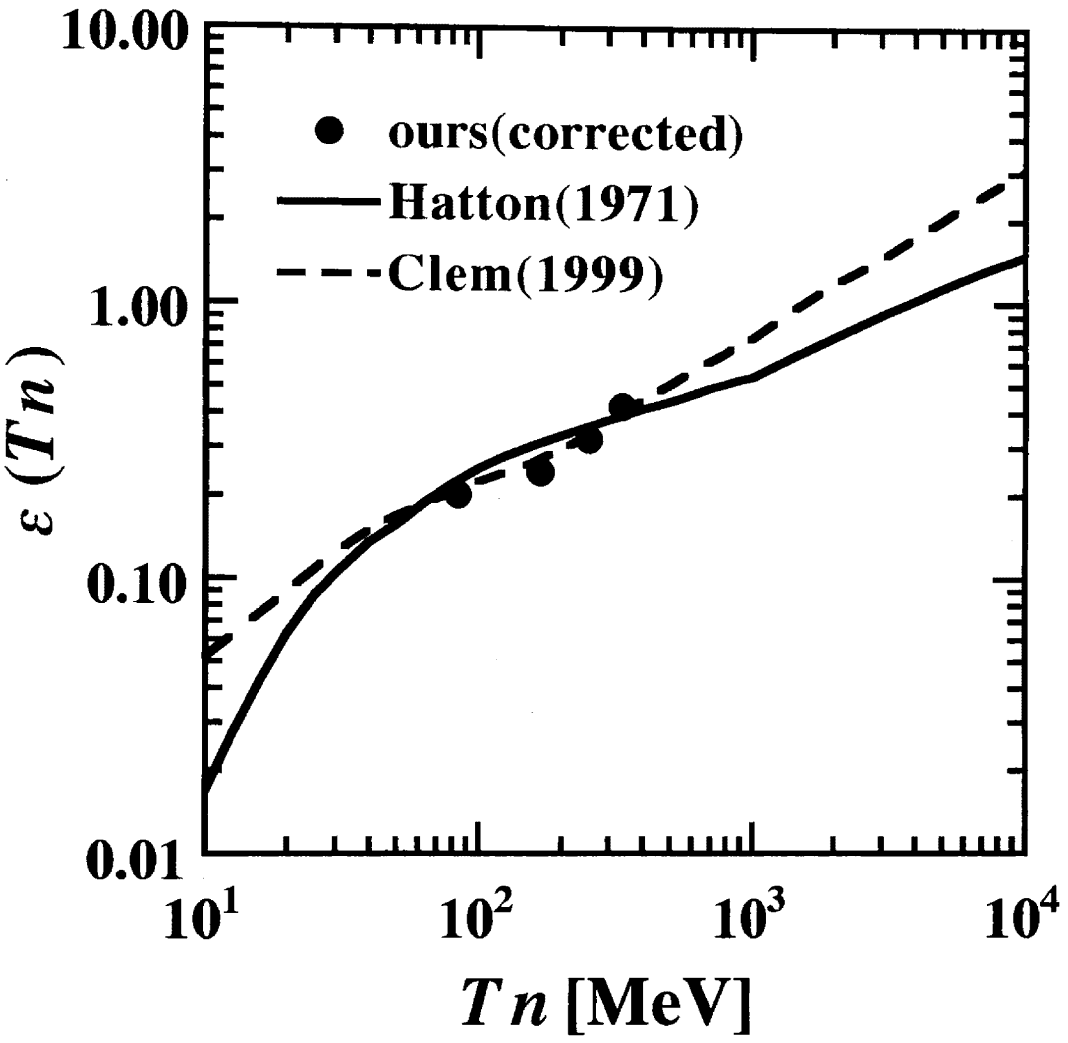

Figure 14: The detection efficiency of the neutron monitor calculated is compared with the experimental results. Solid and dashed lines represent the result of simulation by Hatton [92] and Clem & Dorman [93], respectively. Closed circles represent the experimental result obtained by Shibata et al. [94].

Table 5: Geographical locales of the neutron monitors and cosmic ray rigidities of each station. The contents in the Table are organized by decreasing height. The Longitude and latitude in degrees. R_c means 'cut-off rigidity' at the station. Original data for this table are obtained from `http://ulysses.uchicago.edu/NeutronMonitor/`.

Location	Height(m)	Long.	Lat.	R_c (GV)	Type
Mt. Chacaltaya	5250	291.85	-16.31	12.53	NM64
Yangbajing	4300	90.00	30.00	14.10	NM64
Jungfraujoch	3475	7.98	46.55	4.61	NM64,IGY
Climax	3400	253.82	39.37	2.99	IGY
Alma Ata-B	3340	76.92	43.25	6.61	NM64
Leadville	3094	255.03	39.75	3.03	NM64
Haleakala	3030	203.72	20.72	12.91	NM64,IGY
South Pole	2820	-210.00	-88.00	0.09	NM64
Mt. Norikura	2770	137.55	36.11	11.48	NM64
Gulmarg	2743	74.42	34.07	11.58	IGY
Lomnicky Stit	2634	20.22	49.20	3.98	NM64
Haifa	2300	35.00	32.80	10.75	NM64
Hafelekar	2290	11.38	47.32	4.38	NM64
Mexico City	2274	260.82	19.33	8.61	NM64
Irkutsk-2	2000	100.55	51.37	3.64	NM64
Erevan-B	2000	44.25	40.17	7.58	NM64
Mt. Washington	1909	288.70	44.30	1.46	IGY
Alma Ata-C	1670	76.92	43.25	6.61	NM64
Potchefstroom	1351	27.06	-26.41	7.00	IGY
Tsumeb	1240	17.35	-19.12	9.21	NM64
Calgary	1128	245.86	51.08	1.08	NM64
Erevan-A	999	44.25	40.17	7.58	NM64
Alma Ata-A	775	76.92	43.25	6.61	NM64
Tbilisi	510	44.80	41.72	6.73	NM64
Irkutsk-1	433	104.03	52.47	3.64	NM64
Aligarh	300	78.07	27.91	14.67	IGY

Table 5: (continued)

Location	Height(m)	Long.	Lat.	R_c (GV)	Type
Dourbes	225	4.60	50.10	3.34	NM64
Magadan	220	151.02	60.12	2.09	NM64
Moscow	200	37.32	55.47	2.43	NM64
Apatity	177	33.33	67.55	0.57	NM64
Novosibirsk	163	83.00	54.80	2.87	NM64
Morioka	131	141.13	39.70	10.23	NM64
Kiev	120	30.30	50.72	3.57	NM64
Yakutsk	105	129.43	62.01	1.65	NM64
Fukushima	66	140.48	37.75	10.61	NM64
Rome	60	12.52	41.90	6.32	NM64
Kiel	54	10.13	54.33	2.36	NM64
Sanae	52	357.59	-70.31	0.86	NM64
Newark	50	284.25	39.68	2.09	NM64
Mcmurdo	48	166.72	-77.85	0.00	NM64
Beijing	48	116.26	40.08	10.06	NM64
Goose Bay	46	299.60	53.27	0.64	NM64
Thule	44	291.30	76.50	0.00	NM64
Gif sur yvette	40	2.13	48.68	-1.00	NM64
Terre adelie	35	140.02	-66.67	0.02	NM64
Kerguelen is	33	70.27	-49.35	1.14	NM64
Turku	32	22.60	60.40	1.36	NM64
Mawson	30	62.88	-67.60	0.20	NM64
Hermanus	26	19.23	-34.42	4.58	NM64
Inuvik	21	226.28	68.35	0.17	NM64
Hobart	18	147.33	-42.90	1.84	NM64
Oulu	15	25.47	65.05	0.78	NM64
Durham	0	289.17	43.10	1.58	NM64
Cape Schmidt	0	180.53	68.92	0.00	NM64
Brisbane	0	153.08	-27.42	6.99	NM64

4 Observations using the international network of solar neutron detectors

As mentioned in previous section, we started the construction of solar neutron detectors and have installed them on several high mountains since 1990. The installation of detectors finished in 1998 when solar activity was increasing. From the time of completion of the installation of the detectors to date, 33 X class solar flares have occurred (to September 30, 2000). Tabel 6 shows a brief summary of X class solar flares in solar cycle 23. Until now, many X $\sim$ 1-2 class solar flares have occurred in solar cycle 23, which we consider to be moderate level solar flares except for a few gigantic solar flares. It is uncertain whether neutrons from these moderate solar flares could be detected. However, for a solar flare that occurred on 1998 November 28th, a possible observation of solar neutrons was made by the detector installed in Yangbajing, Tibet. As will be mentioned later, due to the ability to measure arrival directions of incoming neutrons, we believe that this observation is real.

We found one more interesting event on 1997 November 6th, which occurred at the time of the largest solar flare observed in solar cycle 23. In this flare, the detector installed at Mt.Chacaltaya in Bolivia detected a signal of neutrons before the major X9.4 solar flare. This could be very interesting from the point of view that particle acceleration really did occur deep in the solar atmosphere leading to the production of solar neutrons.

In this section, the results of observations by our international solar neutron network are described together with the observations of Yohkoh, BATSE and GOES satellites during these two flares. Before presenting the detailed descriptions of the two events, the general conditions of both observations at the time of the observations around each flare time are given briefly. Figures 15a and b show contour maps of the solar zenith angle for each event. In the color scheme, the color becomes more red as the solar zenith angle becomes smaller. The best observation conditions are for the smallest solar zenith angle. Figure 15a shows the 1998 November 28 event, while Figure 15b shows the 1997 November 6 event. The abscissa and ordinate represent the longitude and the latitude in degrees respectively. In the case of the 1998 November 28 flare, Yangbajing was the most suitable place for detecting so-

Table 6: List of X class solar flares in solar cycle 23.

Date	Start(UT)	Imp.	Opt.	Location at the solar surface
1996 07/09	09:01	X2.6	1B	S10W30
1997 11/04	05:52	X2.1	2B	S14W33
1997 11/06	11:49	X9.4	2B	S18W63
1997 11/27	12:59	X2.6	2B	N17E63
1998 04/23	05:35	X1.2	–	——
1998 04/27	08:55	X1.0	–	S16E50
1998 05/02	13:31	X1.1	3B	S15W15
1998 05/06	07:58	X2.7	1N	S11W65
1998 08/17	21:10	X1.2	–	——
1998 08/18	08:14	X2.8	SN	N33E68
1998 08/18	22:10	X4.9	1B	N33E87
1998 08/19	21:35	X3.9	1F	N32E75
1998 08/24	21:50	X1.0	3B	N35E09
1998 11/22	06:30	X3.7	1N	S27W82
1998 11/22	16:10	X2.5	2N	S30W89
1998 11/23	06:28	X2.2	SF	S28W89
1998 11/24	02:07	X1.0	–	——
1998 11/28	04:54	X3.3	3N	N17E32
1999 08/02	21:18	X1.4	1B	S18W46
1999 08/28	17:52	X1.1	2N	S26W14
1999 10/14	08:54	X1.8	1N	N11E32
1999 11/27	12:05	X1.4	2B	S15W68
2000 02/05	19:17	X1.2	3B	N26E52
2000 03/02	08:20	X1.1	–	——
2000 03/22	18:34	X1.1	2N	N14W57
2000 03/24	07:41	X1.8	2B	N16W82
2000 06/06	13:30	X1.1	–	——
2000 06/06	14:58	X2.3	–	——
2000 06/07	15:34	X1.2	3B	N23E03
2000 06/18	01:52	X1.0	SF	N23W85
2000 07/11	12:12	X1.0	–	——
2000 07/12	10:18	X1.9	2B	N17E27
2000 07/14	10:03	X5.7	3B	N22W07
2000 09/30	23:13	X1.2	SF	N07W91

(a) 1998 November 28th

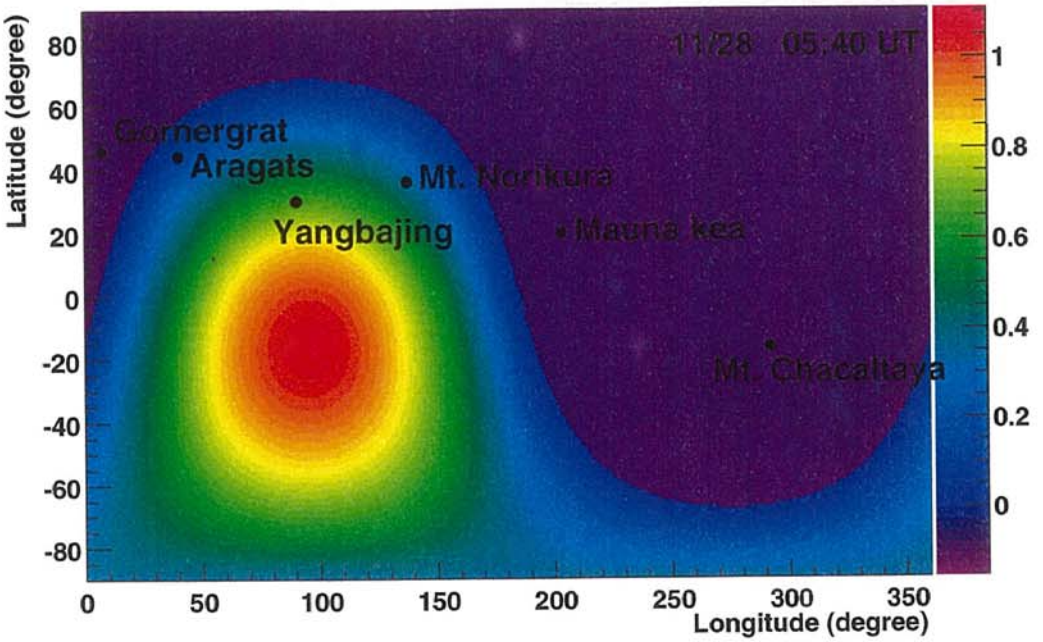

(b) 1997 November 6th

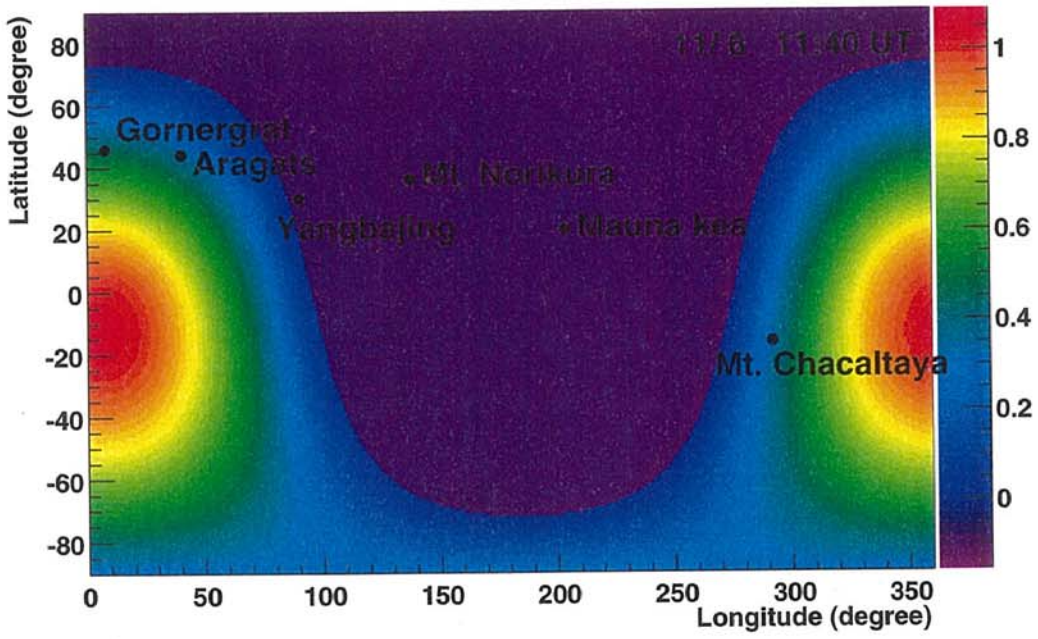

Figure 15: The zenith angle of the sun at each observation time is presented for 1998 November 28th solar flare (a) and for 1997 November 6th solar flare (b). The Figures correspond to the geometrical acceptance conditions for each event. Figures such as these can be freely obtained from following URL on the Internet; `http://binary.stelab.nagoya-u.ac.jp/Neutron/General/`.

lar neutrons although the solar zenith angle was 53°. On the other hand, in the case of 1997 November 6 solar flare, Gornergrat and Mt.Chacaltaya were suitable places. The solar zenith angle for each location at the solar flare times were 63° and 69° respectively. However, a solar neutron detector was not yet installed at Gornergrat for the November's event. Therefore, we could only check the data of the solar neutron detector at Mt. Chacaltaya. At that time, the weather in Switzerland was stormy, so the Jungfraujoch neutron monitor could not identify the neutrons (Flückiger private communication).

4.1 Observations using the Tibet solar neutron detector on November 28, 1998

Active Region 8395 produced a "moderate" solar flare on November 28, 1998. The GOES X ray intensity class and H_α importance were X3.3 and 3N, respectively. As can be seen from Figure 16, the GOES X ray data showed the maximum intensity to be around 5:52 UT. The solar flare continued for more than 1 hour. The location of the solar flare at the solar surface was N17E32. No solar proton event was observed, because of poor connection of the interplanetary magnetic field to the earth. A type II/IV radio burst and a CME were also associated with the solar flare. The X ray and gamma ray data were obtained by the instruments on board Yohkoh and CGRO/BATSE. According to the observation by Yohkoh, there were no strong gamma ray emissions > 1 MeV during the solar flare. Only the hard X ray detector in the energy band 93 - 225 keV detected an increase between 5:39 UT and 5:43:UT with a peak time around 5:41 UT (Yoshimori, 1999 [95]). Furthermore, time profiles of X rays in the energy ranges of 33 - 53 keV and 53 - 93 keV detected by BATSE showed a similar behavior to that detected by Yohkoh. The image of a flare loop in soft X rays observed by Yohkoh indicated a complex loop structure at the time of the solar flare(Masuda, 1999 [96]). The BATSE X ray data in the energy range 30 keV - 58 keV is shown in Figure 17. According to BATSE flare list, the start time, the peak time and the duration of the solar flare recorded by BATSE were 5:31:36 UT, 5:40:46 UT and 2834 seconds, respectively. At the Nobeyama radio heliograph, radio emissions were detected at the 17 and 34 GHz bands with the maximum emission occurring at 5:39:51 UT. The time profile of 17/34 GHz emissions was consistent with the Yohkoh hard X ray data at the peak time. These observations indicate that

electrons were accelerated up to a few MeV. However, no strong evidence was obtained for ion acceleration or neutron production. The 2.223 MeV neutron capture line and π^0 decay gamma ray were not observed. In spite of such a negative suggestions regarding neutron production from satellite observations, the ground level solar neutron detector at Yangbajing in Tibet showed a significant increase in association with this solar flare.

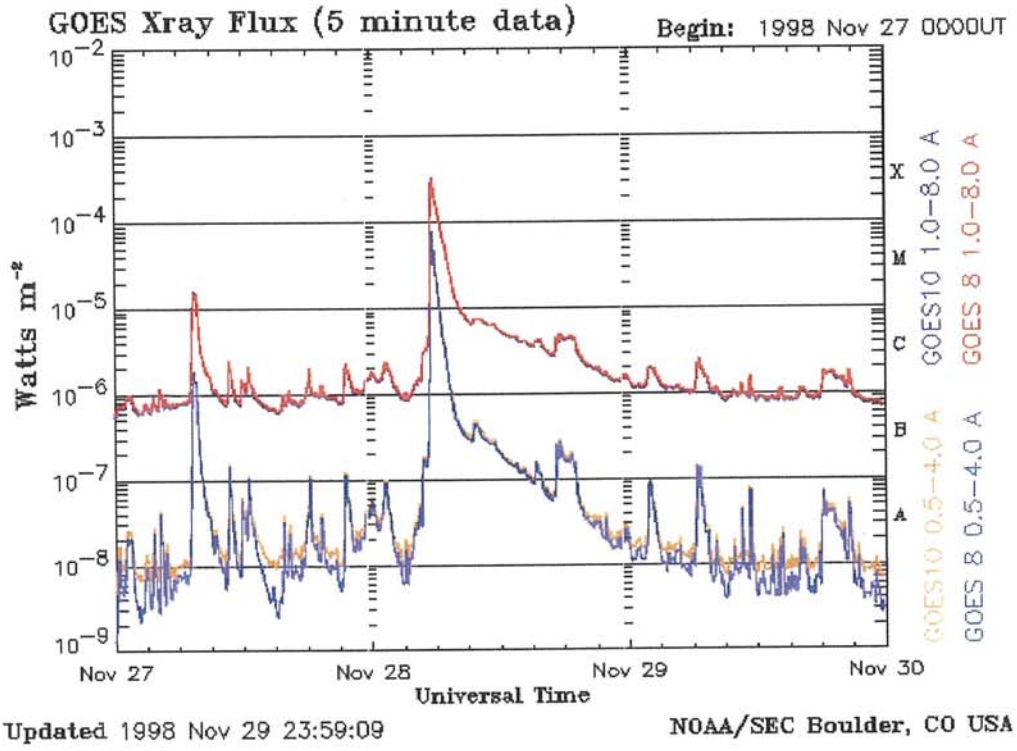

Figure 16: GOES X ray data between November 27 and November 30, 1998.

Figure 18 shows the counting rate of the solar neutron detector at Yangbajing. These data correspond to the channels for neutral particles by monitoring the anti-coincidence of the scintillation counter signals and surrounded proportional counter signals, The energy threshold of each channel shown in Figure 18 corresponds to $>$ 40 MeV, $>$ 80MeV, $>$ 120 MeV and $>$160 MeV. No statistically significant excess was found in association with the solar flare by the upper scintillator data. The BATSE flare onset time is indicated in the graph by a vertical line (see Figure 18). The statistical significance for each channel was 0.081σ, 1.1σ, 1.8σ, 0.79σ respectively. The statistical significance was calculated using the expression $(N_{obs} - N_b)/\sqrt{N_b}$, where N_{obs} and N_b represent raw data and background, respectively.

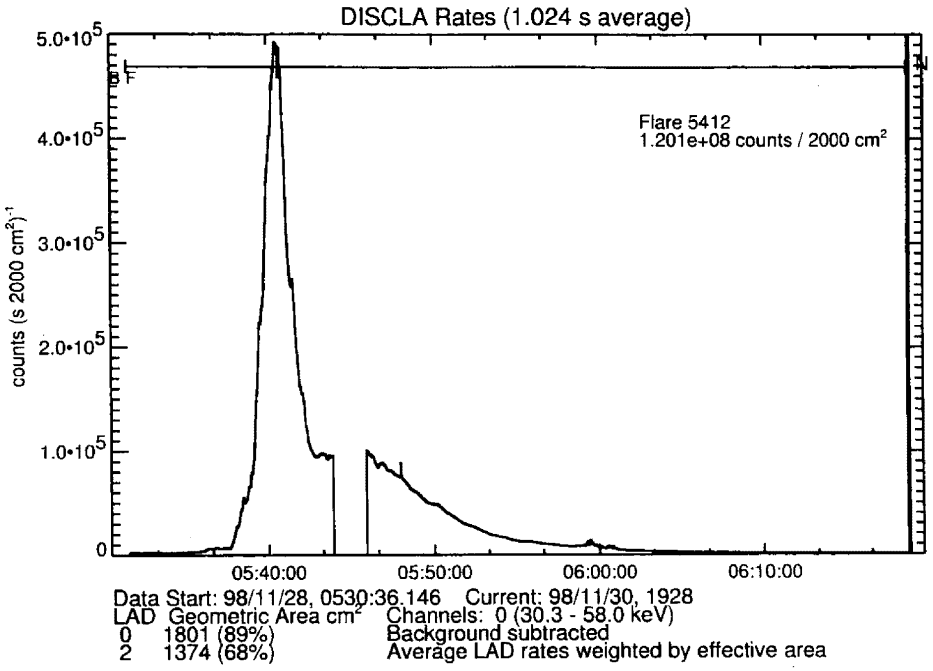

Figure 17: BATSE X ray(30 keV - 50 keV) data around the time of the solar flare. The horizontal axis represents Universal Time.

4.1.1 Analysis taking account of directional information

As mentioned in Section 3, the Tibet solar neutron detector is able to measure the direction of arrival of incoming neutrons. Therefore, we can compare the count for the solar direction(South) with that of the anti-solar direction(North), which allows us to reduce the background. As indicated in Figure 19, the arrival directions can be divided into 25 sectors using the detector. After the summation of the counts of each shadow area in the solar and anti-solar directions, they were compared with one another. This process allows us to reduce the background noise level by a factor of ~ 8.

Figure 20 shows the statistical significance obtained by the telescope for the south direction and the north direction. After the flare onset, a clear peak could be seen in the south direction (solar direction) between 5:38 UT - 5:41 UT, but no clear excess could be seen in the north direction (the anti-solar direction). The statistical significance was positive 4.2σ for the solar direction, and negative -0.4σ for the anti-solar direction over that time interval. The significance maps also are shown in Figure 21 for the interval between 5:25 UT and 5:51 UT. Between 5:38 UT - 5:41 UT, the three components of the south direction showed an enhancement more significant than those of the north direction.

Figure 22 shows the 1 minute counting rate for the south and north directions. A continuous increase between 5:38 UT and 5:43 UT was found for the south direction. The maximum significance at the peak time interval 5:40 UT - 5:41 UT was 4.0σ. Figure 23 shows the 10 second counting rate. The shape of the 10 second counting rate was the characteristic features of a power law energy spectrum and a δ function type production time profile. The dashed line in the top panel of Figure 23 represents the case in which the power index was 3.0.

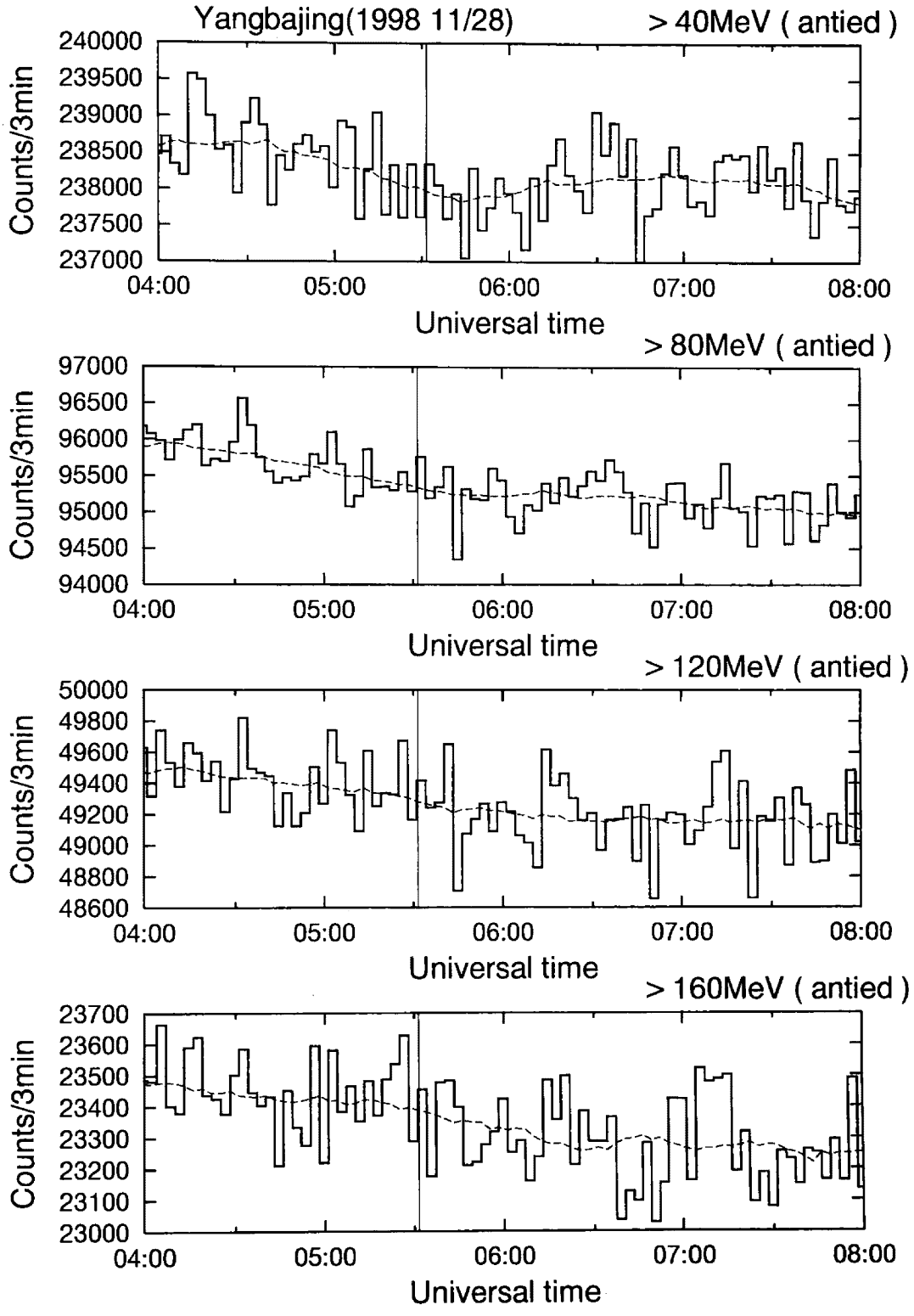

Figure 18: 3 minute counting rate recorded by scintillation counters for neutral particles between 4:00 UT and 8:00 UT. Vertical thin line represents the BATSE flare onset time, which was 5:31:36 UT. The solid and dashed lines indicate the raw counting rate and background level, respectively.

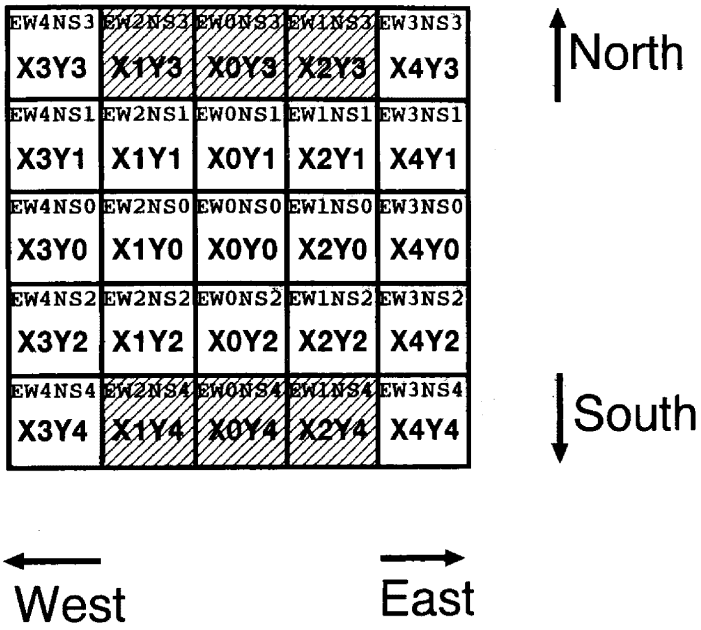

Figure 19: Arrival directions of neutrons at the Tibet solar neutron detector were broken down into 25 directions. Each direction was separated into 25 sectors by combining 5 sets of directional information in the east-west direction and 5 sets of directional information for north and south directions. Shadow sections were used for the analysis and the intensities are compared with one another.

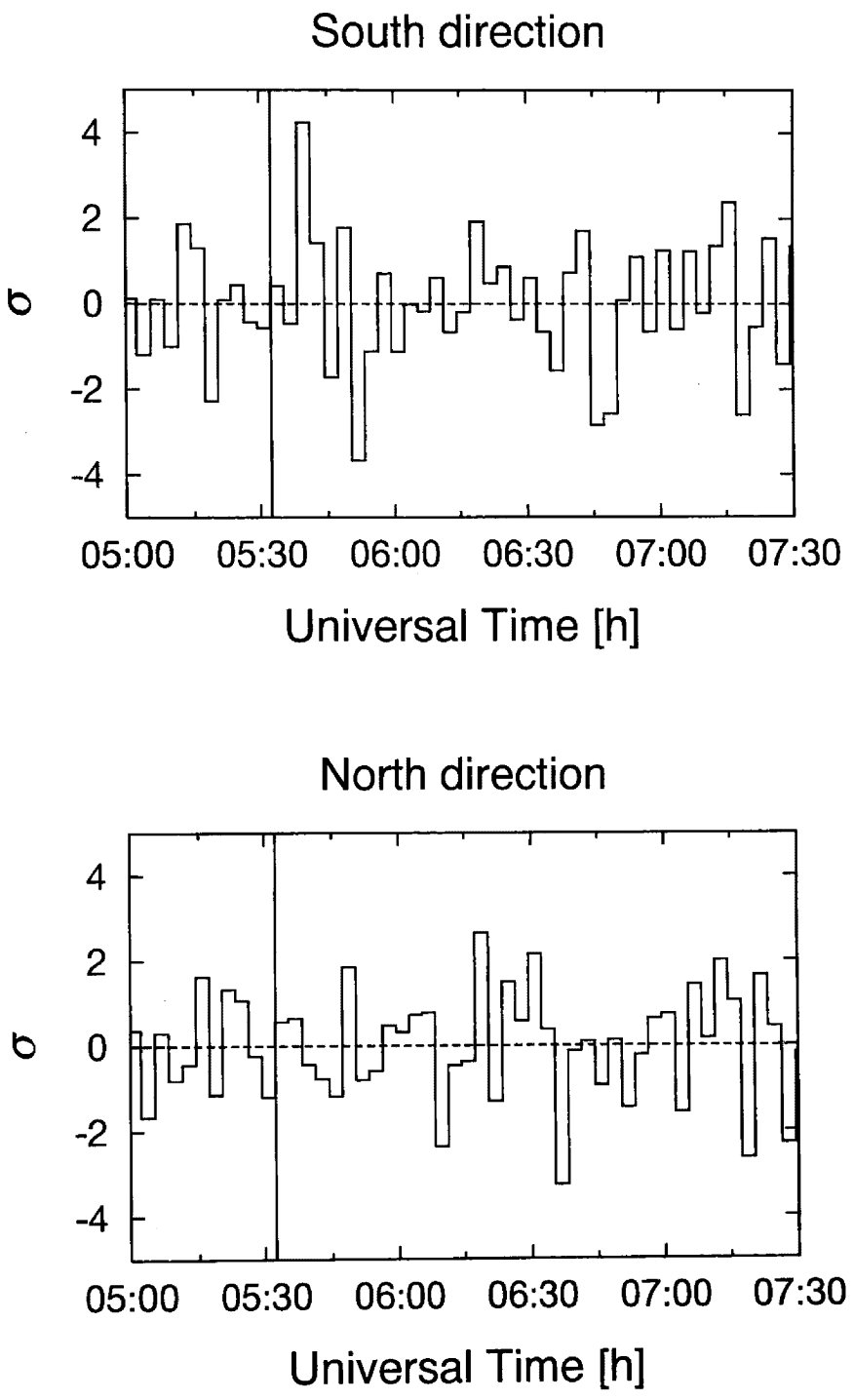

Figure 20: The statistical significances of 3 minutes counting rate are given for the south direction and the north direction. Top panel shows the south direction and the bottom represents for the north side. The horizontal axis represents Universal Time and the vertical axis indicates the statistical significance. The solid vertical line represents the BATSE flare onset time, which was 5:31:36 UT.

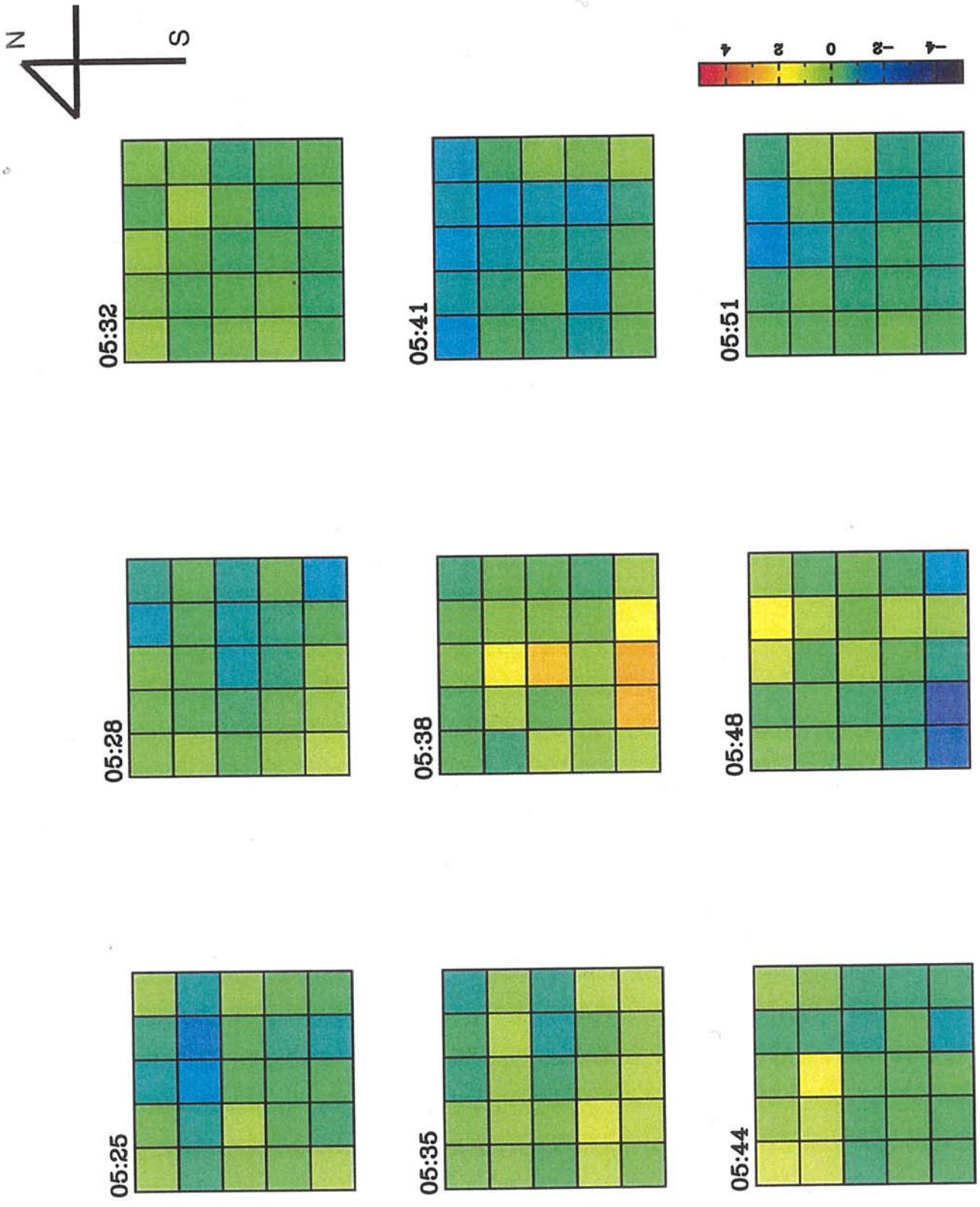

Figure 21: The statistical significance of 25 directions monitored by using the ability of measuring the arrival directions of the solar neutron detector at the time of the solar flare. The color for each section becomes redder as the statistical significance becomes higher.

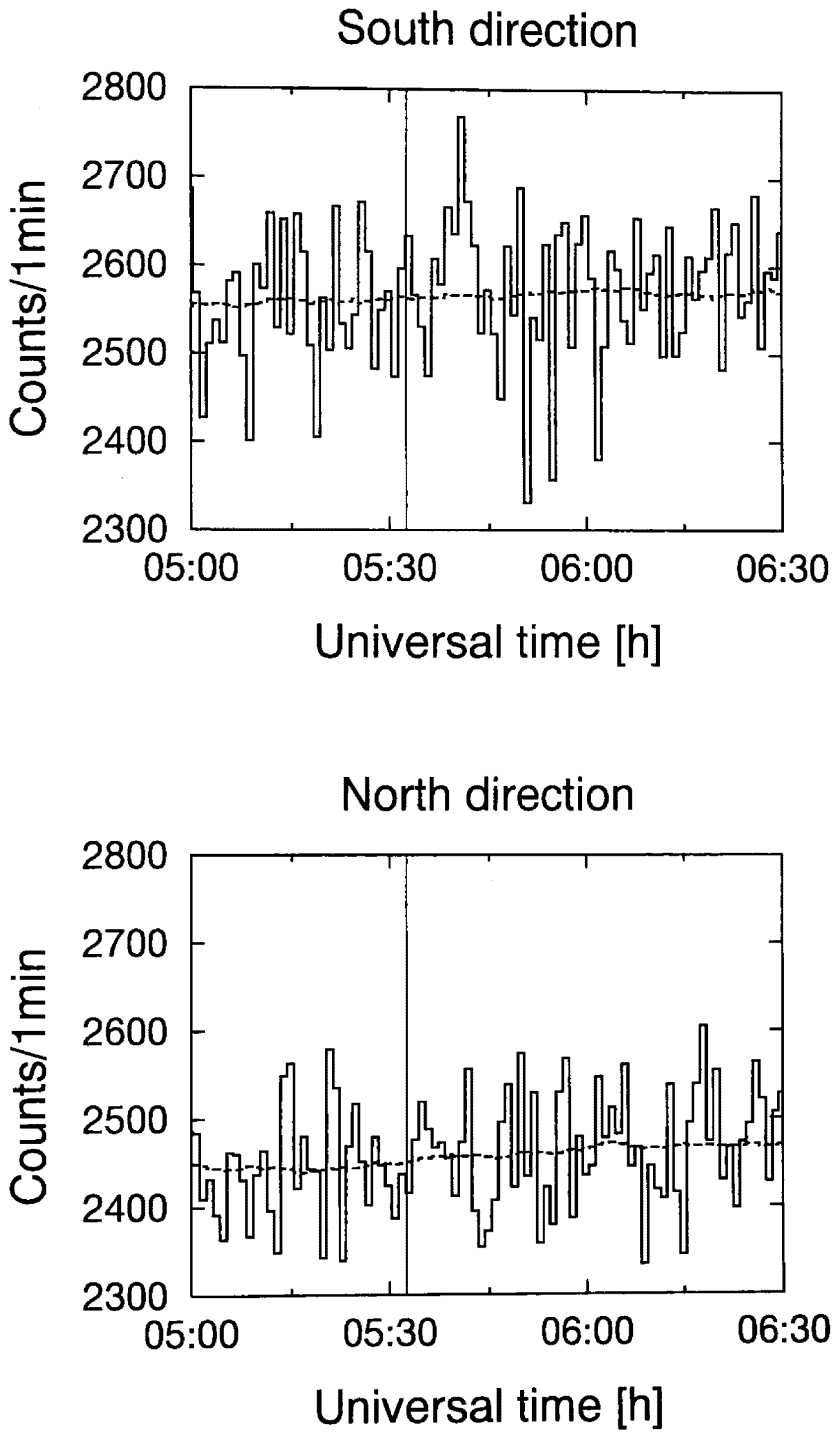

Figure 22: 1 minute counting rate of neutrons for the south and the north directions. The dashed line in the graph represents the average counting rate and the vertical thin line shows the BATSE flare onset time.

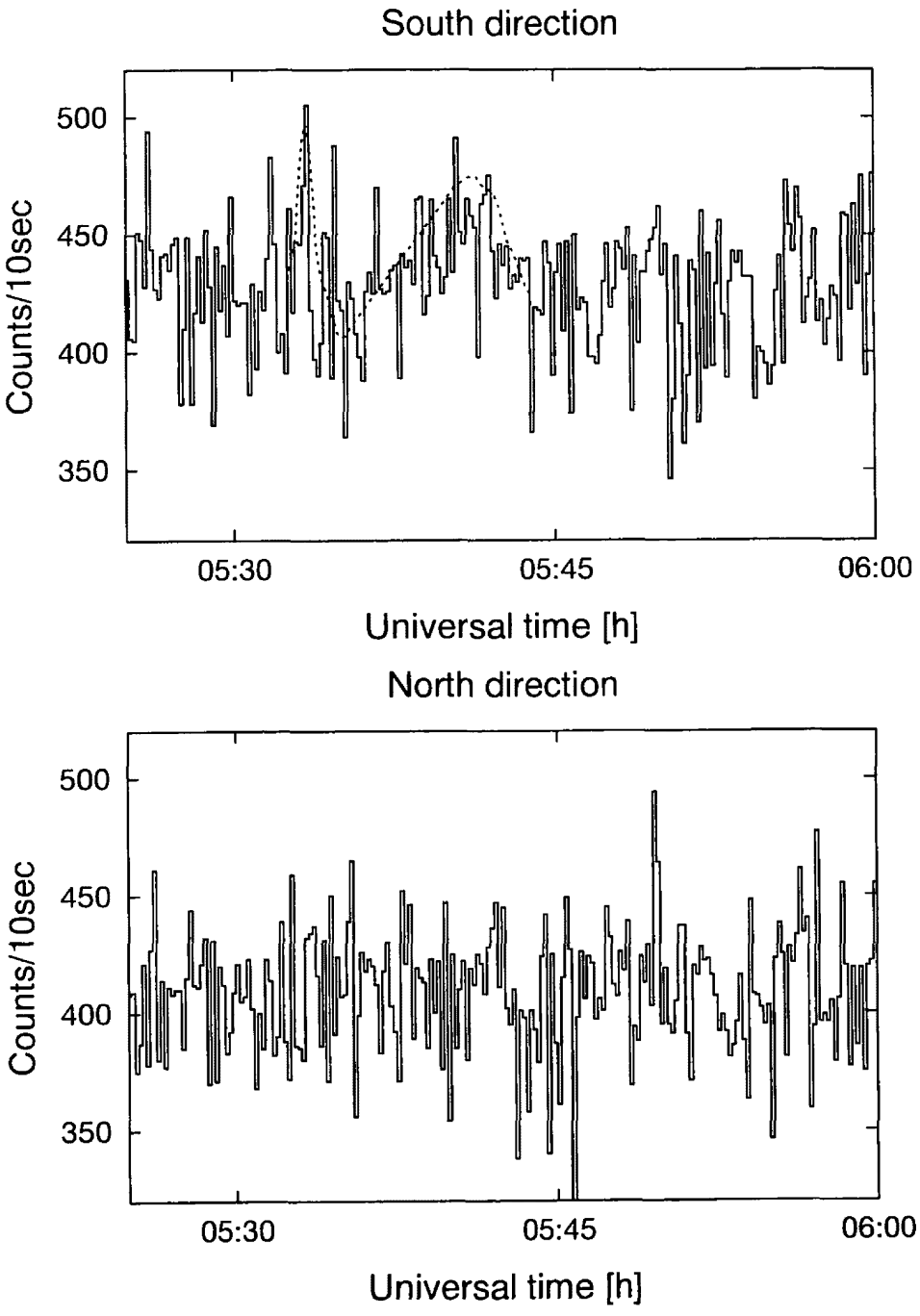

Figure 23: 10 second counting rate of neutrons in the south direction and the north direction between 5:25 UT and 5:45 UT. The dashed line indicates the predicted time profile in the case that neutron production was followed a δ function-like time profile with a power index of 3.0.

4.2 Event detected by the Bolivian solar neutron detector on November 6th, 1997

On 1997 November 6th at 11:49 UT, a huge solar flare with X9.4/2B was observed. Up till now, this is the largest solar flare in solar cycle 23. Soft X ray data obtained by GOES satellite showed that the solar flare continued for about 12 minutes. The GOES soft X ray data and proton data are shown in Figure 24. As can be seen in the bottom panel of Figure 24, since the solar flare occurred at the west limb(S18W63), solar protons and solar energetic particles were also detected by several satellites. They were detected by SOHO, ACE, Ulysses and WIND (Larioo et al., 1998 [97]; Mason et al., 1999 [98]) and also by ground level detectors (Bütikofer & Flückiger, 1999 [99]; Duldig & Humble 1999 [100]; Massetti et al., 1999 [101]). Yohkoh detected a strong impulsive gamma ray emission (up to $\sim$ 20 MeV) from the solar flare between 11:52 UT and 11:56 UT (peak phase) and the derived spectrum indicated gamma ray lines superposed on the bremsstrahlung continuum (Yoshimori et al. 1998 [102];Yoshimori et al., 2000 [103];Yoshimori et al., 2000 [104]). A neutron capture line (2.223 MeV) was also observed (Yoshimori et al., 1999 [105]) and this line shows the neutron production took place during the solar flare. Some of neutrons produced by accelerated ions move into a dense region and slow down to thermal energies via nuclear interactions with ambient hydrogen. As a result, the decelerating neutrons interact with the hydrogen and emit the gamma rays via $n+p \rightarrow d+\gamma(2.223MeV)$. Line gamma rays were also detected by Yohkoh, which were due to the de-excitation processes of C(4.443 MeV) and O(6.129 MeV). These line gamma rays indicate that ions were certainly accelerated in this solar flare. Yoshimori et al. [102] derived the accelerated proton spectrum from the line gamma ray flux. According to their results, the accelerated protons should have a power index of 3.8 - 4.4 and they estimated the number of accelerated protons with the energy greater than 30 MeV as 2.5×10^{32}.

Some detectors on board CGRO also detected this phenomenon. Unfortunately, CGRO was in the high radiation zone of the South Atlantic Anomaly (SAA) at the peak time of the solar flare. For this reason, the 4 detectors on board CGRO missed the observation of the strongest emission of the solar flare. However, the CGRO/OSSE detected a continuous neutron emission in the late phase over the solar flare in the time interval between $\sim$ 12:06 UT

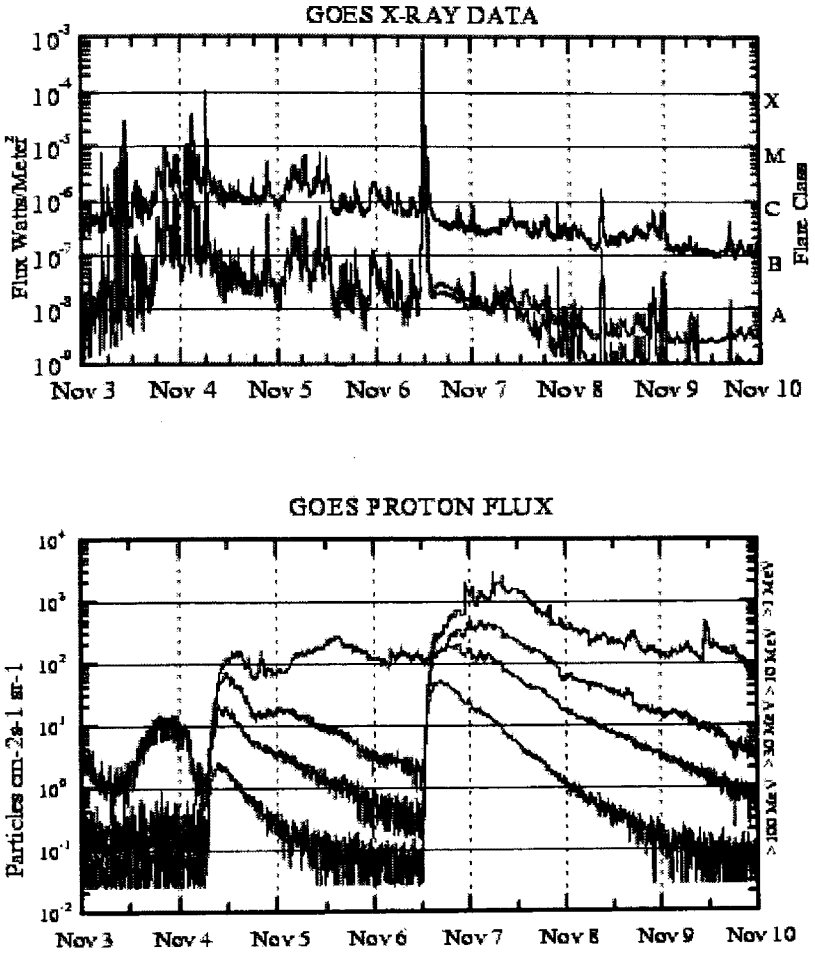

Figure 24: GOES soft X ray and proton time profiles for the period between November 3rd and 10th, 1997. Top panel shows the X ray data and the bottom one shows the proton data. The X9.4 solar flare commenced at 11:49 UT November 6th, 1997.

and 12:28 UT(satellite night) [103]. According to Yoshimori et al. [103], the observed neutrons were produced in both the peak and the extended phases of the solar flare.

At the time of the solar flare, Mt. Chacaltaya was situated in the early morning(7:50 local time in Bolivia). The solar zenith angle was the 69° and the air mass along the line of sight from the sun to the detector was $\sim$ 1500g/cm^2 (540/ cos 69°). In spite of such unsuitable conditions for observing solar neutrons, two significant increases of neutrons were detected by our detector. As shown in Figure 25, the peak was seen 6 minutes after the BATSE flare start time. An increase for the 3 minute counting rate took place between 11:40 and 11:43 UT. The statistical significances for each neutral channel were $3.3\sigma(>$ 40MeV), $3.9\sigma(>$ 80MeV), $2.9\sigma(>$ 120MeV) and $1.7\sigma(>$ 160MeV). The data for the no-anti coincidence mode (no rejection of charged particles) showed no significant enhancement (see in Figure 26). The statistical significance for no-anti channels was $0.5\sigma(>$ 40MeV), $1.2\sigma(>$ 80MeV), $0.4\sigma(>$ 120MeV) and $0.1\sigma(>$ 160MeV). Since the cut-off rigidity of charged particles is high at Mt.Chacaltaya, no ground level enhancement(GLE) due to solar protons was observed in association with this event. The largest enhancement due to neurons was obtained in 2 minute counting rate. The statistical significances for each channel were 5.7σ, 6.8σ, 5.0σ, 3.2σ respectively as presented in Figure 27. In Figure 28, distribution of the statistical significance is given, which corresponds to the the distribution of Figure 27. The four distributions were well fitted with a Gaussian function.

There still remains a question regarding the enhancement in this event. In the main phase of the solar flare, the Bolivia solar neutron detector observed only a 3 σ level excess (as can be seen in Figure 25). The statistical significance for the $>$ 80 MeV channel was 2.6σ. However, there was a clear enhancement detected in the time interval between 11:41 UT and 11:43 UT. It was detected 10 minutes before the major X9.4 solar flare. Figure 29 shows the GOES time profile between 10:00 UT and 12:30 UT on November 6th, 1997. As can be seen in Figure 29, a C4.7 solar flare occurred in advance of the X9.4 solar flare. This C4.7 solar flare started at 11:31 UT and continued until 11:44 UT. The Yohkoh soft X ray images are shown in Figure 30. In the prephase period, complicated loop structures can be seen. Until now, there

has been no report that solar neutrons were produced by a C class solar flare and detected by any detector in space or at the ground level. With regard to the gamma ray observations, one similar event has been reported by Ryan et al.(2000 [106]). The gamma ray emission was detected by COMPTEL on board CGRO in association with a C4 solar flare at 2:21 UT on 20 January, 2000. Did these C class solar flare really cause ion acceleration? If so, the present observations poses a question about the minimum size of a solar flare required for ion acceleration to take place.

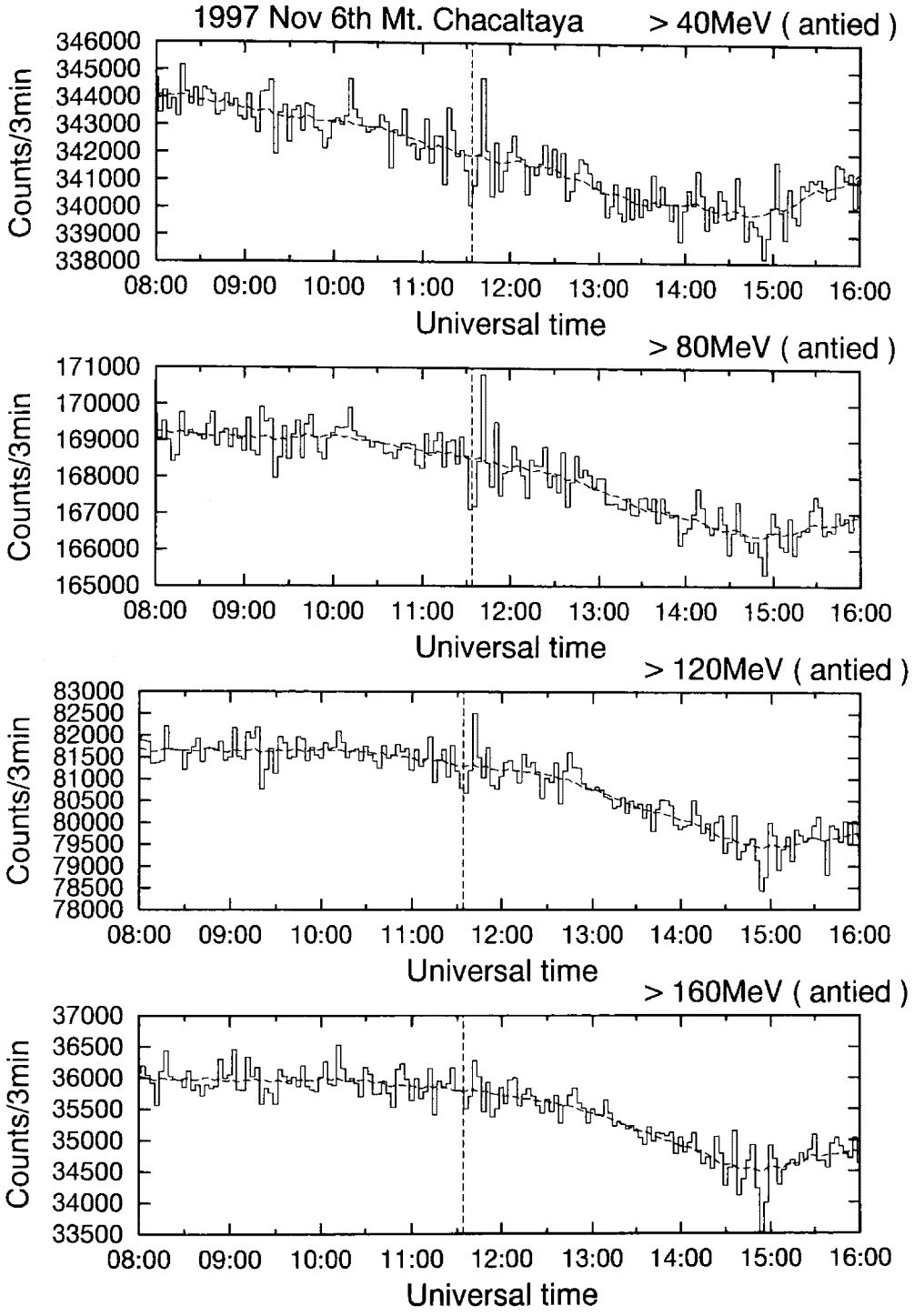

Figure 25: The time profile of the Bolivia solar neutron detector between 8:00 UT and 16:00 UT on November 6th, 1997. The data represent the number of primary neutral particles. The solid and dashed lines represent raw counting rate and average counting rate calculated using moving average method. The vertical dashed line indicates the BATSE flare start time (11:34:02 UT). A clear enhancement was seen between 11:40 UT and 11:43 UT and a weak enhancement was also seen between 11:49 UT and 11:52 UT.

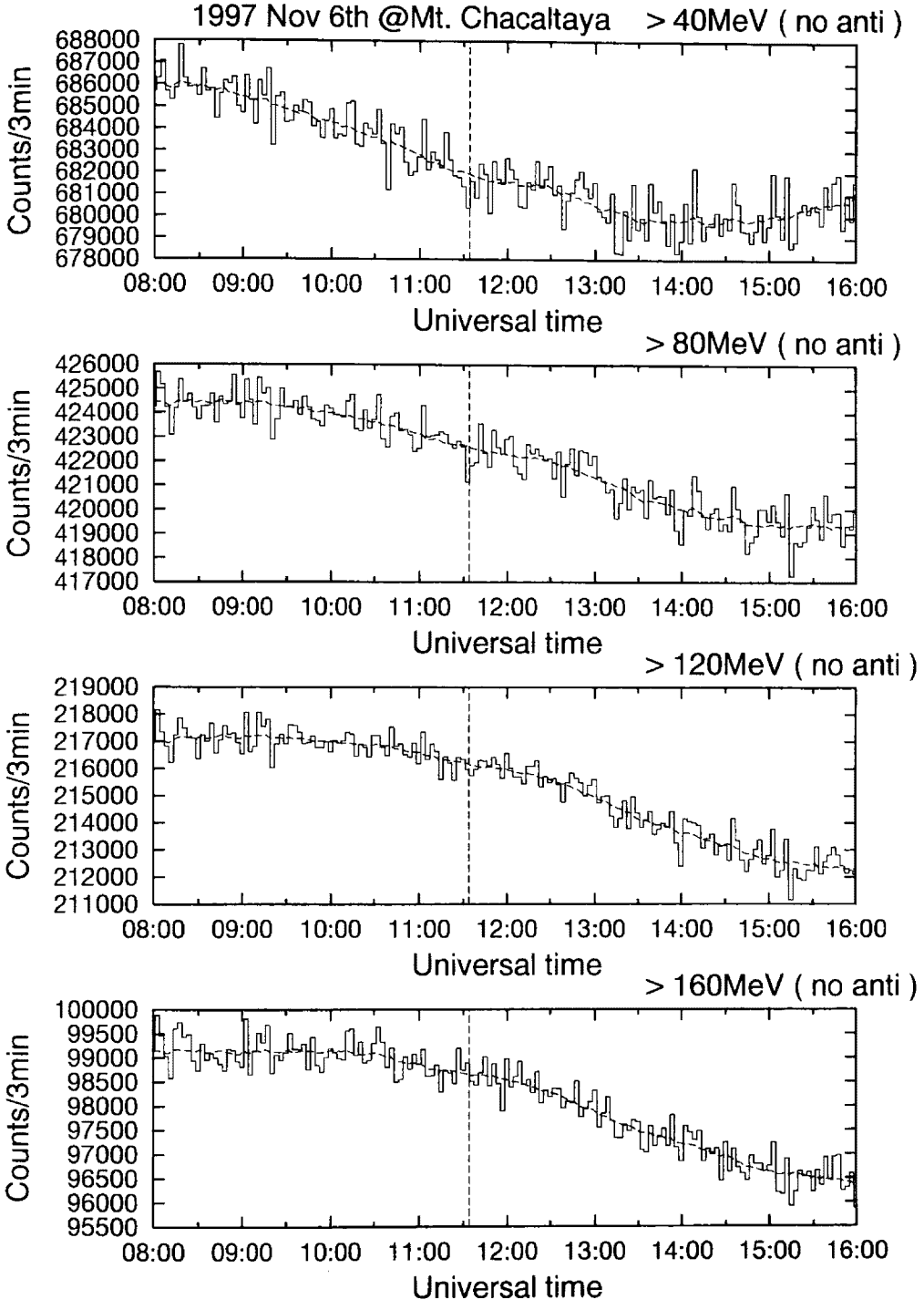

Figure 26: The 3 minute counting rate of total particles recorded by the Bolivia solar neutron detector for the time interval between 8:00 UT and 16:00 UT on November 6th, 1997. The data show the counting rate of the channel including both neutrons and charged particles. The solid and dashed lines represent the raw counting rate and the moving average. There is no peak at 11:43 UT such as that seen in the neutral channel in Figure 25.

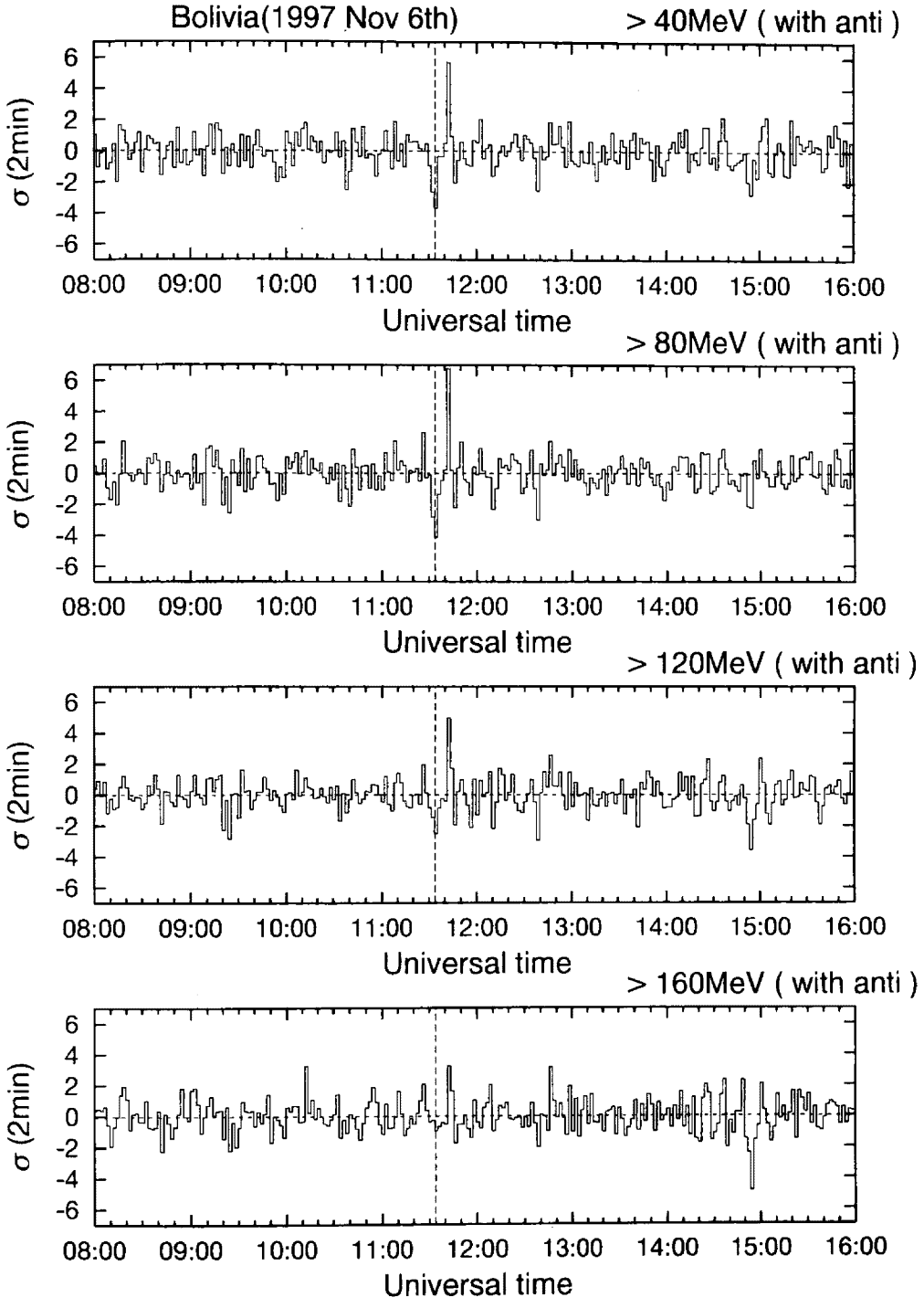

Figure 27: The statistical significances for the Bolivia solar neutron detector for the 1997 November 6th event. The statistical significance indicated here corresponds to the 2 minute counting rate of 4 neutral channels. The vertical dashed line represents the BASTE flare onset time, which was 11:34:02 UT. The most significant signal for each channel was obtained between 11:41 UT and 11:43 UT.

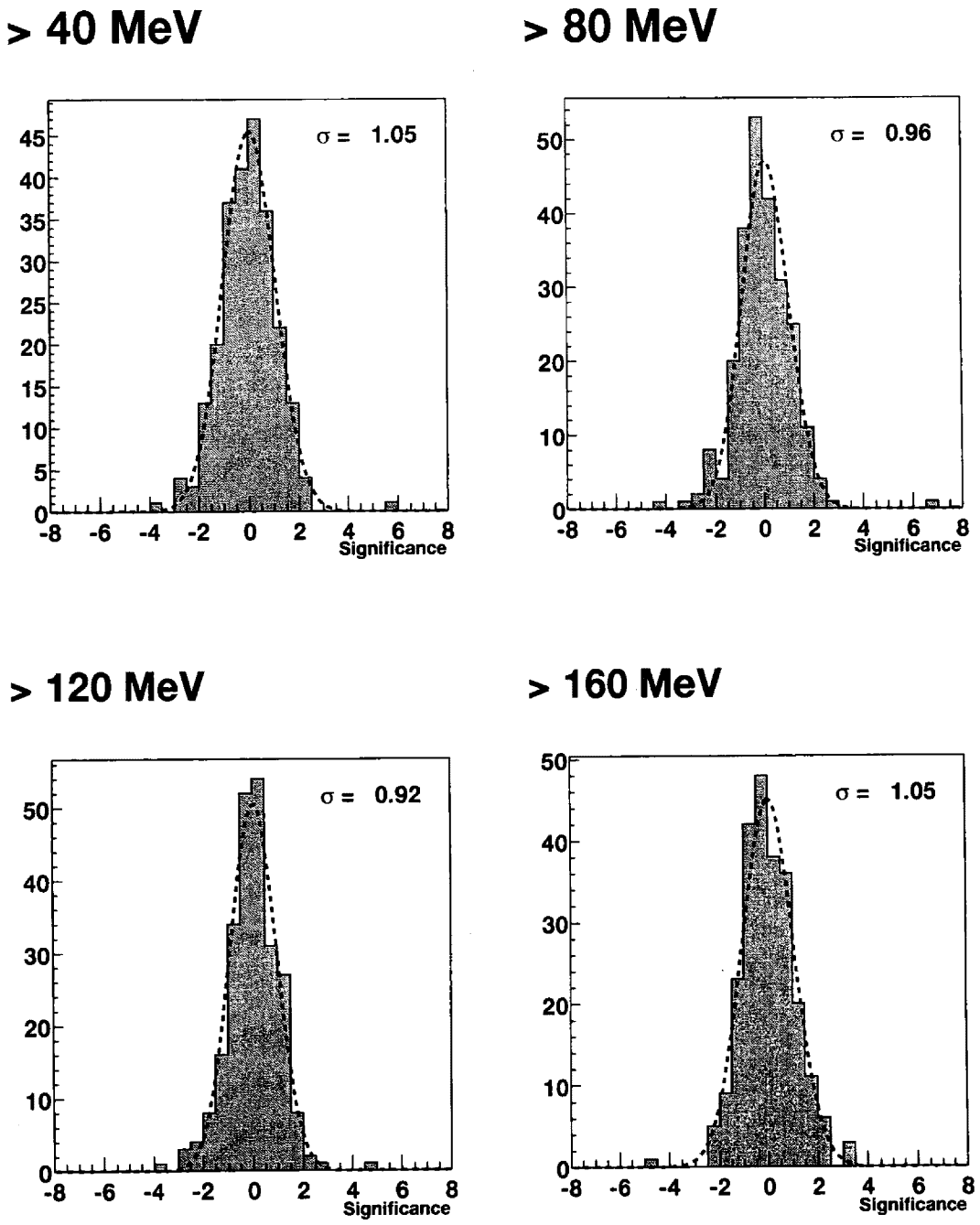

Figure 28: Distribution of the statistical significance of 2 minute counting rate between 8:00 UT and 16:00 UT. Dashed line drawn in each panel represents Gaussian function for fitting the histogram. In each panel, σ represent standard deviation of the Gaussian function.

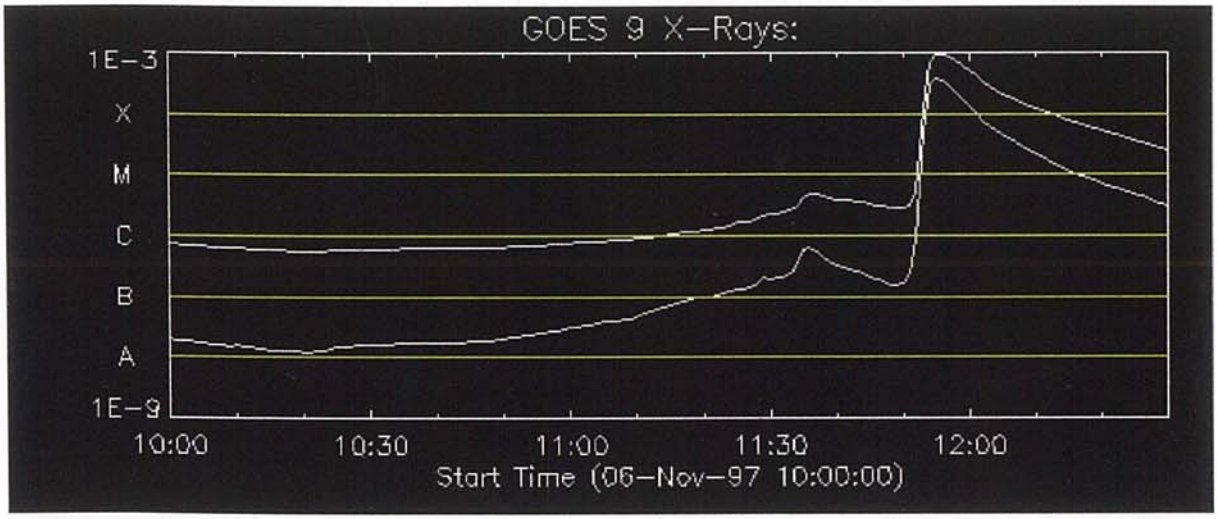

Figure 29: GOES X ray data between 10:00 UT and 12:30 UT for 1997 November 6th event. The graph was obtained from `http://www.lmsal.com/SXT/`.

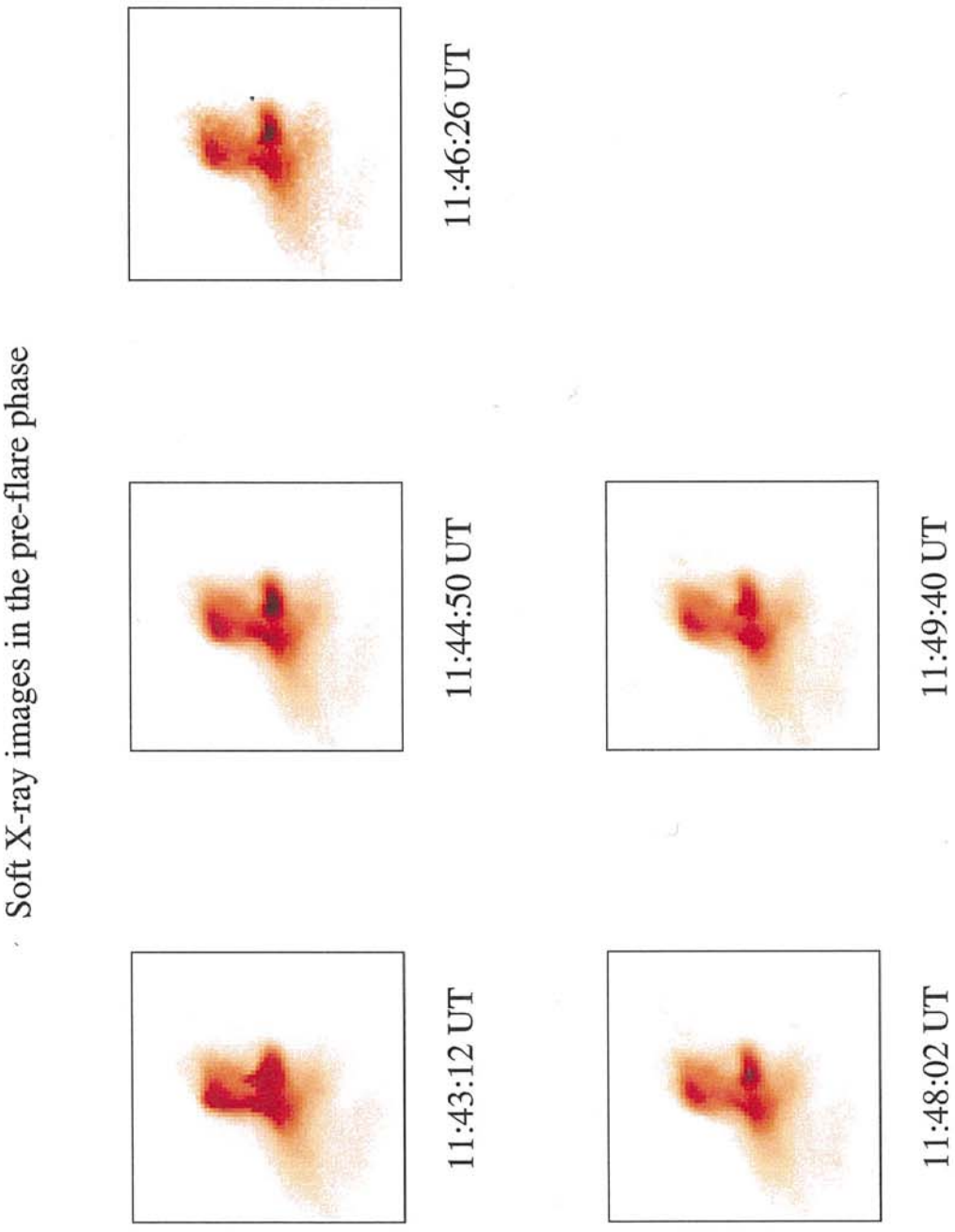

Figure 30: Soft X ray images obtained from Yohkoh X ray telescope in the pre-flare phase of the X9.4 solar flare on November 6th, 1997(The picture was made by S. Masuda.)

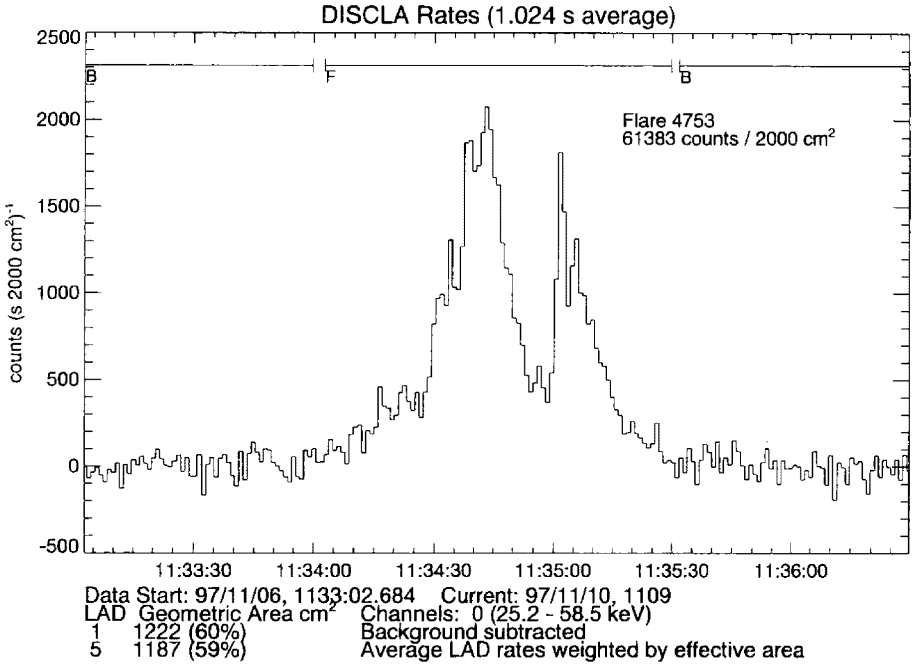

Figure 31: The time profile of X ray emissions detected by BATSE between 11:34 UT and 11:44 UT at the time of 1997 November 6th solar flare.

5 Discussion

5.1 1998 November 28th event

In this section, we discuss the observational results obtained using the Tibet solar neutron detector on 1998 November 28th. Before the discussion, the problems which we will discuss are summarized as follows.

(1) The Attenuation Problem
Since solar flare occurred near the winter solstice, the solar zenith angle was very large (53°) at Yangbajing. For this very large zenith angle, solar neutrons must travel to the detector passing through a very thick atmosphere. The air mass along the line of the sight from the sun to the detector was about $\sim 1000 g/cm^2$ at the time of the flare. It is difficult to imagine that the solar neutrons could travel through such very thick atmosphere and be detected at Yangbajing. In comparison, for the past solar neutron observations such as 1982 June 3rd event and 1991 June 4th event, the atmospheric depths were $\sim 740 g/cm^2$ and $\sim 770 g/cm^2$ respectively.
(2) The Initial Beam Intensity Problem
To date, all observations of solar neutrons on the ground occurred in association with large > X8 class solar flares. However, the signal of the Tibet solar neutron detector on 1998 November 28th was obtained at the time of a weaker X3.3 class solar flare. It is puzzling that such a "medium" size solar flare could produce such an abundant flux of solar neutrons that could be detected at the earth.
(3) The Detection Efficiency Problem
The Tibet solar neutron detector can measure the direction of incident neutrons with high energies. Main role of the upper part of the detector (which consists of the scintillation counters) is to detect low energy neutrons (low energy part), while that of lower part of the detector is to detect high energy neutrons by using four layers of proportional counters and wood (high energy part). A 4.2σ excess over the background count was detected only in the high energy part of the detector. The fact that the significant signal was obtained only by the high energy part and not by the low energy part is another problem. Of course, for the low energy channel, a 2σ level enhancement was also observed as shown in Figure 32.

(4) Weak Gamma Ray Emission Problem
No observation of line gamma rays in association with ion acceleration was reported. However, hard X ray observations by CGRO/BATSE and Yohkoh were obtained. Electron acceleration is responsible for the hard X ray emission. No clear evidence suggesting the presence of ion acceleration was obtained by this event. The question then arises as to whether ions and electrons were accelerated at the same or at different times.

Let us consider first the attenuation problem. For a solar zenith angle of 53°, using a simple formula $h_0/\cos\theta$, where h_0 and θ indicate the vertical atmospheric depth and the solar zenith angle, the corresponding air mass for neutrons is 996g/cm^2. Here h_0 is taken as 600g/cm^2. This thickness of 996g/cm^2 is almost the same as that at sea level(1030g/cm^2). Debrunner et al (1983 [89]) and Shibata (1994 [64]) calculated the attenuation length of solar neutrons in the atmosphere as $\sim$ 100g/cm^2. By using this value and a simple exponential attenuation model, solar neutrons would be attenuated to less than 1/10000. The results of this simple calculation seem to indicate that it would be very difficult to detect solar neutrons at Yangbajing under these conditions.

However, we must consider an "atmospheric refraction effect" proposed by Smart et al (1995 [107]). They reported one event for which we must introduce the atmospheric refraction effect. On 1990 May 24th, solar neutrons were detected by several neutron monitors in North America in association with an X9.3 solar flare. Figure 33 shows the attenuation curve of solar neutrons at that time. The horizontal axis in the Figure indicates the air mass calculated by the formula $h_0/\cos\theta$, where h_0 and θ represent vertical atmospheric depth and solar zenith angle of each station at the time of the 1990 May 24th flare. Under the assumption that solar neutrons were transported to the detector directly, the attenuation length of solar neutrons was calculated as 208g/cm^2. This value was very different from the theoretically predicted attenuation length, 100g/cm^2. There was ,therefore, a discrepancy between the theory and the observation on 1990 May 24th event. Under these circumstances, the atmospheric refraction effect was introduced by Smart et al. in order to explain the discrepancy. Solar neutrons suffered not only the attenuation in the atmosphere but also scattering in the atmosphere during

Table 7: The effective path length of solar neutrons in two cases at Yangbajing. Case 1 is for solar neutrons that are scattered by a constant 6° refraction angle after each scattering. For Case 2, the solar neutron after each scattering has a Gaussian type of angular distribution with standard deviation 6°. At Yangbajing, the vertical atmospheric depth corresponds to 600g/cm^2 (h_0).

Zenith angle θ(degrees)	$h_0/\cos\theta$(g/cm^2)	Case 1	Case 2
15	621	609	606
30	693	632	633
45	849	695	705
60	1200	806	839

their transit. Due to large angle scattering by the interactions and/or multiple small angle scattering, the paths of solar neutrons in the atmosphere were deflected, and were therefore not straight lines. This scattering effect could reduce the total air mass for solar neutrons. Figure 34 shows a simple view of the atmospheric refraction effect. Under the assumption that solar neutrons are scattered by 6° after every scattering with attenuation length 100g/cm^2, the effective path length of solar neutrons turns out to be 747g/cm^2 instead of 996g/cm^2 for the Tibet event. If we choose the scattered angle distribution as a Gaussian distribution with standard deviation 6°, the effective path length becomes 766g/cm^2. Under these two conditions, the total path length of solar neutrons becomes shorter in comparison with the simple calculation of the atmospheric depth by using the $h_0/\cos\theta$ model as shown in Table 7.

Galicia et al.(2000 [76]) calculated the neutron flux taking account of the atmospheric refraction effect and showed the increase of calculated excess counts was quite high; it agrees with the observed increase of each neutron monitor in North America for 1990 May 24th event. They also mentioned that it was very important in observations of solar neutrons to consider the atmospheric refraction effect in the case that the solar zenith angle was large, for example, early morning, late evening and the winter.

Figure 35 shows the attenuation of solar neutrons at an atmospheric depth of 600g/cm^2 in the two cases. Figure 35a shows the result of a Monte Carlo simulation taking into account the atmospheric refraction effect, Figure 35b

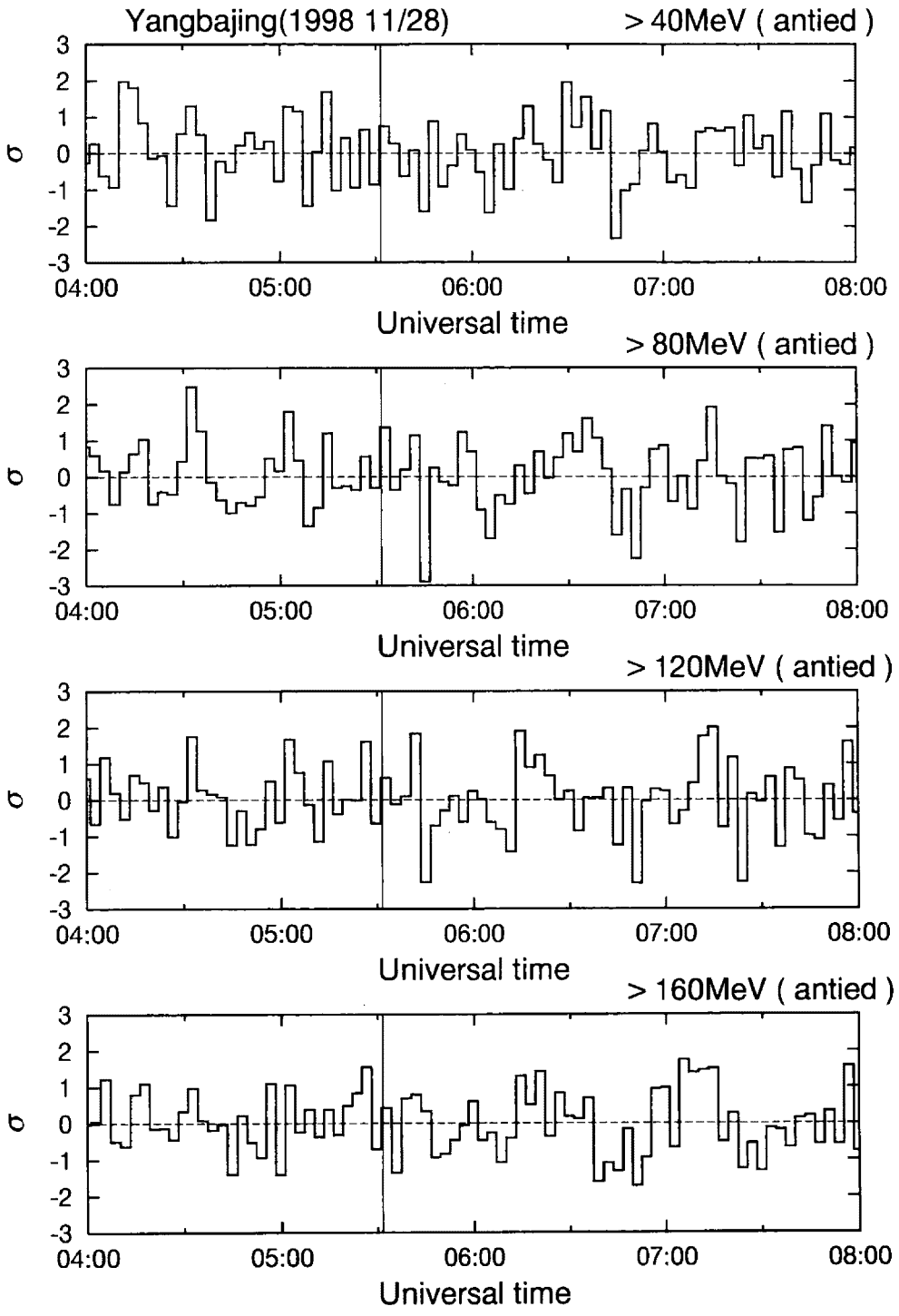

Figure 32: The statistical significance for 3 minute counting rate obtained by the scintillator part between 4:00 UT and 8:00 UT.

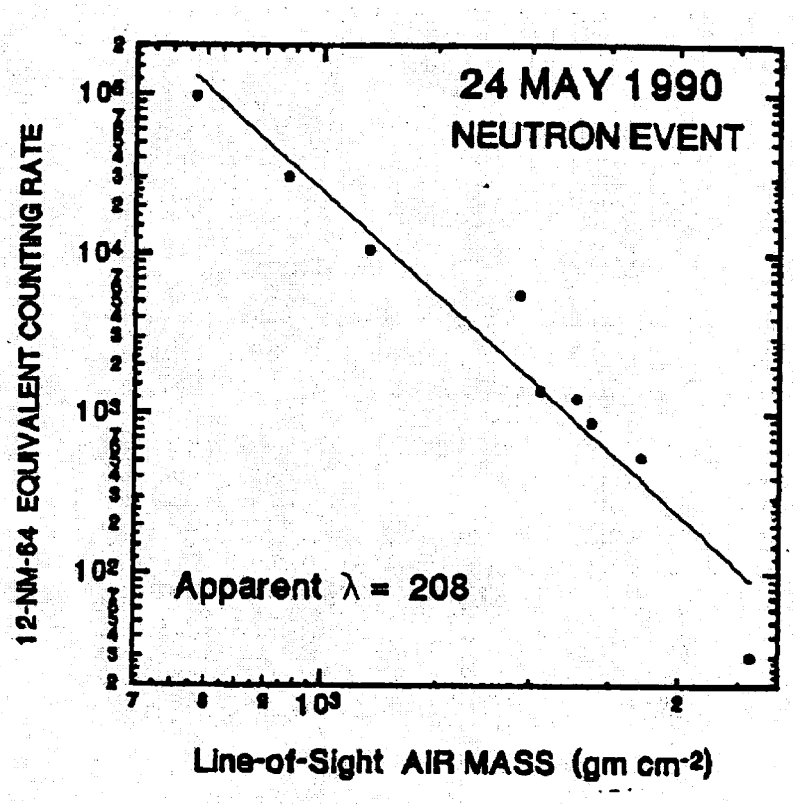

Figure 33: The counting rate recorded by neutron monitors in North America. The counting rate of each neutron monitor was converted to the 12-NM64 type equivalent counting rate. The horizontal axis represents the thickness of the atmosphere of each station. This graph was taken from Ref. [107]. The solid line corresponds to an attenuation length of neutrons of 208g/cm^2, which is twice as large as the theoretical expected value.

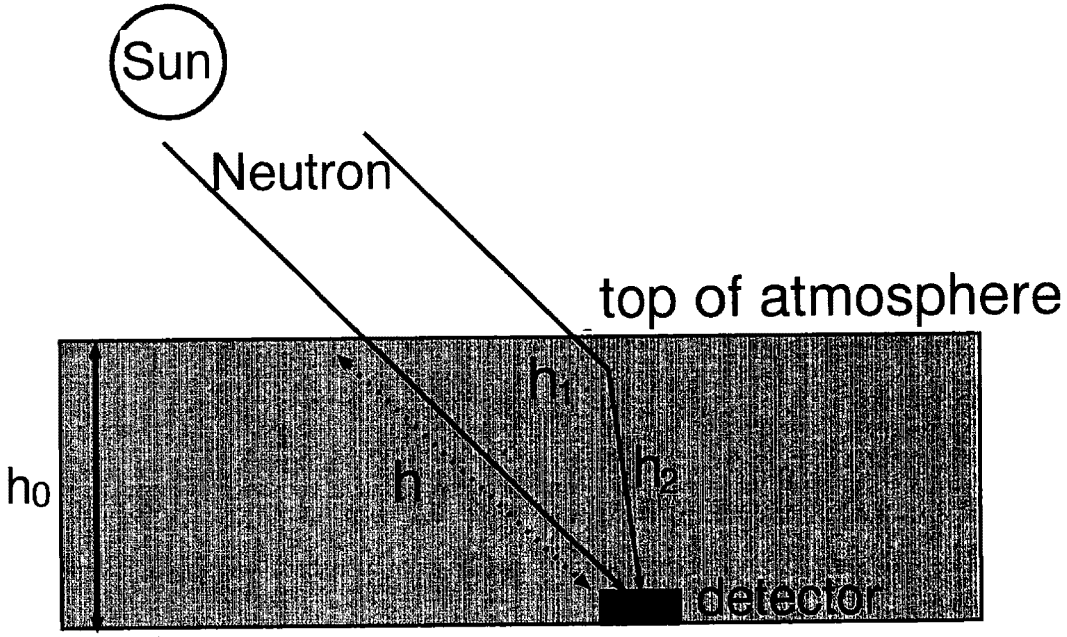

$$h_0 < h_1 + h_2 < h$$

Figure 34: The schematic view of the atmospheric refraction effect showing a neutron being scattered somewhere within the atmosphere. Due to the scattering process, the path length of neutrons in the atmosphere becomes shorter than the straight forward traveling path.

shows the result calculated using a simple exponential attenuation model. As can be seen from Figure 35, the attenuation of solar neutrons with incident angle less than 30° is not much different in the two cases. However, a remarkable difference is seen when the incident angle of solar neutrons exceeds 30°(large angle). It was found that solar neutrons with incident angles larger than 30° were not attenuated as much as was expected when we took account of the refraction effect. Making a comparison of the two attenuation cases for solar neutrons, it was also found that the survival probability of solar neutrons affected by the atmospheric refraction effect was 3.1, 6.6 and 10.0 times higher than that of solar neutrons based only on a simple exponential attenuation model for the kinetic energy of neutrons 200, 500 and 800 MeV. This result indicates that the survival probability is higher than in the previously considered model as the energy of incident neutrons becomes higher.

The attenuation of solar neutrons in three seasons is given in Figure 36. The three seasons correspond to the spring equinox, the summer solstice and the winter solstice. The kinetic energy of incident neutrons is assumed as 800 MeV and the abscissa represents the local time between 8 and 16 o'clock. At local noon in three seasons, the corresponding solar zenith angles are 30°, 6.6° and 53.9° at Yangbajing. The difference between the two attenuation curves in the morning and evening at the spring equinox and the summer solstice is small. However, there is a big difference in the case of the winter solstice. Even at local noon, if we do not take account of the refraction effect, the attenuation value becomes about 1/10000. However, if we consider the refraction effect, the value turns out to be greater than 1/1000. Therefore, in the case of the observations of solar neutrons with oblique incident angles greater than 30°, it is very important to consider the atmospheric refraction effect, because such solar neutrons have a high survival probability compared with the simple attenuation model. Even in the winter time, if an X class solar flare occurs, there will be a possibility of detecting solar neutrons at high altitude like Tibet or Bolivia.

We next consider the possibility of detection of solar neutrons in association with a moderate size X3.3 solar flare. For this purpose, the solar neutron observation in association with an X12 solar flare on 1991 June 4th will be investigated. On 1991 June 4th, the first solar neutron telescope

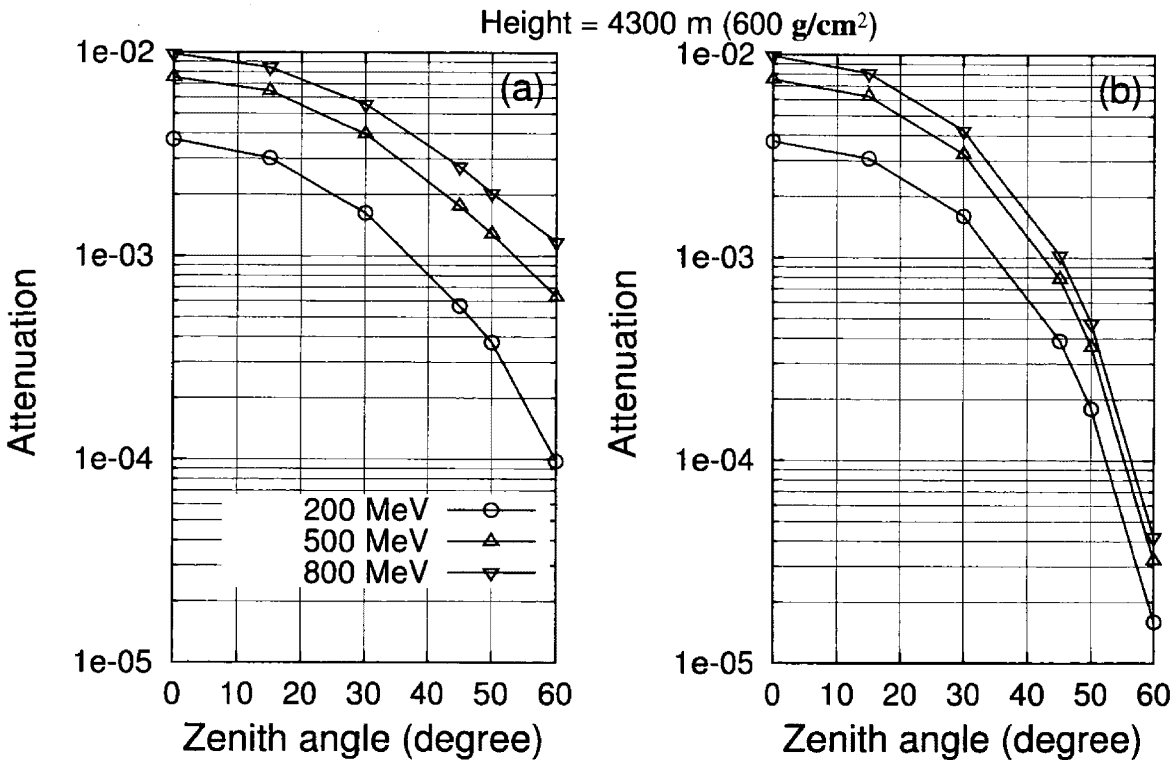

Figure 35: The attenuation curves for two cases are given for the Yangbajing level (vertical atmospheric depth is 600g/cm^2). Left panel (a) shows the attenuation of neutrons taking account the atmospheric refraction effect, while right panel (b) corresponds to the simple exponential attenuation model. The horizontal axis represents the incident angle of solar neutrons at the top of the atmosphere. For three incident energies of solar neutrons, 200 MeV, 500 MeV and 800 MeV, the attenuation curves are given.

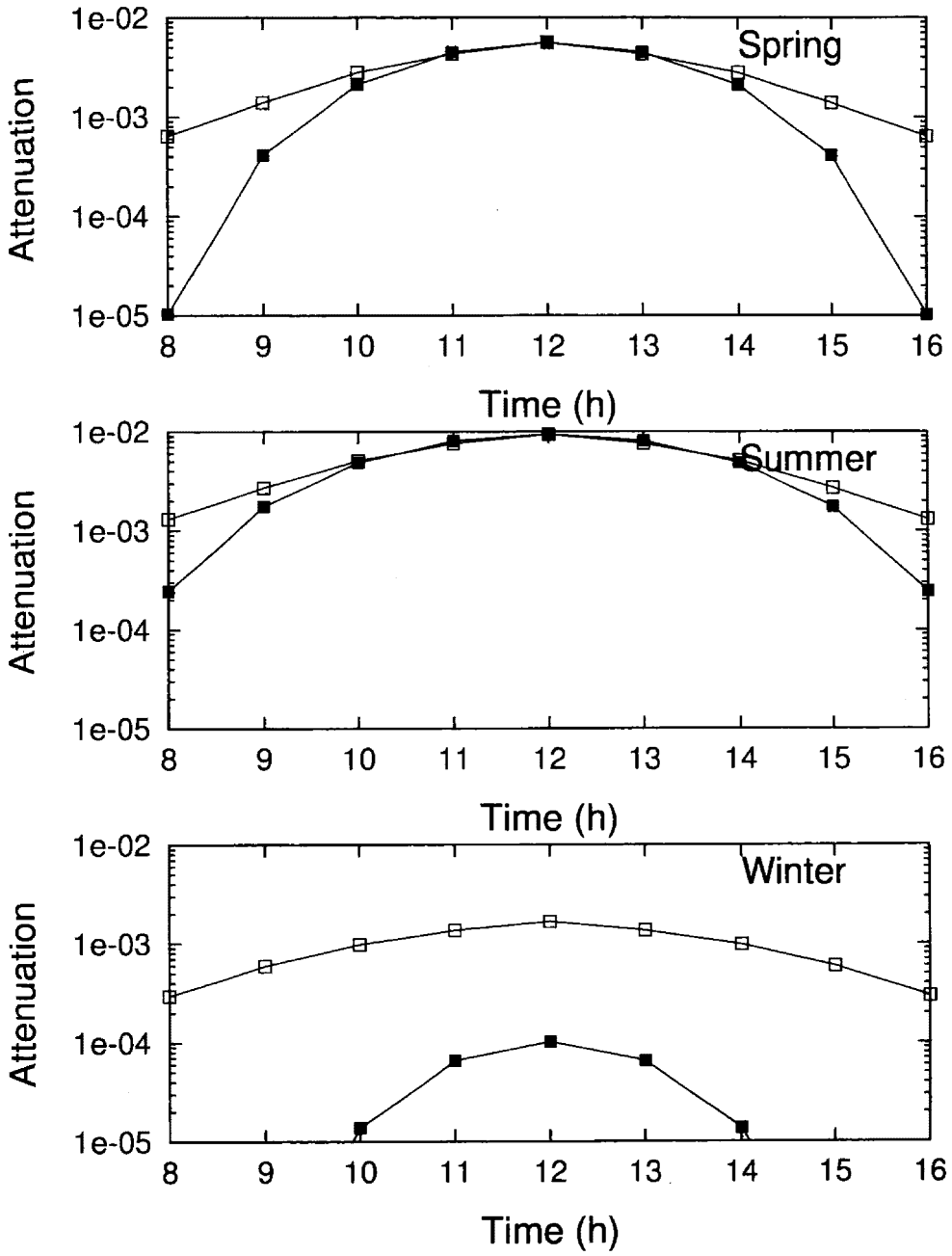

Figure 36: Local time variation of the attenuation of 800 MeV solar neutrons in the atmosphere. The time of each panel represents the local time in Yangbajing. Top, middle and bottom panels correspond to the spring equinox, the summer solstice and the winter solstice respectively. White points indicate the attenuation of solar neutrons in the atmosphere taking account the atmospheric refraction effect while the black points give the prediction for a simple exponential attenuation model.

which was installed at Mt. Norikura detected solar neutrons in association with a gigantic solar flare (Muraki et al., 1992 [36]; Muraki et al., 1995 [38]). Figure 37 shows the time profile in the flare time on 1991 June 4th. The statistical significance obtained by the solar neutron detector was 4.4σ for the 3 minute counting rate in the top panel of Figure 37. The area of the first solar neutron detector was $1m^2$, while the solar neutron detector installed at Yangbajing had an area of $9m^2$ and detected a 4.2σ statistical enhancement for a 3 minute counting rate for the X3.3 solar flare. Up to now, due to a paucity of observations of solar neutron events, it was not possible to investigate whether or not the production rate of solar neutrons was proportional to the flare size as determined by GOES. Table 8 shows the production rate of neutrons at the solar surface which was derived by other authors(Chupp et al., 1982 [54]; Chupp et al., 1987 [34]; Debrunner et al., 1997 [44]). From

Table 8: Neutron production rate at the solar surface in association with major three solar flares.

Date	Class/Imp.	Production rate(/sr)
1980 6/21	X2.6/1B	3×10^{28}
1982 6/3	X8/2B	8×10^{28}
1990 5/24	X9.3/1B	5.6×10^{30}

this Table, the neutron production rates on 1980 June 21st and 1982 June 3rd were nearly proportional to the flare size. But, for the 1990 May 24th event, the neutron production rate was very large and not proportional to the flare size as compared to the other flares. Therefore, the neutron production rate is thought to vary from flare to flare. However, here we assume that the production rate is approximately proportional to the flare size. Under this assumption, the production rate for the X3.3 solar flare is expected to a factor of ~ 4 smaller than for the X12 solar flare.

A comparison of the attenuation of solar neutrons at Yangbajing (4300m a.s.l.) and Norikura (2770m a.s.l.) is shown in Figure 38. The horizontal axis represents the angle of incidence of solar neutrons at the top of the atmosphere. The vertical line drawn in each panel corresponds to the solar zenith angle at the time of each flare. The angle of incidence of solar neutrons in association with the 1991 June 4th solar flare was 18°. Comparing the

attenuation of solar neutrons with the angle of incidence of each event, solar neutrons with the energies of 500 MeV and 800 MeV have almost the same attenuation rate. However, at Yangbajing, solar neutrons with an energy of 200 MeV are attenuated twice as much as at Norikura. Taking account of the differences in flare size, attenuation length and the detector area, a 3.6σ excess of 800 MeV solar neutrons is expected for this event using the Tibet solar neutron detector. Therefore, the detection of solar neutrons in winter by the Tibet detector would be possible.

Now, we consider the acceleration time of ions at the solar surface. As mentioned in Section 4, radio emissions at 17/34 GHz were detected by the Nobeyama radio heliograph showed the peak intensity at 5:39:51 UT. Non thermal hard X ray emissions were started at around 5:36 UT according to Yohkoh observation. The hard X rays with an energy band of 191 keV − 317 keV showed the maximum intensity at around 5:40 UT by Yohkoh. These results imply that electrons were certainly accelerated at the solar surface. On the other hand, the Tibet solar neutron detector detected an increase in the 3 minute counting rate between 5:38 UT and 5:41 UT. Furthermore, the most significant signal in 1 minute counting rate were detected as 4.0σ between 5:40 UT and 5:41 UT. Therefore, the neutron signals almost coincided with the radio and the hard X ray emissions. From this result, we suggest that the electrons and the ions were accelerated at the almost same time.

The time profile of hard X rays for 1998 November 28th event is shown in Figure 17. Although the hard X ray emissions are related to the electron acceleration, it is assumed that ions were accelerated at the rise time of the hard X ray at 5:37:50 UT. This observation indicates that the 4.2σ excess for the 3 minute counting rate occurred between 5:38:19 UT and 5:41:19 UT (see Figure 20). If solar neutrons are produced impulsively, the kinetic energy of solar neutrons can be derived from the time of flight method. Neutrons which arrived at the earth at 5:38:19 UT were delayed by 29 seconds from the production time, 5:37:50 UT. In the case of 5:41:19 UT, the delay time was 209 seconds. The delay time Δt from the production time is represented with

$$\Delta t = \frac{R}{c\beta} - \frac{R}{c} \tag{2}$$

where R is the distance between the sun and the earth (1.496×10^{13}cm) and c and β indicate the light velocity and the ratio of velocity of neutrons to the

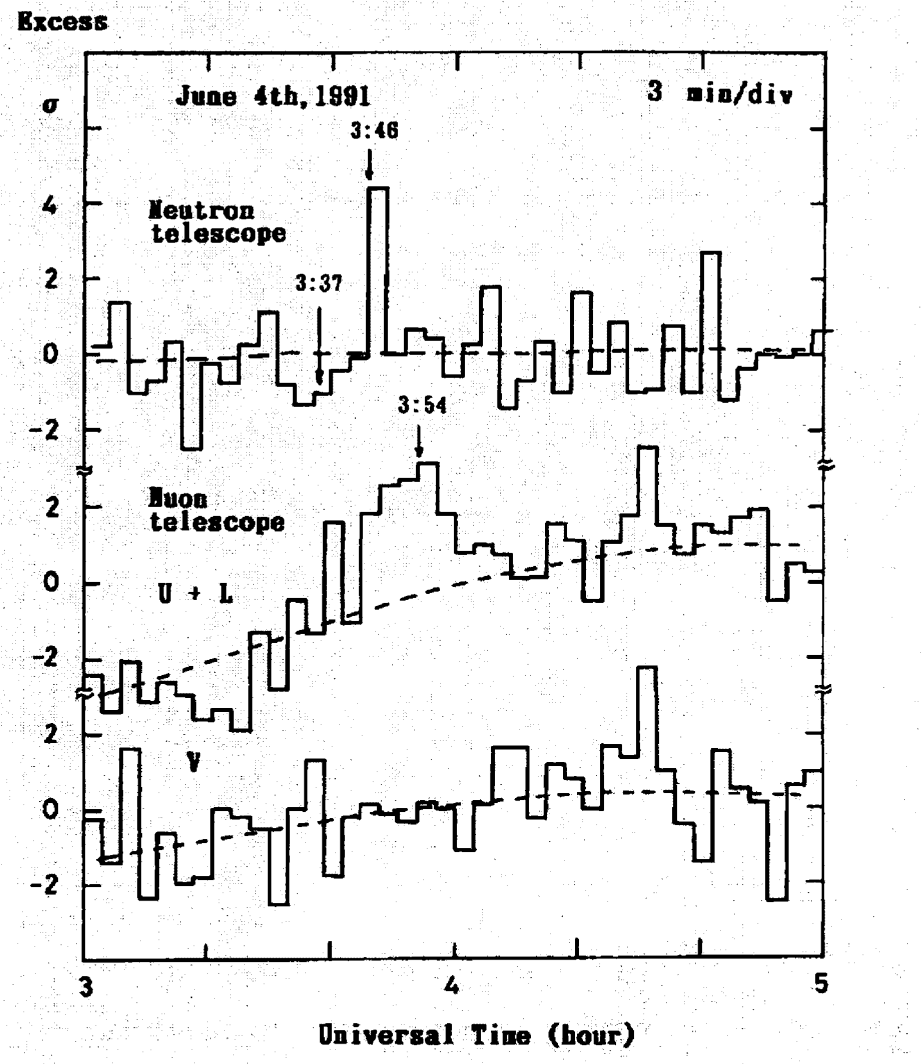

Figure 37: Time profile of the excess recorded by three different type of detectors located at Mt.Norikura on 1991 June 4th. The X12 solar flare occurred at 3:41 UT and solar neutron detector recorded an increase of counting rate between 3:46 UT and 3:49 UT (Top panel). Middle and bottom panels represent the counting rate of the muon telescope and neutron monitor respectively. This figure originated from Figure 2 in [36]

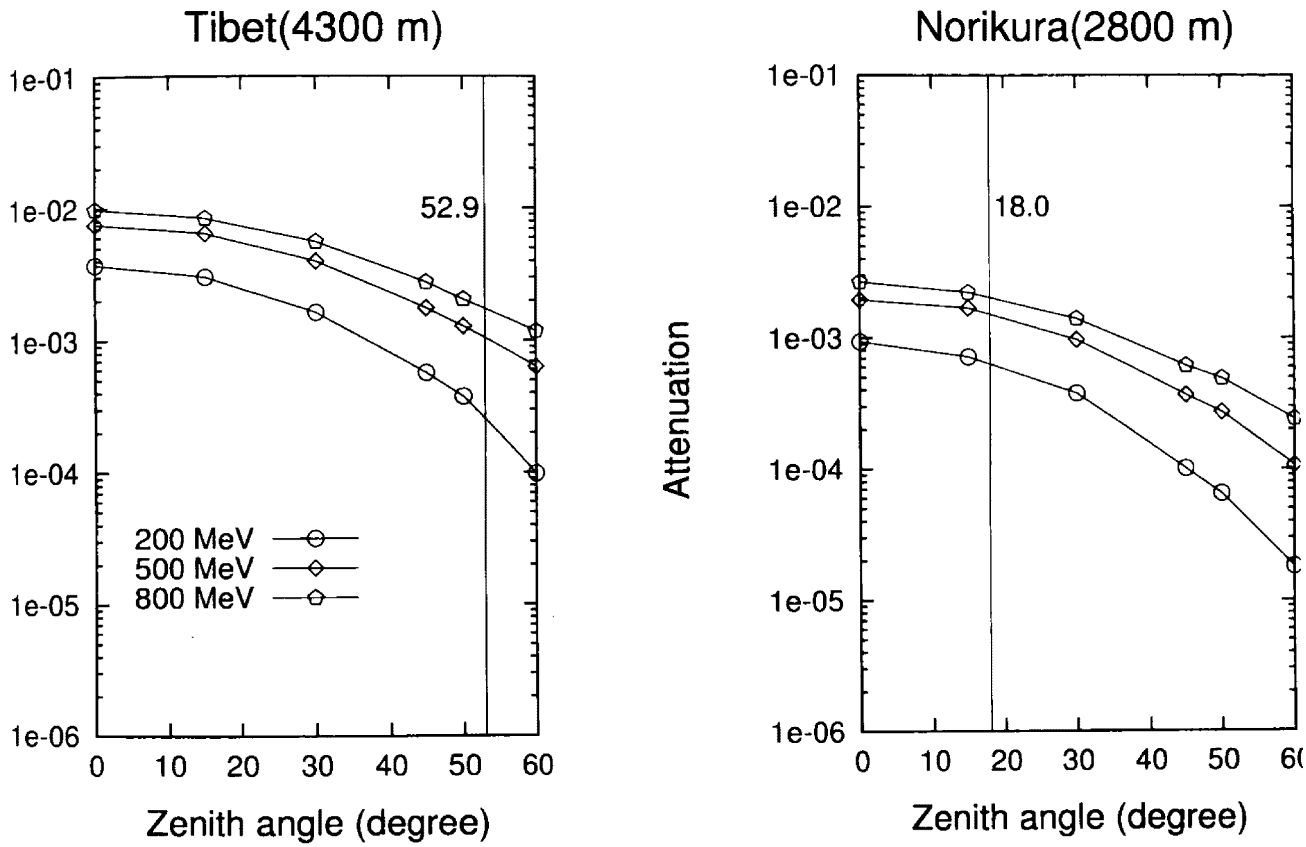

Figure 38: Comparison of attenuation of solar neutrons at two locations. Left panel shows the attenuation at Yangbajing in Tibet and right panel shows the attenuation at Mt. Norikura in Japan. The horizontal axis shows the angle of incidence of solar neutrons at the top of the atmosphere. The vertical line drawn inside each panel represents the zenith angle of the sun for 1998 November 28th solar flare(left panel) and 1991 June 4th flare (right panel).

light velocity. From the equation, β can be shown by

$$\beta = \frac{1}{c\Delta t/R + 1}.$$

Since the delay time corresponding to 5:38:19 UT and 5:41:19 UT was 29 and 209 seconds respectively, so β for each delay time became 0.945 and 0.705. The kinetic energy E_n of neutrons can be given by

$$\begin{aligned} E_n &= (\gamma - 1)M_n \\ \gamma &= \frac{1}{\sqrt{1-\beta^2}}, \end{aligned} \tag{3}$$

where M_n is the rest mass of a neutron. The kinetic energy of neutrons for each delay time was found to be 1944 MeV and 387 MeV. Therefore, neutrons in the energy range between 400 MeV and 2 GeV could have produced the detected signal. The estimation of the energy from the delay time is consistent with our former speculation that the energy of those neutrons must be quite high and the attenuation in the atmosphere must be rather small.

The neutron energy spectrum at the top of the detector can be deduced from the result of observation for the 1 minute counting rate given in Figure 22. For this calculation, the detection efficiency for neutrons by the Tibet solar neutron detector must be taken into account. Figure 39 represents the detection efficiency for neutrons obtained by a Monte Carlo simulation. The "Layer" in the Figure represents the channel which detects the coincidence between the signal of ch1($>$ 40 MeV energy deposit in the scintillator) and the signal each layer in the proportional counters. As the number of layer increases, the recoil protons must penetrate to a deeper layer of the proportional counters, which corresponds to protons converted from higher energy neutrons (see in detail in [88]). North and South in the Figure 39 are defined in the same way as in Figure 19. In the simulation for the detection efficiency, it was assumed that neutrons arriving at the top of the detector would have the zenith angle spectrum described in Figure 40. This angular distribution was deduced from a Monte Carlo simulation with the angles of incidence of neutrons at the top of the atmosphere being 52.9°. As can be seen in Figure 40, neutrons which reach the detector do not have a monochromatic distribution of angles because of the scattering effect and the peak intensity is expected at a zenith angle of 30°.

Using the detection efficiency ϵ and the excess count ΔN between 5:38

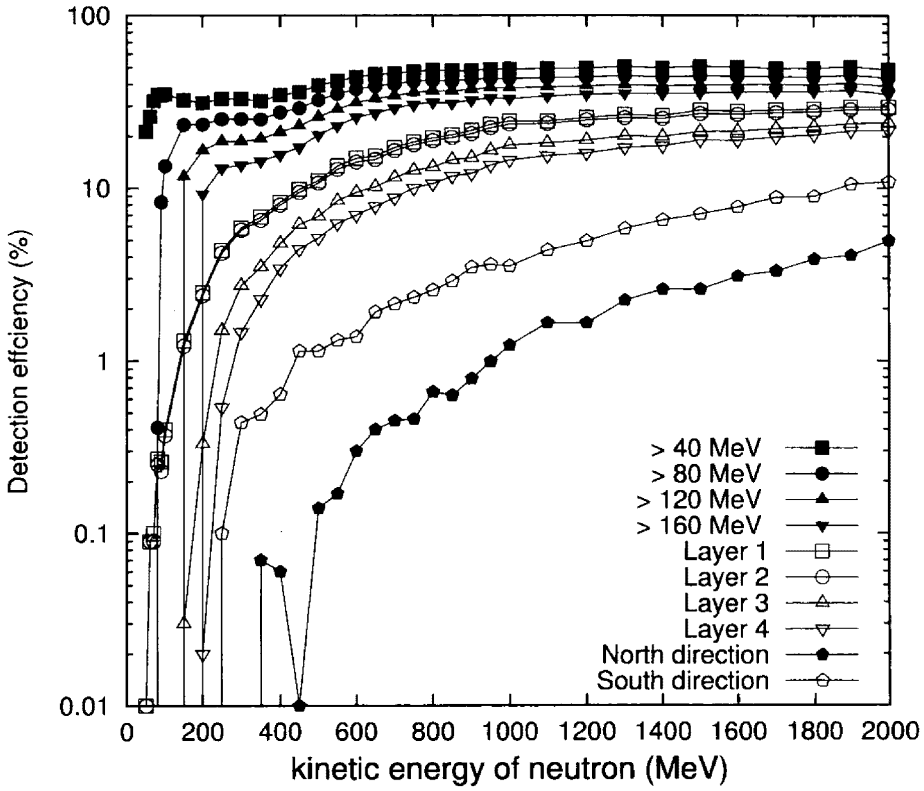

Figure 39: The detection efficiency for solar neutrons with the incident zenith angle 53° at the top of the atmosphere. Horizontal and vertical axes give the kinetic energy of neutrons in MeV and the detection efficiency in %. The numbers > 40, > 80, > 120 and > 160 MeV represent the threshold energies of the 4 channels in the scintillator part of the solar neutron detector. The meaning of "Layer" in the graph is described in the text. The North and South directions represent the channels which were used in analyzing the data from the solar direction (south) and anti-solar direction (north).

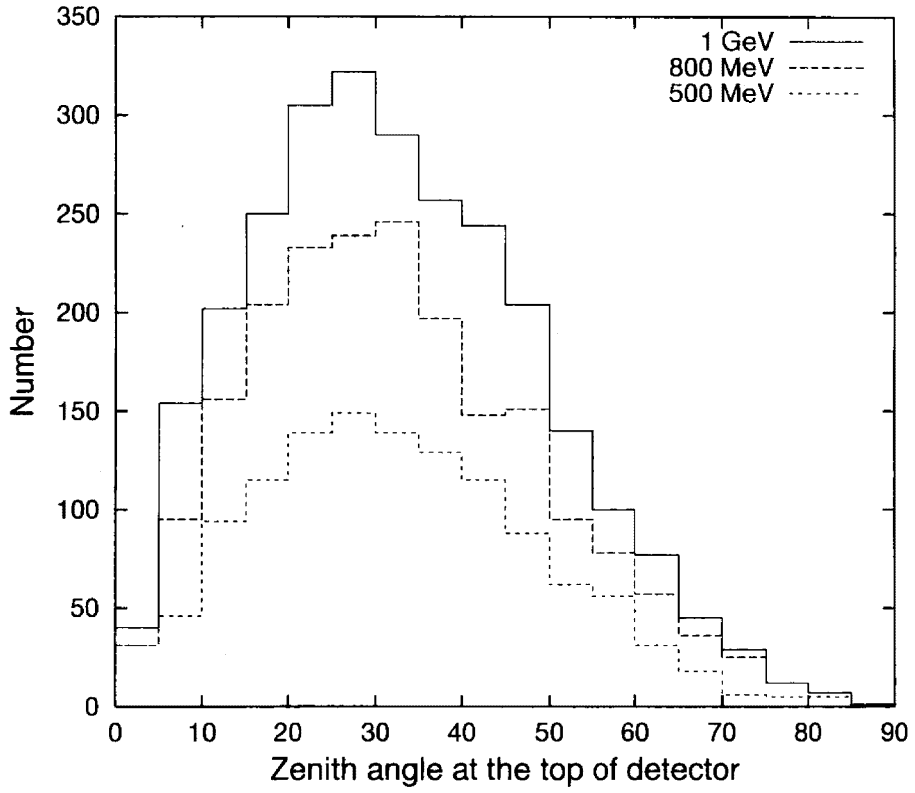

Figure 40: Angular distributions of solar neutrons which arrive at the Yangbajing level for an angle of incidence of the top of the atmosphere of 52.9°. The peak angle is predicted at around 30° from the zenith.

UT and 5:42 UT, the neutron flux can be estimated by the formula;

$$\frac{\Delta N}{\epsilon \times \Delta E_n} \tag{4}$$

where ΔE_n indicates the energy range for each bin of the 1 minute counting rate. In Table 9, ΔN and ΔE_n corresponding to each bin are summarized. The detection efficiencies for each energy bin are given at the average energy E_{ave}. E_{ave} is calculated by the equation below in the case that the shape of

Table 9: The excess between 5:38 UT – 5:42 UT on 1998 November 28th event.

time (UT)	Energy bin ΔE_n(MeV)	Excess count ΔN (/1min)	Excess (%)
5:38 - 5:39	842 - 1944	99	3.90 ± 1.99
5:39 - 5:40	537 - 842	69	2.69 ± 1.99
5:40 - 5:41	388 - 537	228	8.88 ± 1.99
5:41 - 5:42	298 - 388	106	4.13 ± 1.99

neutron energy spectrum is represented by a power law E_n^{α}.

$$E_{ave} = \frac{\int_{E_1}^{E_2} E_n \cdot E_n^{\alpha} dE_n}{\int_{E_1}^{E_2} E_n^{\alpha} dE_n}, \tag{5}$$

where E_1 and E_2 indicate the lower and higher energies for each bin. In equation (5), the average energy corresponding to each energy bin turns out to be 1174, 655, 450, 336 MeV for a power law index $\alpha = 3$, while for a power law index of 2, E_{ave} is estimated as 1235, 665, 453, 338 MeV respectively. No large difference could be found between the power law indices of 2 and 3, so the average energies for $\alpha = 3$ were adopted, taking account of the time profile obtained using 10 second counting rate. Since the detection efficiencies for each average energy are found to be 3.47, 1.29, 0.83, 0.40 (%), the neutron spectrum can be calculated by equation (4); the result is shown in Figure 41. As the result of fitting data points with a power law $C \times (E_n/300)^{\alpha}$, C and α turn out to be

$$\begin{aligned} C &= (1.02 \pm 0.89) \times 10^{-4} \ /\mathrm{MeV/cm^2} \\ \alpha &= -3.52 \pm 3.01. \end{aligned}$$

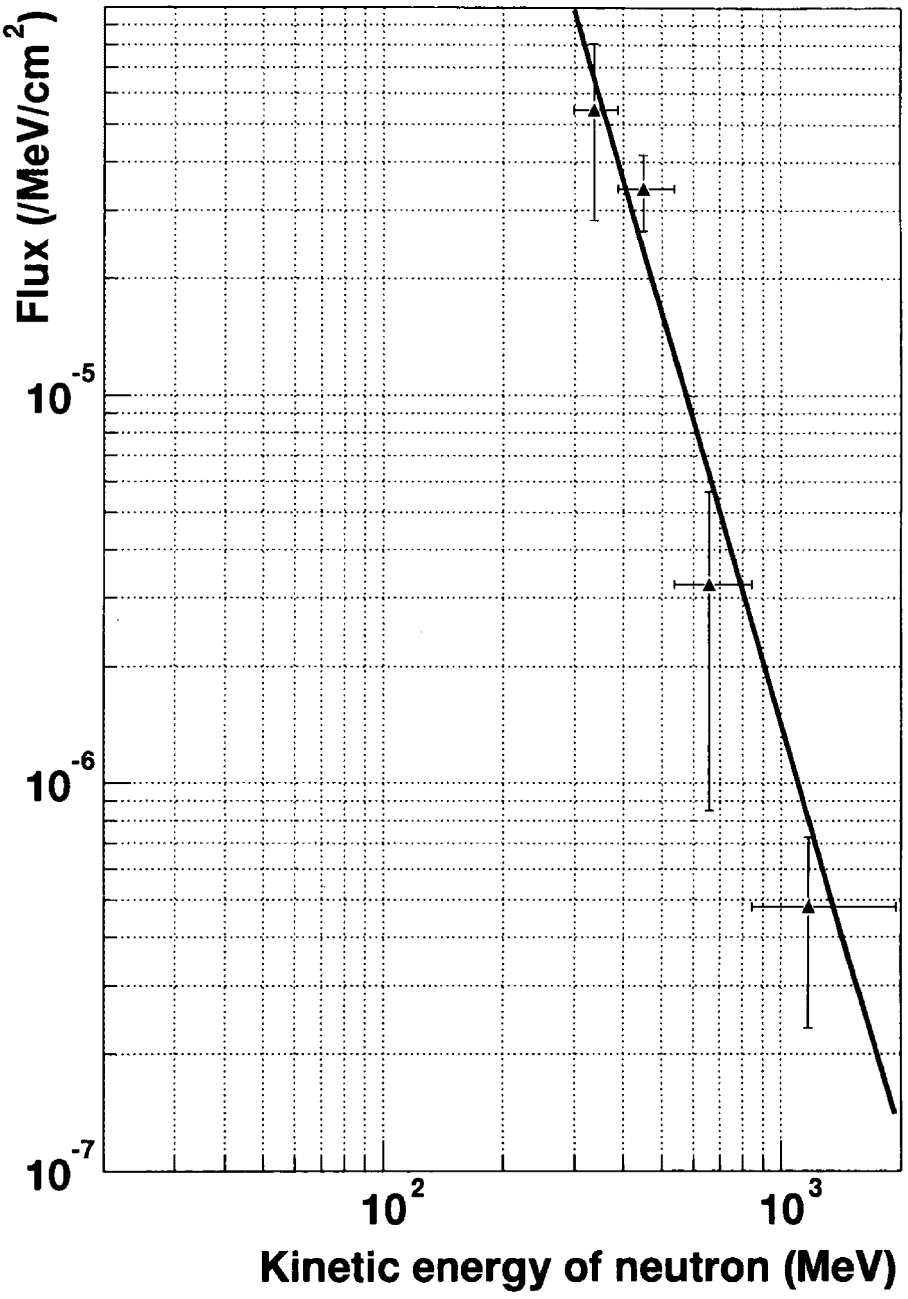

Figure 41: The neutron spectrum at the top of the detector for the 1998 November 28th event. The points represent the average energy.

Table 10: The background neutron spectrum at the Yangbajing level. The process of deriving the spectrum was described in text.

Kinetic energy (MeV)	Flux (/MeV/cm^2)
$2 < E_n < 10$	$2.7 \times 10^{-3} (E_n/10)^{-1.5}$
$10 < E_n < 100$	$1.6 \times 10^{-4} (E_n/100)^{-1.2}$
$100 < E_n < 300$	$1.6 \times 10^{-4} (E_n/100)^{-1.6}$
$300 < E_n$	$2.8 \times 10^{-5} (E_n/300)^{-2.7}$

The fitting function is also shown in Figure 41 as a solid line. In order to compare the derived neutron spectrum with neutron background spectrum at 600g/cm^2, the neutron background at 680g/cm^2 (Miyake, 1983 [108]) is multiplied by exp(-(600-680)/140) = 1.77 and is estimated such as in Table 10. The value of 140g/cm^2 in the exponential factor corresponds to the attenuation length of secondary neutrons produced by primary cosmic rays. Figure 42 represents the result of comparison between the neutron spectrum obtained from the observational data and the neutron background spectrum at 600g/cm^2.

We understand that in this event, high energy neutrons play an important role in the detected signal. The Monte Carlo simulation showed the threshold energy requiring for neutrons to reach the deepest layer of the proportional counter was 230 MeV. As can be seen in Figure 39, the lower energy part of the detector (upper scintillator part) can detect neutrons across wide energy range from low energies to high energies. The detection efficiency of the higher energy part of detector decreases rapidly in the low energy region and, in fact, the higher energy part of detector cannot detect low energy neutrons. This decrease of the detection efficiency arises from using wood as the absorber; this is useful in reducing the background which is dominated by low energy neutrons.

Recoil protons produced by the incident neutrons must penetrate two layers of wood. In the absorber, recoil protons with low energies cannot penetrate the deepest layer so that low energy neutrons are rejected. Furthermore, the background is also reduced using information about the arrival directions of the neutrons. As discussed in Section 4, the background can be reduced $\sim 1/8$ times. Consequently, the Tibet solar neutron detector was

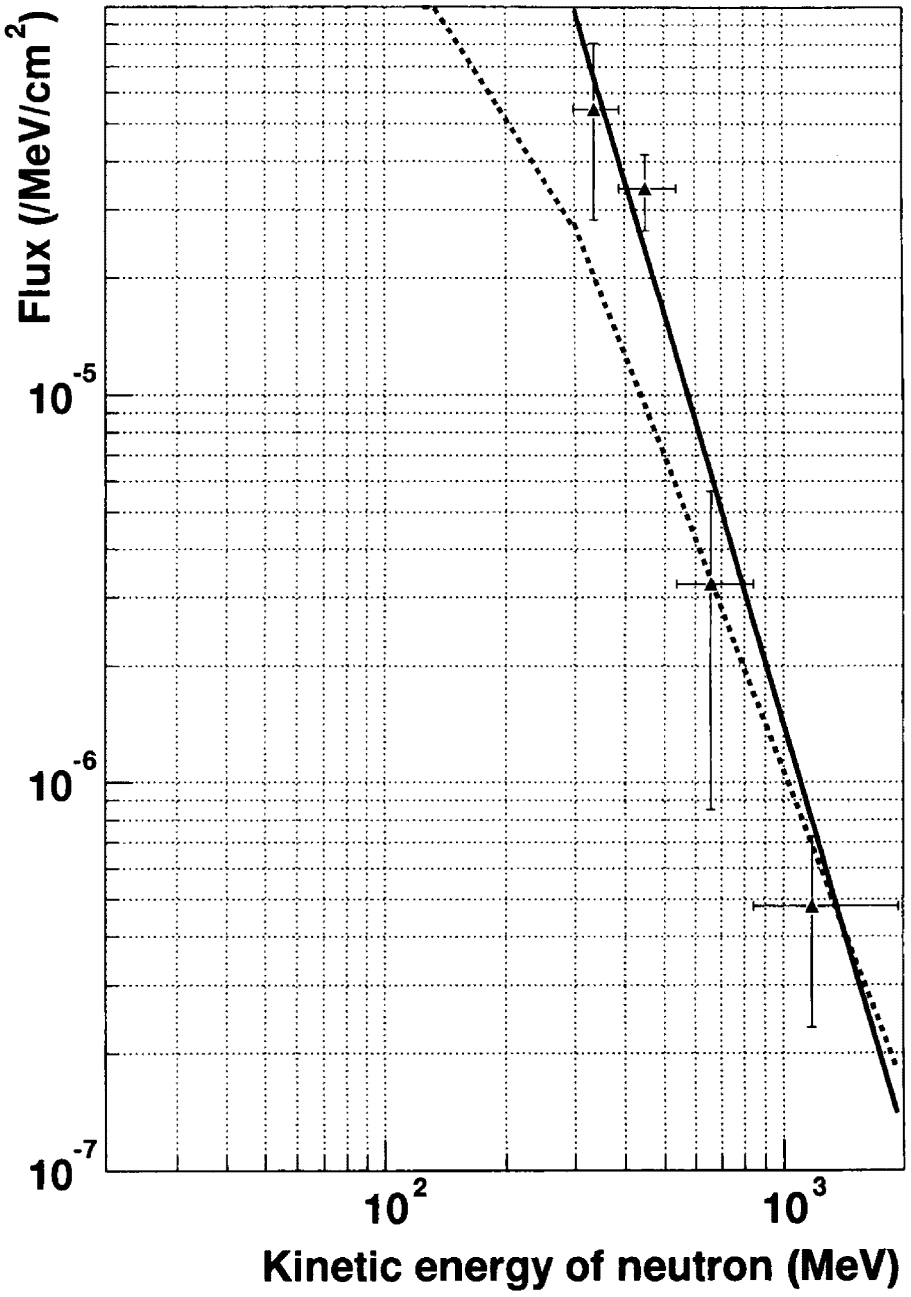

Figure 42: The derived neutron spectrum (solid line) is given in the graph together with the neutron background spectrum at 600g/cm^2(dashed line).

able to detect high energy neutrons which could travel to the bottom of the detector. Comparing the derived flux at the top of the atmosphere for this event with the results of past observations, it is possible that the neutron signal for this event was not as strong at the top of the atmosphere as shown in Figure 43. In the calculation of the flux at the top of the atmosphere, the attenuation values which were used at each average energy were 3.49×10^{-3}, 1.64×10^{-3}, 1.12×10^{-3} and 7.96×10^{-4}.

Here we must mention briefly about the lack of a remarkable excess for this event in the scintillator part (> 40 MeV, > 80 MeV, > 120 MeV and > 160 MeV) and also in the neutron monitor. For the 1998 November 28th solar flare, the solar zenith angle was very large. However, due to the refraction effect, solar neutrons could arrive at the Yangbajing level.

Furthermore, since neutrons passed through two layers of wood and the arrival direction of incident neutrons was measured, the detection was very efficient for high energy neutrons. However, in the scintillator part of the Tibet solar neutron detector, not only solar neutrons but also the omnidirectional low energy components of the background were detected. If this event is interpreted in such a way, it can be argued that the neutron monitors located at Yangbajing could not detect the signal of solar neutrons (Kohno, 1999 [109]). This is because the threshold energy of the neutron monitor for neutrons is a few MeV, so the signal was masked by a large amount of the background same as in the scintillator part of the solar neutron detector. We must note again that the excess was detected by the scintillator part and excess level was only at the 2σ level, which is the same level as fluctuations of the background as shown in Figure 32. Accordingly, making use of the capability to detect the high energy component by using the wood and measuring the arrival direction of neutrons, weak neutron signals were able to detect by the Tibet solar neutron detector in association with 1998 November 28th solar flare.

5.2 1997 November 6th event

In this section, another clear signal obtained from the flare mentioned in the previous section will be discussed.

This event also includes a thick air mass problem as was the case for the 1998 November 28th event mentioned in the previous section. The signal was

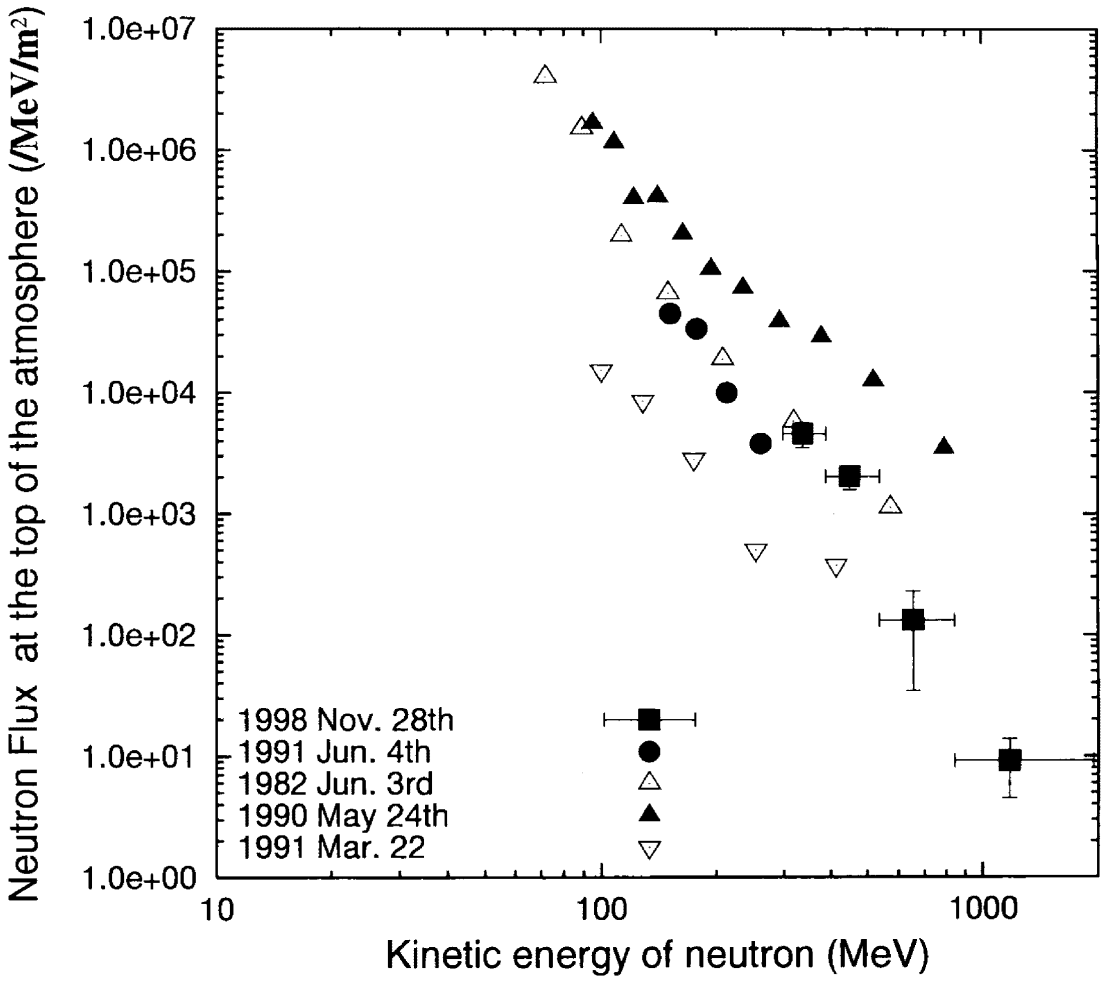

Figure 43: The neutron flux of November 28th event at the top of the atmosphere. Both the November 28th event and the results of past observations are plotted in the Figure.

detected at early morning in Bolivia, at around 7:50 local time(11:50 UT). The zenith angle of the sun was 69°, which was larger than that for Yangbajing for the 1998 November 28th event. The air mass along the line of sight from the sun to the detector was $540(\mathrm{g/cm^2})/\cos 69° \sim 1500\mathrm{g/cm^2}$, where $540\mathrm{g/cm^2}$ corresponds to the vertical atmospheric depth at Mt. Chacaltaya. Although the air mass was very large, it was still possible that solar neutrons could arrive at the detector again, taking account of the atmospheric refraction effect. The attenuation curve for solar neutrons at Mt. Chacaltaya is shown in Figure 44 along with the attenuation curve at Yangbajing for the 1998 November 28th event for comparison. The horizontal axis in the Figure shows the kinetic energy of incident neutron at the top of the atmosphere. In spite of the large zenith angle of the sun for the 1997 November 6th event, the attenuation rate of solar neutrons at Mt. Chacaltaya turns out to be nearly the same as that of Yangbajing for the 1998 November 28th event. This is quite surprising, but taking account of the very high altitude of Mt. Chacaltaya, this turns out to be the case. The effective path length of solar neutrons for this event is 835 $\mathrm{g/cm^2}$ taking account of the scattering effect(instead of $1500\mathrm{g/cm^2}$). According to the attenuation rate and the effective path length, neutrons could reach the detector for this event.

As mentioned in Section 4 and shown in Figure 15b, Gornergrat was also a suitable site for observations on 1997 November 6th. The zenith angle of the sun was 63° at that time at Gornergrat. However, no clear neutron signal could be found at the time of the flare by the neutron monitors which were located at Jungfraujoch near Gornergrat. As can be seen in Figure 45, the attenuation of solar neutrons at Jungfraujoch was much larger than that at Mt.Chacaltaya on 1997 November 6th. This is reason that no significant signal could be detected at Jungfraujoch. But the ground level enhancement due to solar protons was observed because of lower cut-off rigidity as shown in Table 5 [99].

The neutron flux for this event at the top of the atmosphere can be obtained from the observational data. The neutron flux derived from the 30 second counting rate is presented in Figure 46 for the enhancement between 11:41 UT and 11:43 UT. We assume here that the neutron production could be expressed by a δ function type and neutrons were emitted at 11:34:40 UT which corresponds to the time of the maximum counting rate in the

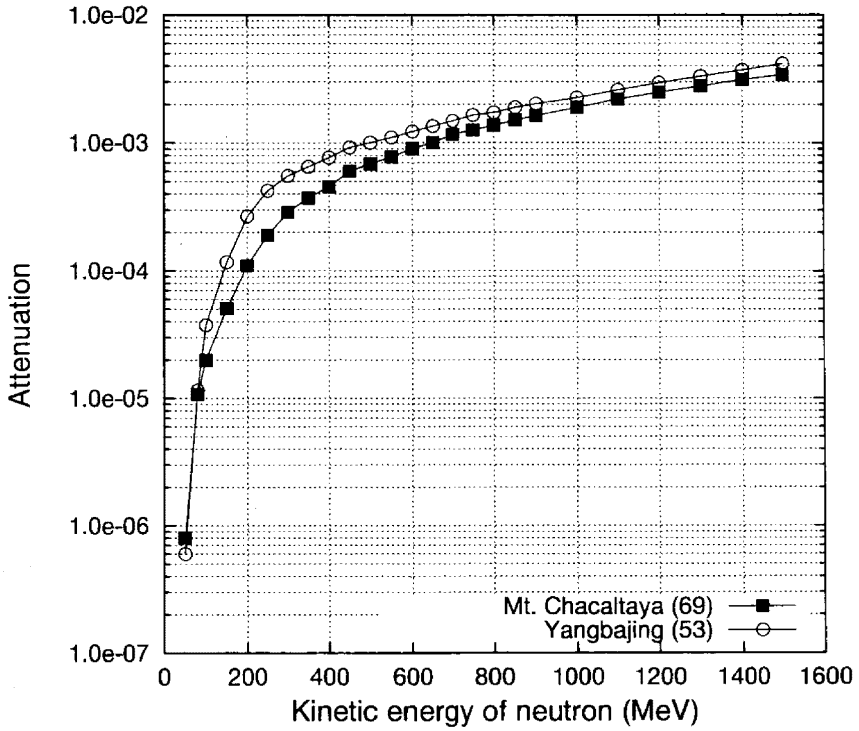

Figure 44: Two attenuation curves for solar neutrons corresponding to the altitudes of Mt. Chacaltaya and Yangbajing. The zenith angle in degrees of the sun for each solar flare event is given in parentheses.

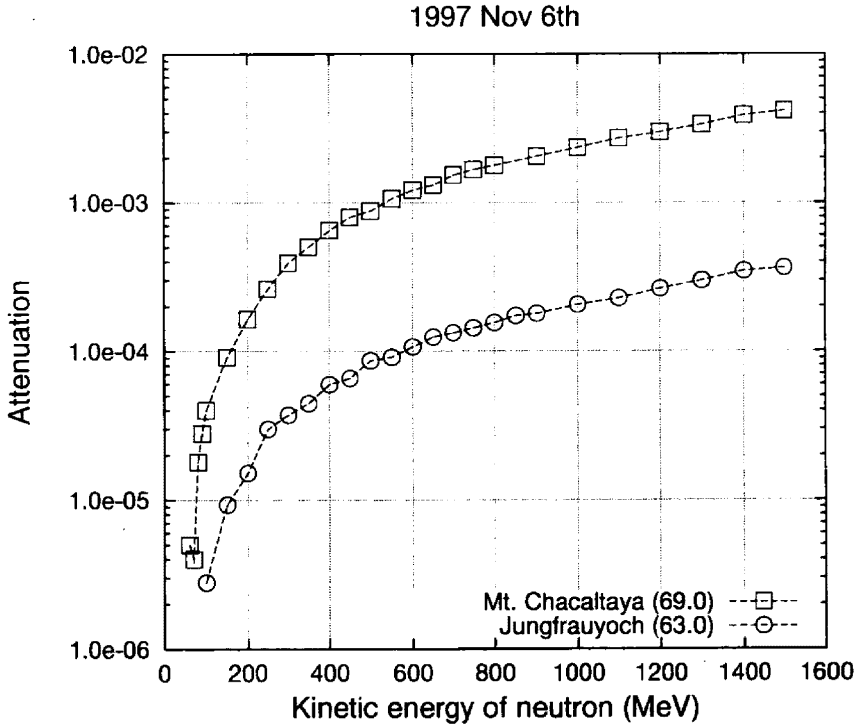

Figure 45: Comparison of two attenuation curves calculated by Monte Carlo simulations. Squares and circles represent the attenuation of solar neutrons at Mt.Chacaltaya and Gornergrat respectively on 1997 November 6th.

X ray emission detected by BATSE. In Table 11, the excess count and the percentage in the flare time are shown. The average energy of each bin is calculated using equation (5) and they turn out to be 176, 162, 150, and 140 MeV respectively. The detection efficiency and attenuation rate of solar neutrons are calculated by Monte Carlo simulation. Fitting the data points with a power law form of $C \times (E_n/100)^{\alpha}$ using the least squares method, C and α become

$$\begin{aligned} C &= (5.88 \pm 4.36) \times 10^6 \quad /\mathrm{MeV/m^2} \\ \alpha &= (-3.28 \pm 1.62). \end{aligned}$$

From the other energy channels, which correspond to > 40 MeV and > 120 MeV, almost the same enhancements were obtained and they are shown in Figure 47. The data obtained by the channel > 160 MeV were not used for calculations of neutron flux because of the lack of statistics. The agreement among the excesses from the three energy threshold channels are quite good. The power law index obtained from the > 40 MeV and > 120 MeV data points turned out to be -3.29 ± 2.89 and -3.26 ± 2.66, respectively.

Table 11: The excess between 11:41:30 UT and 11:43:30 UT on 1997 November 6th event.

time (UT)	ΔE_n(MeV)	$\Delta N(>80\mathrm{MeV})(/\mathrm{m^2})$	Excess (%)
11:41:30 - 11:42:00	169 - 184	139	1.97 ± 0.86
11:42:00 - 11:42:30	156 - 169	164	2.33 ± 0.86
11:42:30 - 11:43:00	145 - 156	172	2.44 ± 0.86
11:43:00 - 11:43:30	135 - 145	104	1.49 ± 0.85

As mentioned in the previous section, there are questions associates with this event. The main problem concerns the detection time. The detector showed an increase of signal about 10 minutes before the major X9.4 solar flare. As for the clear signals, the C4.7 solar flare is thought to be responsible for the excess, because the flare started at 11:31 UT and continued until 11:44 UT. Unfortunately, the Yohkoh satellite was in the shadow of the earth, and OSSE/CGRO did not detect remarkable enhancement during this time (Yoshimori private communication). However, BATSE recorded an excess in the X ray region (25 keV - 59 keV) which related to C4.7 solar flare detected by GOES as shown in Figure 31. Although X ray emission is associated with

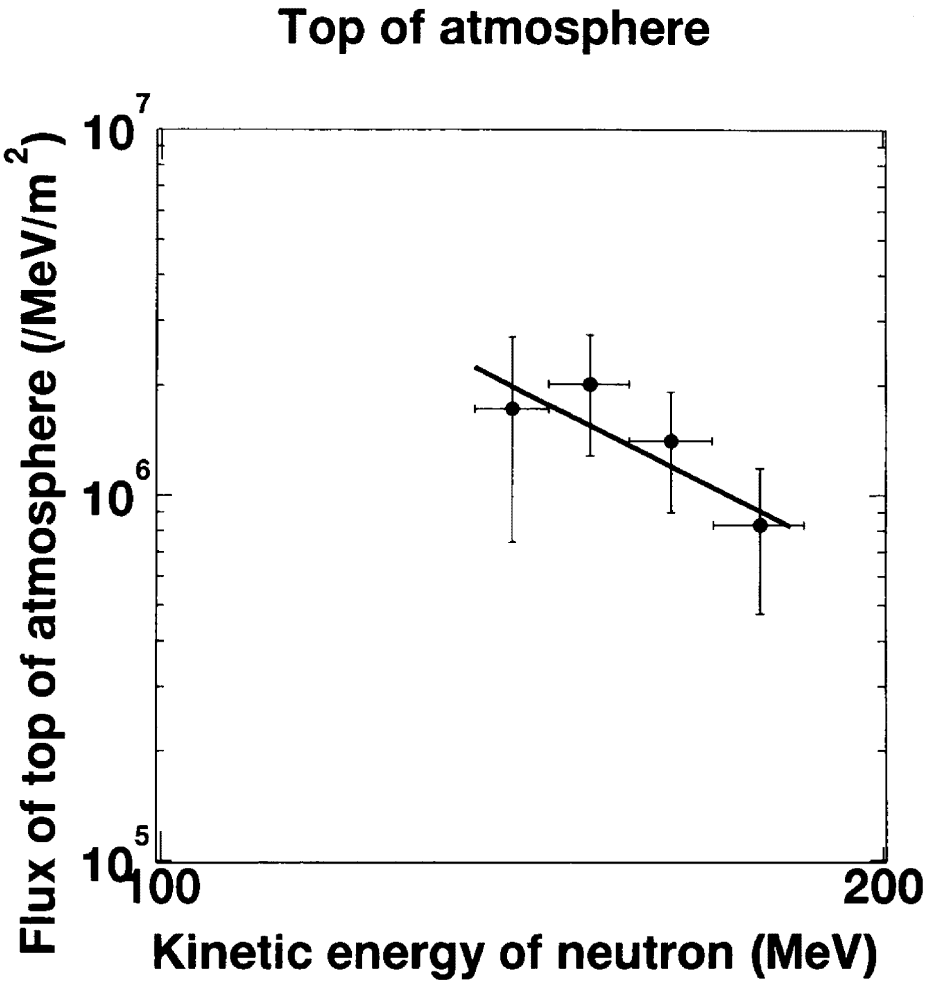

Figure 46: The observed neutron flux at the top of the atmosphere for the 1997 November 6th event. The horizontal axis shows the kinetic energy of neutrons in MeV. The solid line shows the fit to the power law form $C \times (E_n/100)^{\alpha}$.

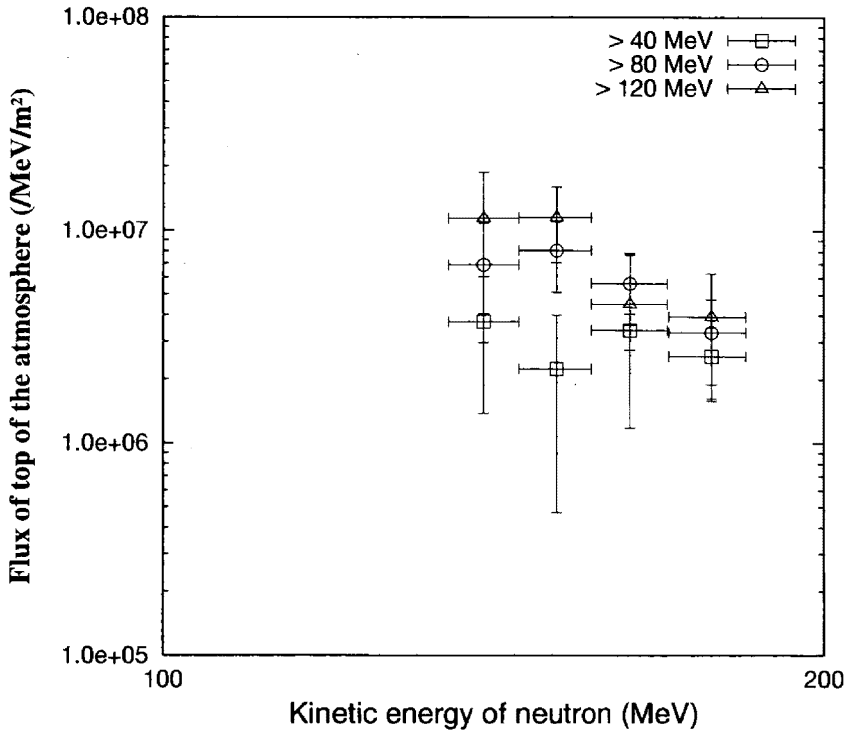

Figure 47: Comparison of the neutron flux derived from three different channels of the threshold energy .

electron acceleration processes, there is a possibility that ion acceleration did also occur at the time. But, no neutron capture line(2.223 MeV) was observed between 11:31 UT and 11:44 UT, while the line gamma rays were observed in the main phase of the X9.4 flare. Therefore, there remains a possibility that no neutron production occurred, which would be consistent with the absence of a neutron capture line. However, there is another possibility, namely that the neutron capture line was strongly masked by the solar atmosphere preventing its detection.

The neutron capture line is attenuated via Compton scattering in solar ambient matter. In particular, in a case in which the location of the emission of the line is at the limb of the solar surface(limb flare), the line is strongly attenuated in comparison with disk flares. This phenomenon is called "limb darking"(Wang & Ramaty, 1974 [110]; Yoshimori et al., 1983 [111]). According to Hua and Lingenfelter(1987 [69]), the intensity of the 2.223 MeV neutron capture line is strongly reduced through absorption by the solar atmosphere when the solar heliocentric angle exceeds 75°. This becomes more apparent when accelerated protons have a harder energy spectrum. Since the solar flare occurred near the limb of the sun (S18W63), it is possible that

Table 12: The composition of the photosphere and the corona (Reams, 1999 [112]). All values in the Table are normalized by the hydrogen value.

	Photosphere	Corona
H	1	1
He	0.098	0.036
C	3.5×10^{-4}	$3.0. \times 10^{-4}$
N	9.3×10^{-5}	7.9×10^{-5}
O	7.4×10^{-4}	6.4×10^{-4}
Ne	1.2×10^{-4}	9.7×10^{-5}
Mg	3.8×10^{-5}	1.2×10^{-4}
Si	3.6×10^{-5}	9.7×10^{-5}
Fe	3.2×10^{-5}	8.5×10^{-5}

limb darking may have happened when the accelerated proton hit the solar surface horizontally.

Estimation of the escape probability of neutrons and 2.223 MeV photons of neutron capture line from the solar atmosphere can be calculated in the following way. The composition of the solar atmosphere is shown in Table 12(Reams, 1999 [112]). The values in Table 12 are normalized by hydrogen abundance. In the calculation, the composition of the photosphere was used. According to the standard solar atmosphere model, the number density of hydrogen in the solar atmosphere has been expressed essentially by an exponential function. In this function, the scale height is chosen as 85 km above the upper photosphere, but the scale height changes at around 300 km depth from the chromosphere and becomes 900 km. The following formulae were used for the number density distribution of hydrogen in the solar atmosphere.

$$\rho(z) = \begin{cases} 5.0 \times 10^{17} \exp(-(z+300)/85) & z > \text{-300 km} \\ 5.0 \times 10^{17} \exp(-(z+300)/900) & z < \text{-300 km} \end{cases} \quad (6)$$

where z is measured from boundary between the photosphere and the chromosphere. Considering the element abundances shown in Table 12 and using equation (6), column density of the solar atmosphere is calculated as a function of the depth z and shown in Figure 48. The horizontal axis represents the depth from the top of the photosphere in km. The depth $z = 0$ shown by

the dashed vertical line in Figure 48, represents the boundary between the photosphere and the chromosphere. Positive(negative) depth values indicate that the point is in the chromosphere(photosphere).

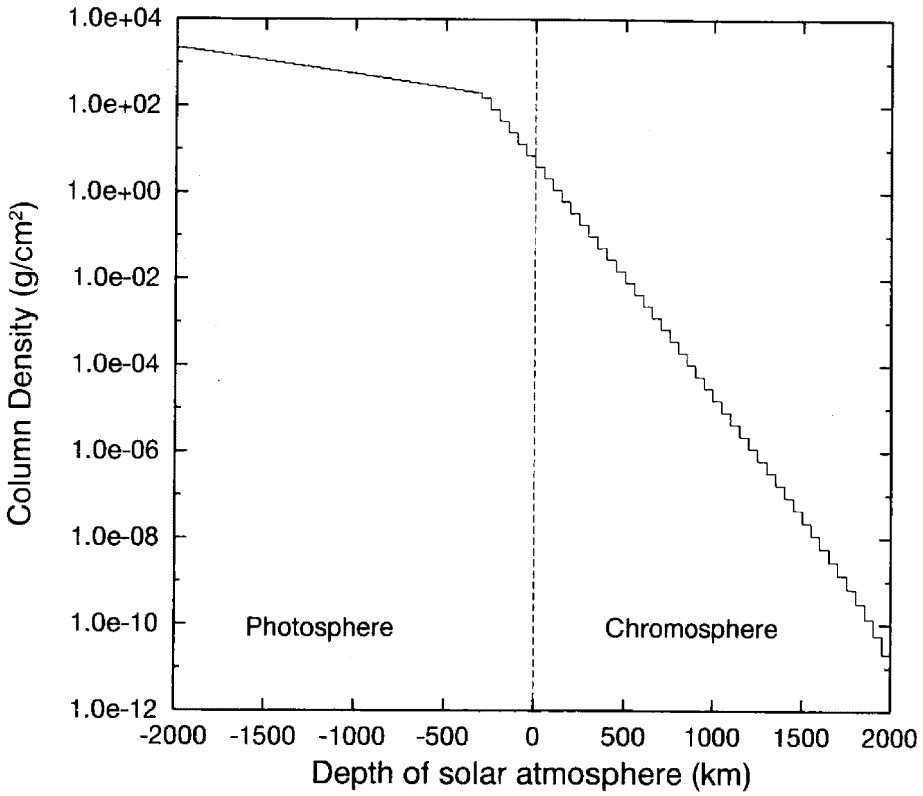

Figure 48: The column density of the solar atmosphere taking account of the element abundances listed in Table 12. The vertical dashed line indicates the boundary between the photosphere and the chromosphere. The horizontal axis shows the depth from this boundary. Positive depth means above the boundary and the chromosphere, while negative z value corresponds to below the boundary and the photosphere.

The attenuation length for 2.223 MeV photons in hydrogen gas is estimated to be 10g/cm^2 (Groom et al., 2000 [113]). The photosphere consists of elements given in Table 12 and so the effective atomic weight A_{eff} can be obtained using $A_{eff} = \sum_i p_i A_i$, where p_i and A_i show relative weight and atomic mass number of ith component. From this relation, A_{eff} of the solar atmosphere turns out to be 1.30. Furthermore, the attenuation length is proportional to $A^{\frac{1}{3}}$ and so the attenuation length taking account of the solar atmospheric composition, λ_{photon}, is 11g/cm^2. The total cross section σ_{np} between hydrogen and neutron with energies of 100 MeV and 200 MeV is 76 and 42 mb, respectively. Using these values and the formula

$1.0/N_A\sigma_{np} \times (A_{eff}/1)^{\frac{1}{3}}$ where N_A is Avogadro constant, the mean free path of neutrons λ_n in the solar atmosphere turns out to be 24 and 43 g/cm^2 at 100 MeV and 200 MeV, respectively.

Figure 49 represents the result of calculation for the escape probability of neutrons and 2.223 MeV photons. In the case that production region of neutrons and 2.223 MeV photons is in the region $z > 0$ in the Figure, they can move almost freely in the chromosphere and escape from their production region. In the region beyond 150 km above the boundary ($z > 150$km), it is still easy for $> 99\%$ neutrons and 2.223 MeV photons to escape. However, when the production region is in the photosphere, the escape probabilities of these neutrons and photons rapidly decrease and the difference of the escape probability between neutrons and 2.223 MeV photons becomes remarkable. According to Hua and Lingenfelter (1987 [69]), the region of the highest production of neutrons is estimated at around 200 km and 300 km inside from the boundary region where accelerated protons have a power index less than 4. At a depth of 200 km (*i.e.*, $z = -200$ km), the ratio of the escape probability of 100 MeV and 200 MeV neutrons to that of 2.223 MeV photons is 25 and 82, respectively. With regard to the production region of the 2.223 MeV photons, it is different from that of neutrons, because the 2.223 MeV photons are produced by the capture process of thermalized neutrons via interaction with ambient protons. Therefore, the production region for the 2.223 MeV photons is deeper than that for neutrons. According to the calculations of Hua and Lingenfelter (1987 [69]), the depth distribution of the captured line gamma ray is shifted approximately 100 km - 200 km deeper in comparison with the maximum neutron productivity region. Taking account of this shift effect of the 2.223 MeV photons, the escape probability of the line gamma rays would be much smaller. In Figure 50, the ratios of the escape probability of the neutrons to that of the 2.223 MeV photons are given. For example if the production of neutrons occurs at $z = -300$ km and the 2.223 MeV photons at $z = -400$ km, the ratio between the escape probability of neutrons (100 MeV) and photons(2.223 MeV) is estimated as 4.0×10^8.

In this event, we assume that the 2.223 MeV photons are produced at the depth of about 400 km $-$ 500 km below the boundary in the photosphere. Despite high ratio of the escape probability of neutrons to that of the 2.223 MeV photons at depths greater than 500 km ($z < -500$ km), the productivity

of both neutrons and 2.223 MeV photons rapidly decreases below $z < -500$ km. From the calculation for the escape probability of neutrons and captured line gamma rays in this thesis, it can be concluded that the 2.223 MeV photons must be masked in this event since the neutron production region must be deeper than 300 km from the boundary between the photosphere and the chromosphere.

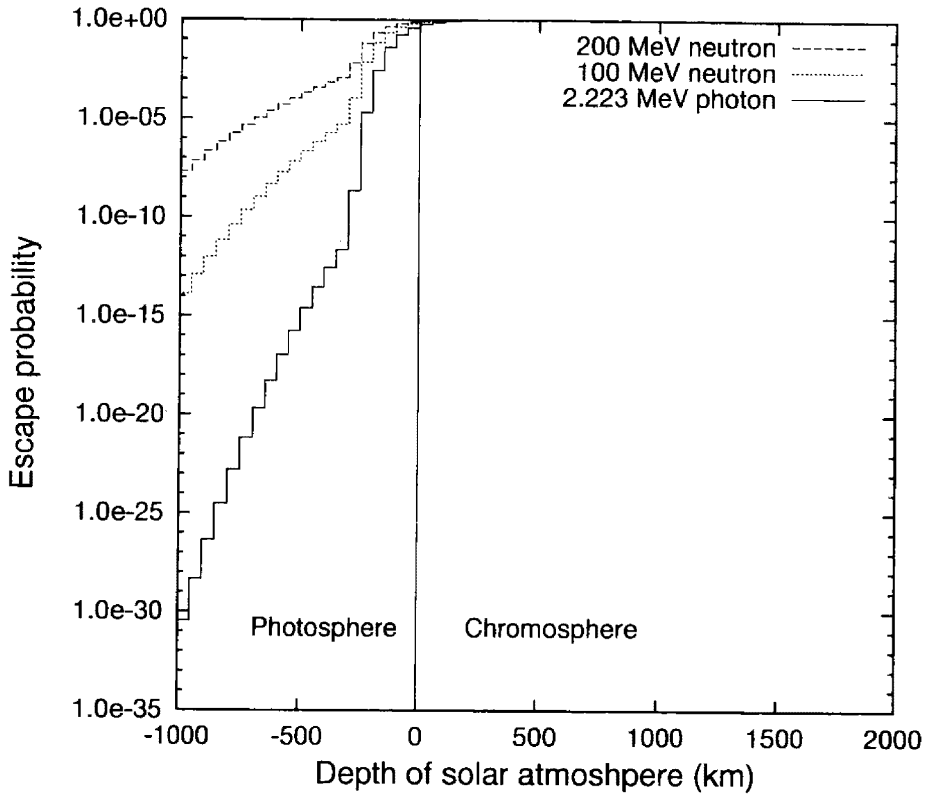

Figure 49: The escape probability of neutrons and 2.223 MeV photons from the solar atmosphere. The solid line represents the probability of 2.223 MeV photons. The dashed and dotted lines correspond to those of neutrons with energies of 200 MeV and 100 MeV.

Until now, there has not been no report of observational evidence for such a masking effect. However, for this event, a clear signal was obtained by the Bolivian solar neutron detector in association with this solar flare, which supports our argument above. Another possibility to explain this 6.8σ signal, is that neutrons which are not associated with solar flare may arrive and produce the signal in the detector. To the present time, the existence of such neutrons with a non-solar flare origin has not been reported either for solar phenomena or astrophysical phenomena. However, there has been some interesting reports about solar energetic particles in association with

solar phenomena(Cliver et al., 1983 [114]; Kahler et al., 1986 [115]).

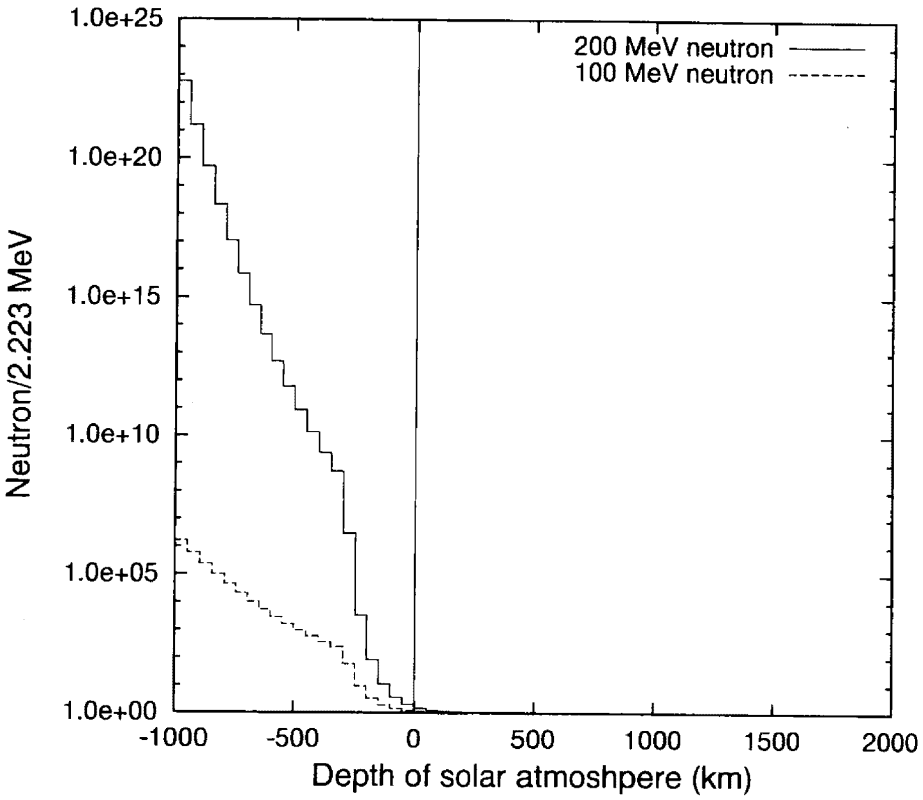

Figure 50: The ratio of the escape probability between neutrons and 2.223 MeV photons. The solid and dashed lines represent the ratio of the neutrons with energies of 200 MeV and 100 MeV to the photons respectively.

6 Conclusions

For the purpose of elucidating the ion acceleration mechanism at the solar surface, a new type of solar neutron detector was installed on high mountains around the world and continuous observation of solar neutrons has been made. Construction of the network of the solar neutron detectors was started in 1990 and seven solar neutron detectors have been installed up to 1998. The new solar neutron detectors have advanced capabilities which classic neutron monitors do not have.

The new solar neutron detector has three major capabilities, which are **(1) Discrimination of incident kinetic energies of neutrons deposited in the detector.**

The traditional neutron monitor responds to neutrons with kinetic energies of $>$ a few MeV, which is a wide energy range. If strong flux of solar neutrons enter the neutron monitor, the neutron signal can be detected by the neutron monitor without being masked by background count. However, in the case of a weak signal, the excess due to the weak neutron flux would be buried within a large number of background counts due to the wide sensitivity of detector. Therefore, the measurement of energy of incident neutrons is indispensable for reducing the background noise level.

As another example why it is important to measure the energy of the neutrons, we consider the interpretation of the 1982 June 3rd event mentioned in Section 2. The problem was whether the neutron production occurred at the solar surface impulsively or continuously. In this event, the neutron monitors at Jungfraujoch detected signals due to solar neutrons between 11:43 UT and 11:55 UT (see Figure 6). The increase in the signals detected by the neutron monitors between 11:50 UT and 11:55 UT could not be explained by original authors (Chupp et al. [34]) without introducing continuous neutron production at the solar surface. However, Muraki et al. [65] were able to explain the increase of the neutron monitors by assuming impulsive neutron production. If impulsive neutron production occurred at the time of the first peak of high energy gamma ray emissions($>$ 25 MeV) between 11:41 UT and 11:42 UT as shown in the middle of Figure 6 (impulsive phase), solar neutrons which had the kinetic energy of $<$ 100 MeV could cause the signals between 11:53 UT and 11:55 UT since neutrons with energies of 100 MeV could arrive at the earth 11 minutes after the arrival of light.

The original authors rejected this possibility, because such low energy neutrons could not reach the neutron monitors at Jungfraujoch according to their attenuation model (Debrunner model). Consequently, the original authors adopted the view that the neutron production occurred not only in the impulsive phase but also in an extended phase. However, according to the Shibata model, neutrons with the energy of < 100 MeV could reach the detector, therefore, Muraki et al. adopted the impulsive neutron production scenario.

The difference between two interpretations could be resolved if the neutron monitors could measure the energy of the incident neutrons. If we can obtain information on the kinetic energy of neutrons, the production time of the neutrons at the solar surface can be identified from the information. Therefore, a solar neutron detector must have the capability to measure the energy of incident neutrons since we must determine whether the neutron production occurs at the solar surface impulsively or continuously in order to understand the ion acceleration mechanism.

(2) Measurement of arrival direction of solar neutrons.

The ability to measure the arrival direction of solar neutrons makes it possible to reduce the background as well as to determine the source of the signal. Secondary neutrons produced by galactic cosmic rays enter the detector as omnidirectional flux. However, solar neutrons arriving at the top of the atmosphere will still be detected as coming from the solar direction regardless of scattering. For this reason, if the solar neutron detector has the ability to measure the arrival direction, the signal of solar neutrons from the sun can be detected by reducing the background of the omnidirectional secondary neutrons. This would permit us to obtain a high signal-to-noise ratio.

(3) Separation of neutrons from charged particles.

Particles produced by the galactic cosmic rays comprise not only neutrons but also charged particles, *i.e.* electrons, muons and pions. Of course, the neutron monitor has an external reflector to reject low energy charged particles. However, according to the results of Clem and Dorman (2000 [93]), it was found that the neutron monitor also had high detection efficiency for charged hadronic components with kinetic energies above 1 GeV at same level as for neutrons. The background of charged particles also enters the solar neutron detector. Therefore, it is very important to reject charged par-

ticles in order to improve the signal to noise ratio. For this purpose, all our solar neutron detectors have been equipped with anti counters, which mainly consist of proportional counters.

A solar neutron detector which had all three functions mentioned above was installed at Yangbajing in Tibet in October, 1998. Fortunately a moderate level X3.3 solar flare occurred at around local noon for Yangbajing on 1998 November 28th just after its installation. The start and end time of the flare were observed by the GOES satellite as 4:54 UT and 6:13 UT, respectively. The Tibet solar neutron detector detected a signal in association with the solar flare. Quite surprisingly, the signal which should be caused by solar neutrons was detected with a significant level of 4.2σ only from the solar direction and no significant signal was detected from the anti-solar direction at the time of the flare. Making use of the ability to measure the arrival direction of incoming neutrons, the signals due to solar neutrons were discovered by reducing the background of neutrons efficiently. The detection of this signal suggested that the energy range of solar neutrons attributed to the signals must be between 400 MeV and 2 GeV if solar neutrons were produced impulsively at the solar surface. Those neutrons were detected between 5:38 UT and 5:41 UT. This time interval coincided with the time in which radio and hard X ray emissions were detected using the Nobeyama radio heliograph and Yohkoh respectively and complex loop structures were also detected in this time interval by soft X ray telescope on board Yohkoh. Therefore, we suggest the simultaneous acceleration of the electrons and ions at the solar surface.

Furthermore, if solar neutrons had been emitted with an energy spectrum of power law shape, $C \times (E_n/300)^{\alpha}$, the constant C and α would have been

$$\begin{aligned} C &= (6.14 \pm 4.88) \times 10^4 \qquad /\mathrm{MeV/m^2} \\ \alpha &= -3.47 \pm 2.60 \end{aligned}$$

at the top of the atmosphere. The detection of solar neutrons using the Tibet solar neutron detector for this event proved that the measurement of the arrival direction of neutrons was very effective method for detecting weak solar neutron flux.

Another interesting event was observed on 1997 November 6th at 11:49 UT when a X9.4 solar flare occurred. At Mt. Chacaltaya in Bolivia, the solar

neutron detector detected clear signals. However, one of the enhancements was detected about 10 minutes before the X9.4 solar flare. It was not clear that solar flare was responsible for the signal. If solar neutrons had really been produced at the solar surface and arrived at the earth, the solar neutrons were produced in association with the preceding C4.7 solar flare with no gamma ray emissions. The detection time of the signal at Mt. Chacaltaya (11:40 – 11:43 UT) and the occurrence time of the C4.7 solar flare (11:31 – 11:44 UT) did correlate with each other. Up till now, no solar neutron observations have been reported in association with a C class solar flare.

From calculation of escape probability of neutrons and 2.223 MeV gamma ray lines from the solar atmosphere, it was found that the 2.223 MeV lines were largely attenuated in the solar atmosphere if production region of the line were deeper than 300 km from the boundary between the photosphere and the chromosphere. Therefore, the calculation also showed that there was a possibility that neutrons could be detected without detecting the 2.223 MeV lines if neutrons were produced in the solar atmosphere deeper than 300 km on 1997 November 6th event. From a gamma ray observations by CGRO/COMPTEL on January 20, 2000, it has been suggested that C class solar flares may cause the ion acceleration [106]. If the signal for this event was related to the C4.7 solar flare, this is the first discovery of solar neutrons in association with C class solar flare. If this is real, the derived neutron spectrum is of the form

$$(5.88 \pm 4.36) \times 10^6 \times \left(\frac{E_n}{100}\right)^{-3.28\pm1.62} \qquad /\mathrm{MeV/m^2}$$

at the top of the atmosphere.

Considering the two events described in this thesis, it was found that atmospheric refraction effect played an important role in the observation of solar neutrons, especially, for the case that arriving solar neutrons had large incident zenith angles at the top of the atmosphere. The zenith angle of the sun for these events was 69°(1997 November 6th) and 53°(1998 November 28th), respectively. According to the present Monte Carlo simulation taking account of the atmospheric refraction effect, *it was found that the survival probability of solar neutrons in the atmosphere was higher than was previously thought.* Particularly, for solar neutrons with zenith angle greater than 30°, this effect must be taken into account and we must consider the solar neutron observations in the early morning, the late evening and during the winter.

The Monte Carlo calculations in this thesis show that there is a possibility of detecting solar neutrons even in such "unsuitable" conditions.

As mentioned above, the effect of the increase of the survival probability due to the refraction effect in the atmosphere and usefulness of directional measurements using the solar neutron telescope as for 1998 November 28th event were demonstrated. Therefore, future solar neutron observations on the ground should be carried out using instrument with the ability to measure both the energy and direction of the incident neutrons. It is necessary to upgrade some of the existing solar neutron detectors which do not have the capability to determine direction of arrival.

As the solar activity still continues to be high until 2003, interesting events similar to the two events in this thesis will certainly be detected in the future. Furthermore, the ground network of solar neutron detectors and neutron monitors must continue the observation of solar neutrons in association with solar flares. At present, there is no satellite operating with an ability to detect solar neutrons in association with solar flares because of the re-entry of the CGRO satellite on 2000 June 4th. However, there are presently plans to design a new type of solar neutron detector which has the capability of detecting solar neutrons in space(Imaida et al., 1999 [116]; Ohno, 2001 [117]; Ryan et al., 1999 [118]). Furthermore, HESSI which has an aim of studying particle acceleration in solar flares will be launched in 2001. Combining various data sets obtained by satellites such as HESSI, Yohkoh and our solar neutron detector for space observation as well as ground based observation, I hope that the essence of the ion acceleration mechanism in association with solar flare will ultimately be elucidated.

Acknowledgment

I am grateful to Prof. Y. Muraki. He gave me, not only the opportunity to observe solar neutrons using solar neutron detectors, but also to take part in many other experiments. Of course, he gave me considerable advice for writing this thesis as well as for analyzing data obtained by the solar neutron detectors.

Prof. T. Yuda suggested our group for construction of the Tibet solar neutron detector when he belonged to Institute for Cosmic Ray Research, University of Tokyo. Thanks to his suggestion, I obtained fruitful experience to go to Yangbajing in Tibet and install the new solar neutron detector.

I deeply thank Associate Prof. Y. Matsubara and Associate Prof. K. Masuda for helping me in my work and experiments. They also gave me considerable knowledge about cosmic ray physics and encouraged me to carry out research in cosmic ray physics through their lecture and private communication. I also thank Assistant T. Sako for his advice in my work and useful discussions on study of solar neutrons as well as that of cosmic rays.

I thank Associate Prof. Shibata (Chubu University) and Dr. T. Koi (International Space Radiation Laboratory National Institute of Radiological Sciences) for useful advice and information on simulation and references. Assistant Y. Katayose (Yokohama National University) also taught me about the simulation using GEANT 3. Prof. Rostoker read and corrected my manuscript.

I greatly and deeply thank those people who joined in construction of international network for solar neutron observation and have maintained each solar neutron detector.

I thank graduates of neutron group of the cosmic ray division in the Solar Terrestrial Environment Laboratory, Mr. S. Ohno, Miss K. Wanatabe and Mr. D. Yamamoto. They discussed the study of solar neutrons with me through regular seminar. I also thank other graduates of cosmic ray division in STE Lab., Mr. T. Murata, Miss S. Noda, Mr. T. Sumi, Mr. M. Kato, Mr. T. Noguchi, H. Toyoizumi, Mr. T. Uemura, Mr. T. Takami and Miss R. Yamada. They supported and helped my work.

Finally, I greatly thank my family for supporting my life as well as my work. Especially, I thank my parents very much for let me continue studying physics.

References

[1] Asakimori, K. *et al.*, *Astrophys. J.* **502**, p. 278 (1998).

[2] Bird, D.J.,*et al.*, *Phys. Rev. Lett.*, **71**, p. 3401 (1993).

[3] Nagano, M. & Watson, A.A., *Rev. Modern Phys.* **72**, 3, (2000).

[4] Koyama, K., *et al.*, *Nature* **378**, p. 255 (1995).

[5] Tanimori, T., *et al.*, *Astrophys. J. Letters* **497**, p. L25 (1998).

[6] Naito, T., *et al.*, *Astrophys. J.* **320**, 4, p. 205 (1998).

[7] Vacanti, G., *et al.*, *Astrophys. J.* **377**, p. 467 (1991).

[8] Tanimori, T., *et al.*, *Astrophys. J. Letters* **492**, p. L33 (1998).

[9] Amenomori, M., *et al.*, *Astrophys. J. Letters* **525**, 2, p. L93 (1999).

[10] de Jager, O.C., *et al.*, *Astrophys. J.* **457**, p. 253 (1996).

[11] Kane, S.R.,*et al.*, *Astrophys. J. Letters* **446**, p. L47 (1995).

[12] Colgate, S.A., *Astrophys. J.* **221**, p. 1068 (1978).

[13] Choe, G.S.& Cheng, C.Z., *Astrophys. J.* **541**, 1, p. 449 (2000).

[14] Tsuneta, S., *et al.*, *Astrophys. J.* **478**, p. 787 (1997).

[15] Shibata, K., *Astrophys. Space Sci.* **264**, 1/4 p. 129 (1998).

[16] Kocharov, G.E., *et al.*, *Adv. Space Res.* **25**, 9, p. 1817 (2000).

[17] Nishio, M., *et al.*, *Adv. Space Res.* **25**, 9, p. 1791 (2000).

[18] Simnett, G. M., *Societa Astrono. Italiana, Memorie* **65**, p359, (1991).

[19] Antiochos, S.K., *et al.*, *Astrophys. J.* **510**, 1, p. 485 (1999).

[20] Innes, D.E., *et al.*, *Solar Phys.* **186**, 1, p. 337 (1999).

[21] Cliver, E. W., *et al.*, *Astrophys. J.* **379**, p. 741 (1991).

[22] Trottet, G., *et al.*, *Astron. Astrophys.* **288**, p. 647 (1994).

[23] Chupp, E.L., *Nucl. Phys. B Proceed. Suppl.* **39**, p. 3 (1995).

[24] Trottet, G., *et al.*, *Astron. Astrophys.* **334**, p. 1099 (1998).

[25] Laitinen, T., *et al.*, *Astron. Astrophys.* **360**, p. 729 (2000).

[26] Masuda, S., *et al.*, *Nature* **371**, p. 495 (1994).

[27] Ramaty, R., *et al.*, *Astrophys. J. Suppl.* **40**, p. 487 (1979).

[28] Cliver, E.W. *et al.*, *18th Inter. Cosmic Ray Conf.(Bangalore)* **10**, p. 342 (1983).

[29] Yoshimori, M., *et al.*, *Astrophys. J. Suppl.* **90**, 2, p. 639 (1994).

[30] Biermann, V.L., *et al.*, *Z. Naturforshch.* **6a**, p. 47 (1951).

[31] Lingenfelter, *et al.*, *J. Geophys. Res.* **70**, p. 4077 (1965).

[32] Lingenfelter, *et al.*, *J. Geophys. Res.* **70**, p. 4087 (1965).

[33] Vestrand, W.T., *et al.*, *Astrophys. J. Suppl.* **120**, p. 409 (1999).

[34] Chupp, E.L., *et al.*, *Astrophys. J.* **318**, p. 913 (1987).

[35] Takahashi, K., *et al.*, *22nd Inter. Cosmic Ray Conf.(Dublin)* **3**, p. 37 (1991).

[36] Muraki, Y., *et al.*, *Astrophys. J. Letters* **400**, p. L75 (1992).

[37] Struminsky, A., *et al.*, *Astrophys. J.* **429**, p. 400 (1994).

[38] Muraki, Y., *et al.*, *J. Geomag. Geoelectr.* **47**, p. 1073 (1995).

[39] Usoskin, I.G., *et al.*, *Ann. Geophysicae* **15**, p. 375 (1997).

[40] Lockwood, J.A. & Debrunner, H., *Space Sci. Rev.* **88**, 3, p. 483 (1999).

[41] Shea, M.A., *et al.*, *Geophys. Res. Letterss* **18**, p. 1655 (1991).

[42] Pyle, K.R. & Simpson, J.A., *22nd Inter. Cosmic Ray Conf.(Dublin)* **3**, p. 53 (1991).

[43] Shibata, S., *et al.*, *23rd Inter. Cosmic Ray Conf.(Calgary)* **3**, p. 95 (1993).

[44] Debrunner, H., *et al.*, *Astrophys. J.* **479**, p. 997 (1997).

[45] Ramaty, R., in *Particle Acceleration Mechanisms in Astrophysics* edited by Arons, J., Max, C. & McKee C., New York, AIP, p. 135 (1979).

[46] Miller, J.A., *et al.*, *Astrophys. J.* **361**, p. 701 (1990).

[47] Bell, A.R., *Mon. Not. R. astr. Soc.* **182**, p.147 (1978).

[48] Bell, A.R., *Mon. Not. R. astr. Soc.* **182**, p.443 (1978).

[49] Ellison D.C. & Ramaty, R., *Astrophys. J.* **298**, p.400 (1985).

[50] Tsuneta, S., *Astrophys. J.* **290**, p. 353, (1985).

[51] Anastasiadis, A., *et al. Astrophys. J.* **489**, p. 367, (1997).

[52] Akimov V.V., *et al.*, *Solar Phys.* **166**, p. 107 (1995).

[53] Ramaty, R., *et al.*, *Astrophys. J. Letters* **455**, p. L193 (1995).

[54] Chupp, E.L., *et al. Astrophys. J. Letters* **263**, p. L95 (1982).

[55] Forrest, D.J. & Chupp, E.L., *Nature* **305**, p. 291 (1983).

[56] Ramaty, R., *et al.*, *Astrophys. J. Letters* **273**, p. L41 (1983).

[57] Lingenfelter, R.E.., *et al.*, *Proc. 18th Inter. Cosmic Ray Conf. (Bangalore)* **4**, p. 101 (1983).

[58] Chupp, E.L., *et al.*, *Proc. 18th Inter. Cosmic Ray Conf. (Bangalore)* **10**, p. 334 (1983).

[59] Efimov, Y.E., *et al.*, *Proc. 18th Inter. Cosmic Ray Conf. (Bangalore)* **10**, p. 276 (1983).

[60] Guglenko, V.G.., *et al.*, *Astrophys. J. Suppl.* **73**, p. 209 (1990).

[61] Ramaty, R., *et al.*, *Astrophys. J. Letters* **316**, p. L41 (1987).

[62] Evenson, P., *et al.*, *Proc. 18th Inter. Cosmic Ray Conf. (Bangalore)* **4**, p. 97 (1983).

[63] Ruffolo, D., *Astrophys. J.* **382**, p. 688 (1991).

[64] Shibata, S., *J. Geophys. Res.* **99**, A4, p. 6651 (1994).

[65] Muraki, Y., *et al.*, *Proc. Suppl. Nucl. Phys. B* **60**, p. 3 (1998).

[66] Mandzhavidze, N. & Ramaty, R., *Astrophys. J.* **389**, p. 739 (1992).

[67] Murphy, R.J., *et al.*, *Astrophys. J. Suppl.* **63**, p. 721 (1987).

[68] Chupp, E.L., *Ann. Rev. Astron. Astrophys.* **22**, p. 359 (1984).

[69] Hua, H.-M. & Lingenfelter, R.E., *Solar Phys.* **107**, p. 351 (1987).

[70] Ramaty, R., *et al.*, *Astrophys. J.* **510**, p. 1011 (1997).

[71] Murphy, R.J., *et al.*, *Astrophys. J.* **510**, p. 1011 (1999).

[72] Hua, H.-M. & Lingenfelter, R.E., *Astrophys. J.* **323**, p. 779 (1987).

[73] Debrunner, H. & Brunberg, E.A., *Can. J. Phys.* **46**, p. 1069 (1968).

[74] Dorman L.I. *et al.*, *Proc. 26th Inter. Cosmic Ray Conf.(Salt Lake City)* **3**, p. 367 (1999).

[75] Dorman L.I. *et al.*, *J. Geophys. Res.* **104**, A10, p. 22417 (1999).

[76] Valdés-Galicia, J.F., *et al.*, *Solar Phys.* **191**, 2, p. 409 (2000).

[77] Miyazaki, H., *Proc. the Cosmic-Ray Res. Sec. Nagaya Univ.* **Vol. 33**, 1, p. 37 (in Japanese) (1992).

[78] Matsubara, Y., *et al.*, *Proc. 23rd Inter. Cosmic Ray Conf.(Calgary)* **3**, p. 139 (1993).

[79] Muraki, Y., *et al.*, *Proc. 25th Inter. Cosmic Ray Conf.(Durban)* **1**, p. 53 (1997).

[80] Matsubara, Y., *et al.*, *Proc. 25th Inter. Cosmic Ray Conf.(Durban)* **1**, p. 37 (1997).

[81] Flückiger, E.O., *et al.*, *in Medina, J. (ed.), rayos cósmicos 98, Proc. 16th European Cosmic Ray Symposium, Departamento de Fisica, Universidad de Alcalá, Spain* , p. 219 (1998).

[82] Tsuchiya, H., *Proc. the Cosmic-Ray Res. Sec. Nagaya Univ.* **Vol. 39**, 1, p. 241 (in Japanese) (1998).

[83] Hoshida, T., *et al.*, *Proc. 26th Inter. Cosmic Ray Conf.(Salt Lake City)* **6**, p. 38 (1999).

[84] Katayose, T., *et al.*, *Proc. 26th Inter. Cosmic Ray Conf.(Salt Lake City)* **6**, p. 58 (1999).

[85] Matsubara, Y., *et al.*, *Proc. 26th Inter. Cosmic Ray Conf.(Calgary)* **6**, p. 46 (1999).

[86] Tsuchiya, H. *et al.*, *Proc. 26th Inter. Cosmic Ray Conf.(Salt Lake City)* **3**, p. 363 (1999).

[87] Ter-Antonyan, V.S., *Thesis submitted to Yereven State Univ for Bachelor degree.* (2000).

[88] Tsuchiya, H. *et al.*, *Nucl. Inst. Meth. A* in press (2000).

[89] Debrunner, H. *et al.*, *Proc. 18th Inter. Cosmic Ray Conf.(Bangalore)* **4**, p. 75 (1983).

[90] Debrunner, H. *et al.*, *Nucl. Inst. Meth. A* **278**, p. 573 (1989).

[91] Usoskin, I.G.*et al.*, *Ann. Geophysicae* **15**, p. 375 (1997).

[92] Hatton, C.J., *Progress in Elementary Particle and Cosmic Ray Physics* **Vol. X**, edited by Wilson, J.G. and Wouthuysen, S.A., p. 1, North-Holland, Amsterdam (1971).

[93] Clem, J.M. & Dorman, L.I., *Space Sci. Rev.* **93**, 1, p. 335 (2000).

[94] Shibata, S. *et al.*, *Nucl. Inst. Meth. A* in press (2000).

[95] Yoshimori, M., *Proc. mini conf. on the solar neutron event on 1998 November 28th (Solar-Terrestrial Enviroment Lab., Nagoya Univ. (Feb. 22 - 23))* p. 29 (1999).

[96] Masuda, S., *Proc. mini conf. on the solar neutron event on 1998 November 28th (Solar terrestrial enviroment lab., Nagoya Univ. (Feb. 22 - 23))* p.18 (1999).

[97] Lario, D., *et al.*, *Geophys. Res. Letterss* **25**, 18, p. 3649 (1998).

[98] Mason, G. M.,*et al.*, *Geophys. Res. Letterss* **26**, 2, p. 141 (1999).

[99] Bütikofer, R. & Flückiger, E.O., *26th Inter. Cosmic Ray Conf.(Salt Lake City)* **6**, p. 395 (1999).

[100] Duldig, M.L. & Humble, J.E., *26th Inter. Cosmic Ray Conf.(Salt Lake City)* **6**, p. 403 (1999).

[101] Massetti, S., *et al.*, *26th Inter. Cosmic Ray Conf.(Salt Lake City)* **6**, p. 387 (1999).

[102] Yoshimori, M., *et al.*, *Proc. Nobeyama Symp. (Solar Physics with Radio Observations)* (1998).

[103] Yoshimori, M., *et al.*, *Adv. Space Res.* **25**, 9, p. 1801 (2000).

[104] Yoshimori, M., *et al.*, *In Acceleration and Transport of Energetic Particles Observed in the Heliosphere:ACE 2000 Symp.* edited by Mewaldt, R.A., *et al.*, AIP Proc. 528, AIP, New York, NY (2000).

[105] Yoshimori, M., *et al.*, *26th Inter. Cosmic Ray Conf.(Salt Lake City)* **6**, p. 5 (1999).

[106] Ryan, J.M., *et al.*, *American Astron. Soc., SPD meeting* #32, #14.08 (2000).

[107] Smart, D.F., *et al.*, *Proc. 24th Cosmic Ray Conf. (Roma)* **4**, p. 171 (1995).

[108] Miyake, S., In *Cosmic Ray Astrophys. (in Japanese)* edited by Oda, M., Nishimura, J. & Sakurai, K. (1983).

[109] Kohno, T., *et al.*, *Proc. 26th Cosmic Ray Conf. (Salt Lake City)* **6**, p. 62 (1999).

[110] Wang, H.T., & Ramaty, R., *Solar Phys.* **36**, p. 129 (1974).

[111] Yoshimori, M., *et al.*, *Proc. 18th Cosmic Ray Conf. (Bangalore)* **4**, p. 89 (1983).

[112] Reams, D.V., *Space Sci. Rev.* **90**, p. 413 (1999).

[113] Groom, D.E. *et al.*, *The European Physical J.* **C15**, 1 (2000).

[114] Cliver, E.W. *et al.*, *Astrophys. J.* **264**, p. 699 (1983).

[115] Kahler, S.W. *et al.*, *Astrophys. J.* **302**, p. 504 (1986).

[116] Imaida, I., *et al.*, *Nucl. Inst. Meth. A* **421**, p. 99 (1999).

[117] Ohno, S., *Master Thesis submitted to Nagoya Univ.* (in Japanese) (2001).

[118] Ryan, J.M., *Proc. SPIE* **3768**, p. 496 (1999).